Engineering of Bispecific T Cell Receptors using Mammalian Display Technologies

Entwicklung bispezifischer T-Zell-Rezeptoren mithilfe von Säugetier-Display-Technologien

Von der Fakultät Energie-, Verfahrens- und Biotechnik der Universität Stuttgart zur Erlangung der Würde eines Doktors der Naturwissenschaften (Dr. rer. nat.) genehmigte Abhandlung

Vorgelegt von
Janine Dilchert
aus Herne

Hauptberichter:	Prof. Dr. Roland Kontermann
Mitberichter:	Prof. Dr. Matthias Peipp

Tag der mündlichen Prüfung:	05.Dezember 2022

Institut für Zellbiologie und Immunologie der Universität Stuttgart
2022

Summary

The main goal of immunotherapy in oncology is to use the power of the patient's own immune system to fight cancer. Therefor many bispecific antibodies were developed mainly for redirecting T cells to cancer cells. A novel and promising class of biotherapeutics are increasingly recognized, namely bispecific T cell receptor (TCR)-based molecules capable of redirecting and activating T cells towards tumor-specific peptides presented by human leucocyte antigens (HLA). The usage of TCR-based molecules allows for targeting of novel tumor antigens including intracellular antigens and thus significantly widens the accessible target space in cancer immunotherapy. In contrast to antibodies, TCRs naturally exhibit a low binding affinity and stability and thus a complex maturation process is required for successful generation of TCR-based biotherapeutics. We developed a Chinese hamster ovary (CHO) cell display system for the maturation of TCR-based biomolecules, such as T cell engaging receptor (TCER®). Unlike previously used phage or yeast display systems, the mammalian system is capable of engineering TCRs in the final TCER® format making the step of reformatting of matured TCRs dispensable. The display approach is based on a recombinase-mediated cassette exchange for efficient and stable single copy integration of bispecific agents into a predefined genetic locus of the CHO cell. This work describes the setup of the CHO display, the membrane-bound expression of different TCR-based formats as well as its successful application for engineering of TCER® molecules using TCR variable domains from a model TCR recognizing preferentially expressed antigen in melanoma (PRAME). Affinity-improved TCER® molecules were isolated from a library encoding different complementarity determining region (CDR) variants in the final format. The selected TCER® candidates were evaluated in the CHO display system regarding their binding to the PRAME pHLA target as well as 11 peptides with high degree of sequence similarity to the PRAME peptide as part of specificity testing. TCER® variants expressed as soluble proteins showed strong reactivity against PRAME-positive tumor cells linked with a pronounced cytokine release from activated T cells. This study supports feasibility of the CHO-based maturation system for TCR affinity maturation in the final TCER® format and demonstrate data consistency between membrane-bound and soluble TCER® format.

Zusammenfassung

Das Hauptziel der Immuntherapie in der Onkologie besteht darin, die Kraft des eigenen Immunsystems des Patienten zur Krebsbekämpfung zu nutzen. Zu diesem Zweck wurden viele bispezifische Antikörper entwickelt, die vor allem T-Zellen auf Krebszellen umlenken sollen. Eine neue und vielversprechende Klasse von Biotherapeutika wird zunehmend anerkannt, nämlich bispezifische Moleküle auf der Basis von T-Zell-Rezeptoren (TCR), die in der Lage sind, T-Zellen auf tumorspezifische Peptide umzulenken und zu aktivieren, die von menschlichen Leukozytenantigenen (HLA) präsentiert werden. Die Verwendung von TCR-basierten Molekülen ermöglicht die gezielte Ansprache neuartiger Tumorantigene, einschließlich intrazellulärer Antigene, und erweitert damit den für die Krebsimmuntherapie zugänglichen Zielbereich erheblich. Im Gegensatz zu Antikörpern weisen TCRs von Natur aus eine geringe Bindungsaffinität und -stabilität auf, so dass für die erfolgreiche Herstellung von TCR-basierten Biotherapeutika ein komplexer Maturierungsprozess erforderlich ist. Wir haben ein CHO-Zell-Display-System für die Maturierung von TCR-basierten Biomolekülen, wie z. B. dem T cell engaging receptor (TCER®), entwickelt. Im Gegensatz zu den bisher verwendeten Phagen- oder Hefe-Display-Systemen ist das Säugetiersystem in der Lage, TCRs im endgültigen TCER®-Format zu präsentieren, so dass der Schritt der Neuformatierung von gereiften TCRs überflüssig ist. Der Display-Ansatz basiert auf einem Rekombinase-vermittelten Kassettenaustausch zur effizienten und stabilen Integration von bispezifischen Molekülen in einen vordefinierten genetischen Lokus der CHO-Zelle in einer einzigen Kopie. Diese Arbeit beschreibt den Aufbau des CHO-Displays, die membrangebundene Expression verschiedener TCR-basierter Formate sowie die erfolgreiche Anwendung für das Engineering von TCER®-Molekülen unter Verwendung variabler TCR-Domänen eines Modell-TCRs, der ein preferentially expressed antigen in melanoma (PRAME) Peptid erkennt. TCER®-Moleküle mit verbesserter Affinität wurden aus einer Bibliothek isoliert, die für verschiedene Varianten der komplementäritätsbestimmenden Region (CDR) im endgültigen Format kodiert. Die ausgewählten TCER®-Kandidaten wurden im CHO-Display-System auf ihre Bindung an das PRAME pHLA Target sowie an 11 Peptide mit

hoher Sequenzähnlichkeit zum PRAME Peptid im Rahmen von Spezifitätstests untersucht. TCER®-Varianten, die als lösliche Proteine exprimiert wurden, zeigten eine starke Reaktivität gegen PRAME-positive Tumorzellen, verbunden mit einer ausgeprägten Zytokinfreisetzung von aktivierten T-Zellen. Diese Studie unterstützt die Möglichkeit des CHO-basierten Maturierungssystems für die TCR-Affinitätsreifung im endgültigen TCER®-Format und demonstriert die Datenkonsistenz zwischen membrangebundenem und löslichem TCER®-Format.

Content

List of Abbreviations

Abbreviation	Meaning
%	Percentage
°C	Degree Celsius
μL	Microliter
μM	Micromolar
Ab	Antibody
ADC	Antibody drug conjugates
ADCC	Antibody-dependent cell mediated cytotoxicity
ADCP	Antibody-dependent cellular phagocytosis
AID	Activation-induced cytidine deaminase
APC	Allophycocyanin
bp	base pairs
BsAbs	Bispecific antibodies
CAR	Chimeric antigen receptor
CDC	Complement-dependent cytotoxicity
CDR	Complementarity determining region
C_H	Constant heavy chain
CHO	Chinese hamster ovary
C_L	Constant light chain
CO_2	Carbon dioxide
CRISPR/Cas9	Clustered regularly interspaced short palindromic repeats/ CRISPR-associated protein 9
CRS	Cytokine release syndrom
DNA	Deoxyribonucleic acid
E.coli	*Escherichia coli*
EDTA	Ethylenediaminetetraacetic acid
Fab	Fragment antigen binding
Fc	Fragment crystallizable

g	G-force
GFP	Green fluorescent protein
GOI	Gene of interest
h	Hour
H_2O	Water
HEK	Human embryonic kidney
HLA	Human leucocyte antigen
HSA	Human serum albumin
Ig	Immunoglobulin
IgA	Immunoglobulin A
IgD	Immunoglobulin D
IgE	Immunoglobulin E
IgG	Immunoglobulin G
IgM	Immunoglobulin M
K_D	Dissociation constant
kDa	Kilodalton
LDH	Lactatdehydrogenase
LDH-AM	Lactatdehydrogenase assay medium
mAbs	Monoclonal antibodies
MFI	Mean fluorescence intensity
min	Minute
mio	Million
mL	Milliliter
nm	Nanometer
nM	Nanomolar
NSCLC	Non-small cell lung cancer
pHLA	Peptide HLA complex
PBS	Phosphate buffered saline
PDGFR	Platelet-derived growth factor receptor

PE	Phycoerythrin	
pH	Potential of hydrogen	
pM	Picomolar	
PRAME	Preferentially expressed antigen in melanoma	
RFP	Red fluorescent protein	
rH	Relative humidity	
RMCE	Recombinase-mediated cassette exchange	
RNA	Ribonucleic acid	
rpm	Rotations per minute	
RT	Room temperature	
RTs	Recombination target sites	
SABC	Specific antigen binding capacity	
scFv	Single-chain fragment variable	
SCS	Single cell sort	
scTv	Single-chain T cell receptor variable	
sec	Second	
SHM	Somatic hypermutation	
SSR	Site-specific recombinases	
TAA	Tumor-associated antigen	
TALEN	Transcription activator-like effector nuclease	
T-BsAbs	T cell engaging bispecific antibodies	
TCER	T cell engaging receptor	
TCM	T cell medium	
TCR	T cell receptor	
TILs	Tumor-infiltrating lymphocytes	
TM	Transmembrane domain	
TME	Tumor microenvironment	
U	Enzyme unit	
V$_H$	Variable heavy chain	

V$_L$	Variable light chain
wt	Wildtype
IL-2	Interleukin-2

1 Introduction

1.1 History of Immunotherapy

The field of immunotherapy has raised high expectations as diagnostics and therapeutic tools[1–3] with an expected world-wide size of 126.9 billion US$ by 2026 exhibiting a growth rate of 9.6 %[4]. This story of success was not foreseeable in the 1980s with the first attempts to use monoclonal antibodies (mAbs) for clinical use mainly failing[5]. Since then, mAbs and immunotherapy have come a long way to one of the great hopes in cancer therapy. Nevertheless, it took up to 1997 until the first anti-cancer mAb, Rituximab, has been approved. Since then, more than 27 therapeutic antibodies (Abs) have gotten the approval for cancer treatment in a broad range of cancer entities[6]. Despite the wide range of therapeutics available the majority of cancer patients does not benefit from current immunotherapies[7], for example due to a suppressive tumor microenvironment (TME)[8]. This medical need led to the invention of a plethora of different therapeutic options comprising bispecific Abs (BsAbs), immunomodulators, chimeric antigen receptor (CAR)-T cell therapy[4], T cell receptor (TCR)-T cell therapy, and TCR-based bispecifics[9,10].

1.2 Antibody Based Therapeutics

1.2.1 Natural Antibodies

Antibodies belong to the family of glycoproteins called immunoglobins (Ig) with five different classes: IgA, IgD, IgE, IgG, and IgM with IgG being the most abundant one with 4 different subtypes. The general structure of the IgG molecule compromises two heavy and two light chains with both constant and variable regions (Figure 1). The variable parts of the light (V_L) and the heavy chain (V_H) mediate target binding whereas the constant part (C_L and C_H) facilitates the effector functions. The variable regions can be further discriminated into hypervariable parts, the so-called complementarity determining regions (CDRs), and parts with lower variability, the framework regions. The whole antibody can be divided into two separate parts – the fragment antigen binding (Fab) and the fragment crystallizable (Fc) domain (Figure 1)[11].
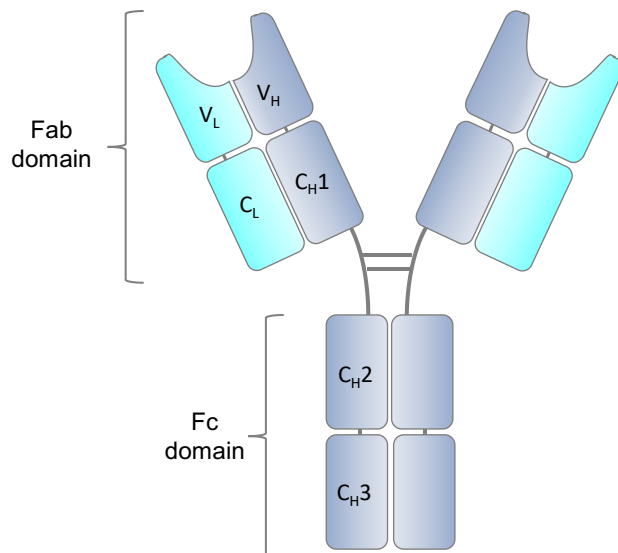
Figure 1: General structure of an IgG1 antibody. The light chain (light blue) comprises a variable (V_L) and a constant (C_L) region. Whereas the heavy chain (dark blue) consists of a variable part (V_H) and three constant regions (C_H1-3). Fab: fragment antigen binding; Fc: fragment crystallizable.

1.2.2 Mode of Action of Monoclonal Antibodies

Antibodies can be used to mediate a wide range of effector mechanism to induce cell death of target cells. These mechanisms can be discriminated in direct and immune-mediated cell killing[12]. Direct cell killing is initiated via receptor binding either blocking a pathway and inducing apoptosis[13] or binding to so-called death receptors and directly inducing cell death[12]. Furthermore, mAbs can be deployed to deliver a toxic payload quite specifically to target cells. These constructs are called antibody drug conjugates (ADC)[12]. ADC therefore enables the use of drugs that are either not suited for a systemic administration or in an unconjugated form[13]. Immune-mediated cell killing can be divided into antibody-dependent cellular phagocytosis (ADCP), antibody-dependent cell mediated cytotoxicity (ADCC), and complement-dependent cytotoxicity (CDC). This group of killing mechanism is mediated by the interaction of the Fc part of an antibody with the Fcγ receptors of different immune cell populations or with the C1q component for CDC[14].

1.2.3 Engineering Antibody Formats

1.2.3.1 Bispecific Antibodies

In contrast to antibodies with only one specificity bispecific antibodies have two well-defined ones[15] to mediate among others immune cell recruitment to cancer cells[2]. There is a plethora of different formats which are subdivided depending on the presence or absence of an Fc region. Fc mediated effector functions like ADCC or CDC will not be activated by molecules lacking a Fc region. Furthermore, these molecules have a shorter half-life since they are not recycled via the neonatal Fc receptor[15]. Since the effector functions are in some cases unwanted silencing mutations have been discovered to inhibit the immune activation while keeping the half-life extension[16–18].

One of these Fc-less formats is the single-chain fragment variable (scFv) composed of two genetically fused variable regions of an antibody[19] (Figure 2). Due to their lower size smaller molecules show rapid and effective distribution, allow a good control over their level in the circulation, and can be quickly cleared from the circulation, if needed[15]. A Fab fusion molecule comprised of the Fab region of an antibody and an added specificity for selected targets shows in general a low aggregation tendency and has a good stability under physiological conditions[15].
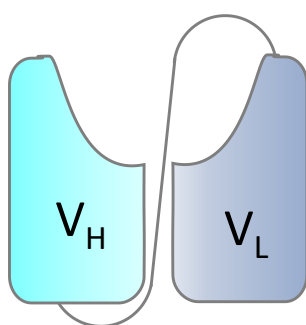
Figure 2: Structure of a scFv fragment. An scFv fragment is composed of the V_H (light blue) and the V_L (dark blue) region of an antibody connected by a linker sequence.

Moreover, antibody derivatives cannot only be discriminated by the presence or absence of a Fc part but also by the number of binding sites. An IgG antibody with a different specificity on each arm would have one binding site for a specific target on each site. It would therefore be classified as a bivalent format. A doubling of the binding sites for each specificity would result in a tetravalent construct. Additionally, also the number of specificities can be increased

resulting in for example tri- or tetra specific formats[15]. Since many of the above-mentioned formats have two different chains and require the formation of heterodimers for the wanted bispecific specificity, it is aimed to increase the likelihood of heterodimerization. To achieve this goal the Fc part can be engineered. In general, the dimerization is mediated by the C_H3 domain and the hinge region of an IgG format[20]. This knowledge led to the invention of many strategies creating complementary chain surfaces to favor heterodimerization. Today, a concept known as "knobs-into-holes" is widely used favoring heterodimerization by the exchange of amino acids to generate a knob with larger side chain on the one chain and a hole with smaller side chains on the other[21–23].

1.2.3.2 T cell Engaging Bispecific Antibodies (T-BsAbs)

T cell engagers are bispecific molecules that redirect native T cells mainly via an anti-CD3 scFv moiety and an anti-tumor-associated antigen specificity to target cells[6,24]. The binding to the CD3 complex of the T cell leads T cell activation associated with the release of cytokines and chemokines, cytotoxic molecules, and the induction of T cell proliferation resulting in targeted tumor cell killing[25]. While the majority of T-BsAbs use the same T cell engaging domain, they can be discriminated via the targeting domain. Here, the targeting moiety can be either derived from an antibody or from an TCR[9].

1.2.3.3 Antibody Derived T-BsAbs

This class of T-BsAbs redirects T cells to the target cells without the human leucocyte antigen (HLA) restriction in normal T cell recruitment. They mainly target surface expressed tumor targets like CD19 in Blinatumumab (anti-CD19/anti-CD3) and many other T-BsAbs in clinical trials[26,27]. Since they are not targeting an antigen presented via the HLA, they are not affected by the downregulation of antigen presentation often observed in immune escape[9]. Nevertheless, restriction to mainly non-HLA presented targets is also one limitation of antibody derived T-BsAbs because the number of surface antigens is limited and more tumor-associated antigens (TAA) can be exploited also considering intracellular and extracellular peptides presented via the HLA.

1.2.3.4 TCR Derived T-BsAbs

TCR derived T-BsAbs use the affinity matured binding moiety of a TCR and for example an anti-CD3 binding domain. Compared to antibody derived T-BsAbs, TCR-based molecules need a complex maturation process until the TCR binding domain can be used in a soluble format. Since TCRs are instable as soluble proteins, they show a high aggregation tendency, and have naturally a low affinity towards their targets (1-100 µM)[9,28,29]. In contrast to antibodies TCRs recognize short (8-20 amino acids) peptide antigens from intracellular, membrane or extracellular proteins presented in the HLA context. Due to the challenging maturation process, there is only a limited number of TCR derived T-BsAbs in clinical trials and only one in clinical use, a gp100 targeting ImmTAC from Immunocore[9]. The KIMMTRAK called molecule was approved 2022 for the treatment of metastatic uveal melanoma[30]. An example of the molecules still in clinical trials is the ABBV-184 molecule by AbbVie. This molecule targets the surviving pHLA complex on tumor cells for the treatment of refractory or relapsed acute myeloid leukemia and non-small cell lung cancer (NSCLC)[31]. Beyond these molecules already in clinical trials there are others to come such as Immatics' T cell engaging receptor (TCER®) molecule. The TCER® molecule consists of an effector-function silenced Fc part, an anti-CD3 scFv and an anti-tumor single-chain TCR variable (scTv) domain (Figure 3).
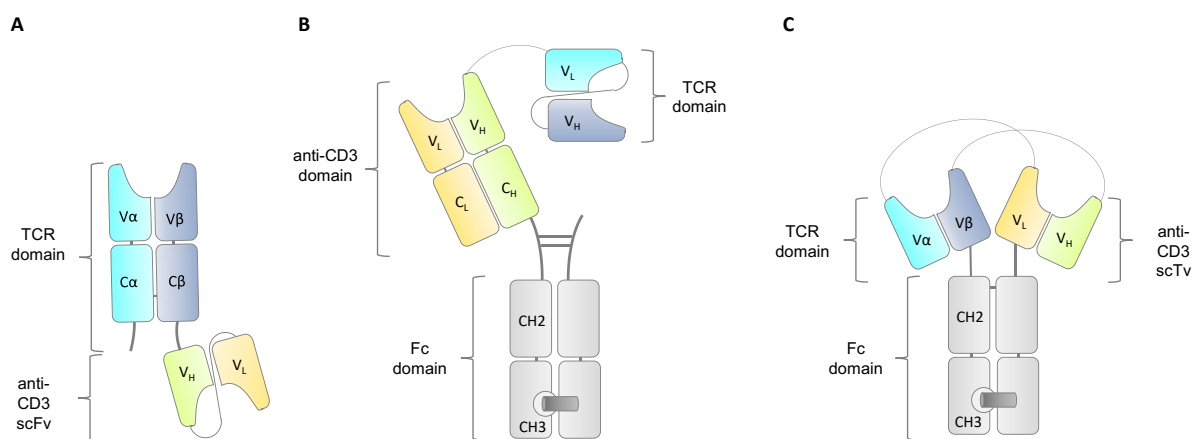
Figure 3: Overview of the different T cell engaging formats in clinical or pre-clinical development. A) ImmTAC format from Immunocore consisting of a targeting TCR domain (light and dark blue) and an anti-CD3-scFv (green, orange). B) ABBV-184 format from AbbVie with a Fc (knob into hole) (grey), an anti-CD3 domain (green, orange), and a surviving targeting scFv (light and dark blue). C) TCER® format is composed of an effector-silenced Fc part (knob into hole) (grey), a tumor targeting scTv (light and dark blue) and an anti-CD3 scFv (green, orange).

1.3   T cells

T cells belong to the group of lymphocytes and have an important role in the adaptive immune response. They are characterized by the presence of a membrane bound TCR for the recognition of foreign peptides[32]. T cells are subdivided into CD4^{+} and CD8^{+} subpopulations, helper and killer T cells, respectively. Helper T cells can indirectly mediate target cell killing by cytokine secretion and subsequent activation of dendritic cells or CD8^{+} T cells. Compared to that, killer T cells can directly eliminate a target cell. For this the additional activation by a co-receptor like CD28 is required as a safety mechanism[32,33]. Upon activation the immunological synapse is built between the target and effector cell. During this process, the T cell releases cytokines and cytotoxins (perforin and granzyme) to induce apoptosis in the target cell[32].

1.3.1   TCR Structure and Target Recognition

The TCR is the antigen recognition structure of T cells. The receptors are membrane-bound and do not appear in a soluble form as B cell receptors and antibodies. Nevertheless, they are related to the immunoglobin family regarding their general architecture[32]. A TCR consists of two distinct chains with constant and variable regions with hypervariable domains (CDRs) determining their specificity resulting in a heterodimeric structure. The majority of the T cells belongs to the α/β subtype whereas only a small number is ranked as the γ/δ type. The TCR itself has a certain resemblance to the antibody Fab fragment and is associated with the CD3 complex for signal transduction and stability (Figure 4).
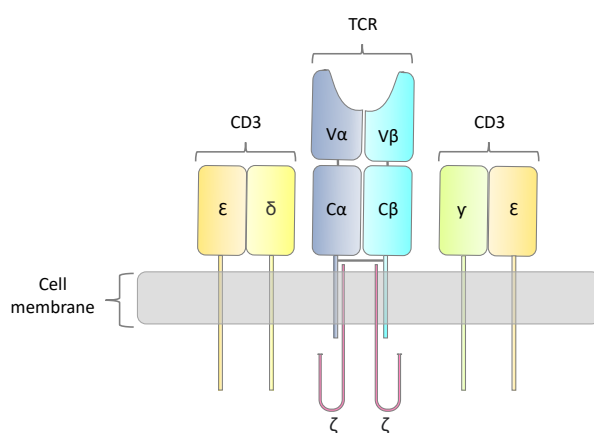
Figure 4: General structure of the α/β T cell receptor CD3 complex. The TCR consist of two chains, α (dark blue) and β chain (light blue) with variable and constant regions. The receptor is complexed with CD3 proteins (ε (orange), δ (yellow), γ (green), and ζ (rose)) for signal transduction.

The TCR can only recognize antigens in a linear and HLA bound fashion, thus the actual target is the peptide: HLA complex (pHLA)[34], since the TCR binds to the linear peptide as well as to the HLA backbone. Here the separate binding profiles of the different CDRs come into play. Whereas the CDR1 and CDR2 are mainly orientated over the HLA backbone, the CDR3 loops are primarily in contact with the peptide[32]. There are two distinct subtypes of the HLA molecule – HLA I and HLA II. The different HLA molecules have not only a different structure, bind different antigens but also bind to different T cell subsets. The HLA I complex consists of three α chain domains and one non-covalently bound β2 microglobulin. Domain α1 and α2 form a groove for peptide binding. The α3 domain anchors the complex to the cell membrane. The HLA II complex consists of two membrane-bound chains – α and β. The α1 and β1 domain fold into a peptide-binding cleft whereas α2 and β2 mediate membrane-anchoring[32] (Figure 5). The HLA I complex is recognized by cytotoxic CD8⁺ T cells. The Class II complex in contrast is associated with CD4⁺ T helper cells. Both interactions result in T cell responses[35].
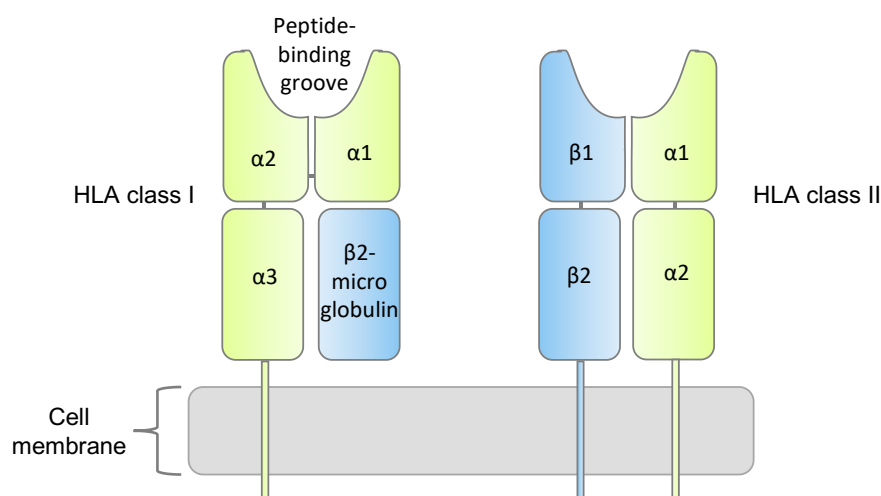
Figure 5: Schematic structure of HLA I and HLA II molecules. HLA class I consists of three α domains (green) with a transmembrane domain and one β2 microglobulin domain (blue). HLA II complex is composed of two chains both anchoring the HLA II to the membrane. The two chains are subdivided into α1 and α2 (green) and β1 and β2 (blue).

Naturally, TCRs have a quite low affinity towards the pHLA complex with K_D in the µM range[36,37] to maintain self-tolerance[38] and they show a great cross-reactivity towards different peptides[39–41]. These characteristics and the fact that the natural presentation level of the pHLA complex can be very low (< 10 copies per cell[42]), make a large maturation effort

necessary to use a TCR-based binding moiety for a bispecific molecule to achieve a specific affinity in the pM range[43,44].

1.3.2 Tumor Antigens

Tumor antigens are proteins or other molecules that discriminate normal cells from cancer cells[45]. The group of tumor antigens has three subgroups: Firstly, tumor-associated antigens which are highly overexpressed on cancer but are also expressed on healthy cells[46]. Secondly, tumor specific antigens that are only expressed on cancer tissues and arose from single non-synonymous variants only present in cancer cells[47]. The third subgroup is the group of cancer testis antigens since they are not expressed on normal tissues except for the testis[48]. Compared to conventional antibody-based approaches TCR-based immunotherapy has the potential to detect also intracellular antigens as they are processed and delivered to the cell surface as small peptides in the context of the HLA[49].

1.3.2.1 PRAME

PRAME (Preferentially expressed antigen in melanoma) is a cancer antigen associated with melanoma and various other non-melanocytic cancer entities, like cutaneous and uveal melanoma[50] and in breast cancer[51], renal cell cancer[52], ovarian carcinoma[53], NSCLC[54] as well as leukemia[55], synovial sarcoma[56], myxoid liposarcoma[57,58] and neuroblastoma[59] making it an attractive target for immunotherapy[48].

1.3.3 Off-targets

Off-targets are peptides with a sequence or motif similarity to the actual tumor target. In contrast to the tumor target, which is mainly or solely expressed on tumor cells, off-targets are expressed on healthy tissue. They can be discovered via mass spectrometry to allow counter-selection during the development of immunotherapies[60].

1.3.4 T cells in the Anti-Tumor Response

Since cancer cells show distinct variations from healthy cells the peptides presented by the HLA complex differ. This often triggers an immune response against cancer cells. The presence of so-called tumor-infiltrating lymphocytes (TILs) is an important prognostic marker in different tumor entities[61–64], but these immune responses are frequently not sufficient for

tumor elimination[65], since there are many immune-suppressive mechanism in place in the TME[66,67]. Additionally, the pHLA complex is often down regulated to escape the T cell based immune response[9]. All these effects hinder a sufficient natural anti-tumor response[66,67].

The power of T cells can, nevertheless, be exploited via the administration of T-BsAbs. CD3-targeting T-BsAbs have the advantage that they are not restricted to the activation of a specific T cell subpopulation. T cells in general are greatly suited as target cells for immune cell recruitment to fight cancer cells due to their high abundance, killing efficiency and high proliferation capacity[2]. Thus, CD3-targeting T-BsAbs can initiate a polyclonal T cell response against the tumor. Hereby, the tumor targeting moiety binds to the target cell and recruits T cells via binding to the CD3 complex[68]. This leads ideally to a robust anti-cancer response and tumor lysis via formation of an immunological synapse (Figure 6) with subsequent cytotoxin and cytokine release[6]. However, an associated challenge with increased T cell activation during immunotherapies is the cytokine release syndrome (CRS)[69,70]. This condition is evoked by a fast increase of cytokines in the serum of the patients leading to life threatening conditions[71–73]. Therefore, it is necessary, to find a good balance between the affinity of the target binding moiety and the anti-CD3 binding one to keep the resulting T cell activation and cytokine release in check[74,75].
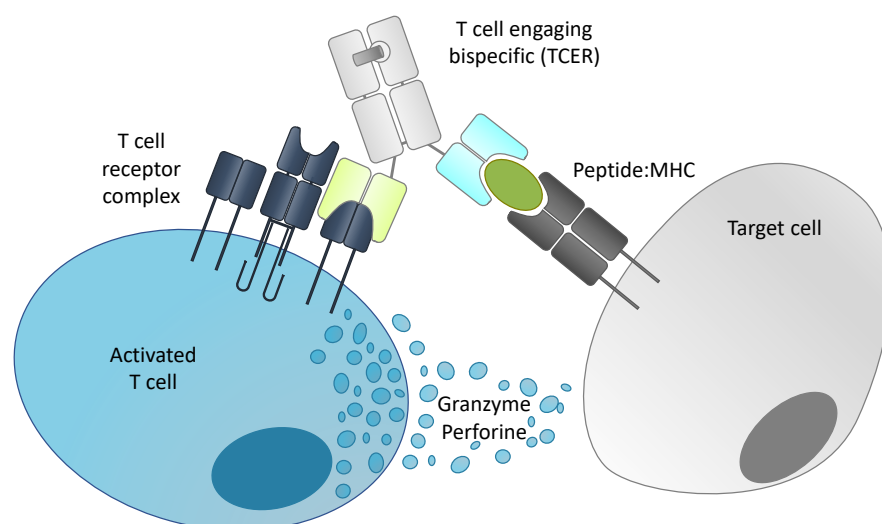
Figure 6: Schematic overview of T-BsAb mediated tumor cell killing. The T-BsAbs (TCER®) binds the pHLA (grey/dark green) on the target cell (light grey) with the TCR domain (light blue) and recruits and activates a T cell (dark blue) via the CD3 binding domain (light green). The released granzymes and perforins lead to subsequent target cell killing.

1.3.5 Engineering of T cell Receptors

TCRs are naturally quite unstable and must therefore undergo stability maturation. For this purpose, various display methods have been previously exploited for antibody maturation[35]. But despite the structural similarities of antibodies[76] and TCRs, the previously established methods like phage, yeast, or mammalian display can just be used to a limited extend, since native TCR constructs are too instable to be displayed [35]. Therefore, it needs a stabilization of the TCR chains facilitated by Boulter and colleagues via the introduction of a modified disulfide bond at TRAC T84C and TRBC S57C (IMGT numbering)[77]. Wagner et al. used these modifications to screen full-length TCRs for high affinity and soluble expression in a Chinese hamster ovary (CHO) cell display system[78]. Other approaches mature the TCR not in full-length but as smaller units such as scTv and circumvent the stability problem[79].

1.4 Display Technologies

Phage, yeast, and mammalian surface display are often used to isolate mAbs therapeutics[80–82] and are more and more used to display and mature TCRs. The prerequisite for all these techniques is the linkage of the phenotype to the genotype of the respective cell to extract the genomic information of the clones after selection[76].

1.4.1 Phage Display

In 1985 it was first shown that peptides can be detected on filamentous phages[83]. Hereby, a peptide sequence is fused to the virus capsid protein and displayed on the outer surface. This fusion allows the detection and selection of peptide variants with higher affinity compared to the wildtype peptide[84]. Since then, this technique is often used to screen for high affinity antibodies against a selected target via biopanning[85]. Phage display has a high degree of flexibility since it allows full-length Igs[86] as well as fragment expression[87–89]. However, the biggest advantage is the possibility to generate very large libraries with up to 10^{11} different variants[76,90,91]. Despite these high usage for antibody-screening it took until 1995 for phage display being used to display TCRs[92] and 10 more years until it was exploited for TCR affinity maturation[44].

1.4.2 Yeast Display

This technique was pioneered by Boder and Wittrup in the year 1997 and is based on the fusion of a protein of interest to a surface protein and the subsequent expression on the cell surface[93]. Mainly the a-agglutinin subunits Aga1p and Aga2p are used to anchor the protein of interest on the surface. Yeast display allows N- or C-terminally linkage[93,94] and expression of full-length Igs[95,96] as well as fragments[93,97–100]. Furthermore, yeast display can also be used to screen TCR-based formats like the scTv format comparable to the antibody-based scFv[101]. In contrast to phage display only smaller libraries with up to 10^9 clones are possible[102–104]. One advantage over phage display is the fact that yeast cells as eucaryotes have a better protein folding machinery and allow the expression of more complex molecules[105–107]. Moreover, it can be combined with flow cytometry enabling 2D sorting for affinity and expression and allows real-time analysis of the clones[93,107,108]. Selected clones can directly be analyzed on the yeast surface and sequence information can easily be obtained via sequencing[76]. It is mainly used for mAbs affinity maturation[93,109,110] but can also be used for TCR-based constructs[111,112].

1.4.3 Mammalian Cell Display

Mammalian cell display made huge progress in the last years. This is mainly due to the possibility to use gene editing techniques like clustered regularly interspaced short palindromic repeats/CRISPR-associated protein 9 (CRISPR/Cas9)[113], transposons[114], transcription activator-like effector nuclease (TALEN)[113], and recombinases[115–117] to achieve a targeted integration at a specific genomic locus[118]. Targeted genomic integration can be used to modify a broad spectrum of cells like human embryonic kidney (HEK) 293T or CHO cells[117,119,120]. To achieve the display of a membrane-bound protein of interest in one of the cell lines the protein of interest will be genetically fused to a transmembrane (TM) domain for example from the murine H-2Kk protein or from the platelet-derived growth factor receptor (PDGFR)[113,121]. With the new gene editing methods, the generation of stable transfected libraries rapidly increased due to a more convenient workflow with more selection rounds possible without plasmid loss[113,114,122–124] and a steadier genotype phenotype coupling[113]. Compared to the beforementioned display techniques this method has the great advantage that the later expression host can also be used for the selection of the clones. Moreover, mammalian cells have a particularly suited expression machinery for

proper folding of full-length Ig molecules with a human-like glycosylation and post-translational modifications[125,126]. These characteristics and the combinability with flow cytometry enables a profound selection of candidates based not only on binding affinity but also on aspects of developability[127]. Furthermore, mammalian cells can be used to express mAb fragments[128] as well as full-length Igs[117,121,129–132] making a re-formatting into the final product format often accompanied with problems regarding impaired binding, folding, or expression expandable[128]. Besides, mAb selection mammalian cell display is also used for TCR identification[133] or maturation[78]. The major downside of mammalian display is the relatively small library size that can be generated. Larger libraries range around 10^9 via random integration[114] and 10^7 using directed integration into a pre-defined locus[113]. Random integration has not only the disadvantage of variation in the expression level depending on the transcriptional activity at the integration site[76] but can also lead to multiple integration[122,123]. Multiple integrations coding for different variants can interfere with the important phenotype genotype coupling and hamper the selection of favorable clones substantially[76]. To address both of these problems site-specific integration at pre-defined loci is more and more used[78,113,117]. Additionally, the implementation of somatic hypermutation (SHM) in vitro led to an increase in library size[117,129,132]. In this case cells are transfected with the enzyme activation-induced cytidine deaminase (AID) mediating the cytosine to uracil exchange and subsequent amino acid substitutions naturally during antibody affinity maturation in B cells[134–136]. To induce SHM in cells without endogenous AID expression it can be transfected[137–139] generating the same mutations as observed in *in vivo* SHM[140].

1.5 Site-specific Integration into Mammalian Cells

As mentioned before site specific integration can mediate the integration of a gene of interest (GOI) into a targeted locus of the host genome[118]. This has the advantage to achieve transcriptional normalization due to the insertion into the same genomic locus[141] and it makes stable expression more convenient[113,114,123,124]. Enzymes that mediate side-specific integration are called site-specific recombinases (SSR) and are very well suited for the insertion or deletion of larger deoxyribonucleic acid (DNA) stretches[118]. The SSR most frequently used for mammalian cell modification are bacteriophage P1-derived Cre, bacteriophage derived ΦC31 integrase, and the Flp recombinase from *Saccheromyces*

cerivisisae. SSR have the advantage of being very specific since they recognize a 30-40 base pair (bp) sequence[118], called recombination target sites (RTs)[141]. The RTs for Cre and Flp are *LoxP* and *FRT* sites, respectively[142]. The recombination using Cre or Flp allows also for a reversion or a reuse of the targeted locus since the RTs remain unchanged after recombination. However, it has the disadvantage that the excision reaction is favored for thermodynamic and kinetic reasons[143]. In contrast to this, the recombination by ΦC31 using the RTs *attP* and *attB* leads to formation of *attL* and *attR* sites, respectively, making a further excision or reusage of the locus impossible since the *attL* and *attR* sites are not recognized by the ΦC31 recombinase[118]. When the GOI is flanked by two RTs the recombination technique is called recombinase-mediated cassette exchange (RMCE) (Figure 7).
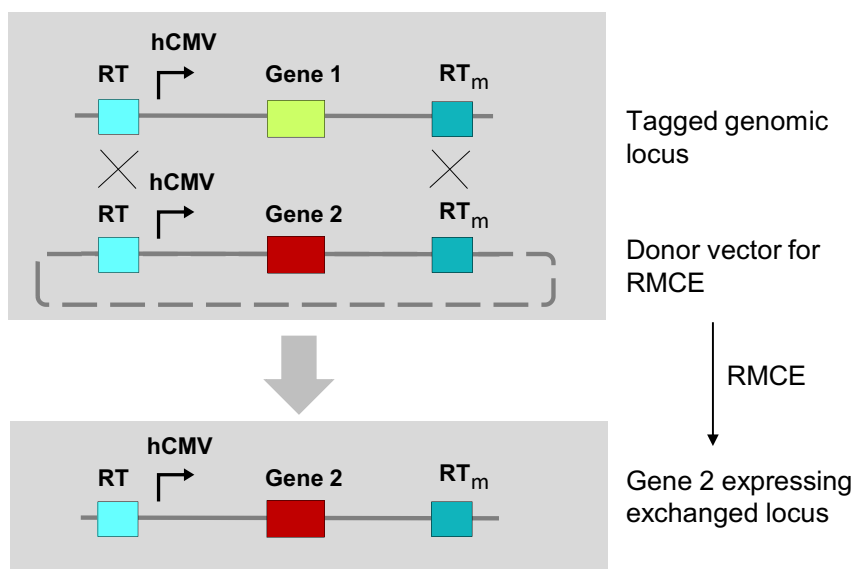
Figure 7: Schematic principle of recombinase-mediated cassette exchange. The genomic host locus is tagged with a pair of recombination sites (turquoise and petrol) flanking gene 1 (green). Adding of a recombinase leads to an exchange of the cassette indicated by the grey crosses resulting in Gene 2 (red) being integrated into the host genome at a specific site.

To enable a directed integration into the tagged locus by RMCE heterospecific RTs were exploited which are unable to recombine with each other. For Flp or Cre mediated RMCE these could be for example F3[144] or LoxP2272 sites[145], respectively. Both variants have been shown to be unreactive with the wildtype (wt) RTs[144,145]. Instead of using heterospecific RTs the RTs from Cre and Flp can also be mixed[146]. To increase the compatibility with mammalian cell culture conditions the temperature-sensitive wt Flp was modified. The resulting Flpe variant is stable at 37 °C and can therefore be used for mammalian cell engineering[147]. Even though SSR are very suited for targeted DNA editing, they still have a few drawbacks. One of

these is their very low but still detectable off-target recombination mediated by pseudo-sites similar to their RTs[118] leading to a background signal due to random integration[148]. The best studied example the ΦC31 has around 100 of those pseudo-sites in the human genome. Furthermore, the expression of certain SSR like Cre[118] or ΦC31 can be toxic for the host especially when expressed highly or stably[118].

2 Aim of the Study

Immunotherapy including mAb and TCR-based bispecifics have raised high expectations in the last years in the treatment of cancer. Nevertheless, there is still a large group of patients not benefiting from the already approved therapies indicating a great medical need for novel therapeutic agents. For the improvement of the preclinical development of such novel therapeutics a mammalian display system should be generated allowing the screening and maturation of TCR-based bispecifics. The mainly used maturation platforms like phage or yeast display exhibit the above-mentioned shortcomings. The implementation of a mammalian cell display platform could therefore be an important step towards a faster and more profound selection of therapeutic candidates. A master cell line with a single copy tagged locus in CHO cells for RMCE should be generated as a first step to allow screening and maturation of molecules at a normalized expression level and assure the important phenotype genotype linkage. Flow cytometric measurements were conducted to screen for high and stable expression of the gene of interest from the tagged locus and to show that membrane-bound expression of various TCR-based bispecific formats is possible from the tagged locus. The newly established system is used to show the feasibility of screening and selecting TCER® candidates from a PRAME pHLA specific library applying target and off-target screening. Selected candidates from this library are tested for their *in vitro* potential assessing their target cell killing, effector cell activation and cytokine-release ability.

All in all, this study should improve the preclinical development of TCR-based immunotherapies with high affinities and favorable specificity profiles helping to bring the power of T cells to cancer patients.

3 Material and Methods

3.1 Material

3.1.1 Medium and Additives

Name	Manufacturer
CD CHO	Gibco by Thermo Fisher Scientific, Waltham, MA, USA
Cell Boost™ 7A - ADCF	Cytiva, Marlborough, MA, USA
Cell Boost™ 7B - ADCF	Cytiva, Marlborough, MA, USA
ClonaCell™-CHO ACF Supplement	Stemcell™ Technologies, Vancouver, Canada
ClonaCell™-CHO CD	Stemcell™ Technologies, Vancouver, Canada
DMEM	Gibco by Thermo Fisher Scientific, Waltham, MA, USA
DMEM high glucose	Gibco by Thermo Fisher Scientific, Waltham, MA, USA
Fetal Calf Serum	Gibco by Thermo Fisher Scientific, Waltham, MA, USA
Geneticin	Gibco by Thermo Fisher Scientific, Waltham, MA, USA
Gentamycin	Biozym, Hessisch Oldendorf, Germany
GlutaMAX	Gibco by Thermo Fisher Scientific, Waltham, MA, USA
HT Supplement	Gibco by Thermo Fisher Scientific, Waltham, MA, USA
Human serum	c.c. pro, Oberdorla, Germany
HyClone ActiPro™	Cytiva, Marlborough, MA, USA
HyClone CDM4CHO™	Cytiva, Marlborough, MA, USA
HyClone HyCell CHO™	Cytiva, Marlborough, MA, USA

HyClone™ ActiSM™	Cytiva, Marlborough, MA, USA
HyClone™ CDM4PerMAb™	Cytiva, Marlborough, MA, USA
Hygromycin B	Invitrogen by Thermo Fisher Scientific, Waltham, MA, USA
InstiGRO CHO	SAL Scientific Ltd, Fordingbridge, UK
InstiGRO CHOPLUS	SAL Scientific Ltd, Fordingbridge, UK
MEM NEAA, 100x	Gibco by Thermo Fisher Scientific, Waltham, MA, USA
Penicillin/Streptomycin	Lonza, Basel, Switzerland
Pluronic™ F-68 non-ionic surfactant	Gibco by Thermo Fisher Scientific, Waltham, MA, USA
RPMI 1640 GlutaMax	Gibco by Thermo Fisher Scientific, Waltham, MA, USA
RPMI 1640 without phenol-red	Gibco by Thermo Fisher Scientific, Waltham, MA, USA
S.O.C. Medium	Thermo Fisher Scientific, Waltham, MA, USA

3.1.2 Cell Lines

Name	Organism	Disease	Reference
A375	Homo sapiens	Melanoma	Giard et al.[149]
FreeStyle™ CHO-S™	Cricetulus griseus		Puck et al.[150]
HS695T	Homo sapiens	Melanoma	Creasey et al.[151]
SET-2	Homo sapiens	Essential thrombocytemia	Uozumi et al.[152]
T98G	Homo sapiens	Glioblastoma multiforme	Stein[153]
UACC-257	Homo sapiens	Melanoma	Leibovitz[154]

3.1.3 Chemicals and Reagents

Name	Manufacturer
0.25 % Trypsin/EDTA	Gibco by Thermo Fisher Scientific, Carlsbad, CA, USA
1 kb DNA Ladder	New England Biolabs, Ipswich, MA, USA
10 % Pluronic® F-68	Gibco by Thermo Fisher Scientific, Carlsbad, CA, USA
100 bp DNA Ladder	New England Biolabs, Ipswich, MA, USA
Accutase	PromoCell, Heidelberg, Germany
Acetic Acid 100 %	Merck, Darmstadt, Germany
Ampicillin	Carl Roth GmbH, Karlsruhe, Germany
Ampuwa (sterile injection water)	Fresenius Kabi, Bad Homburg, Germany
Bacillol AF	Bode Chemie GmbH, Hamburg, Germany
Benzonase	Merck, Darmstadt, Germany
Bovine Serum Albumin	Sigma-Aldrich, St. Louis, MO, USA
Citric acid monohydrate ($C_6H_8O_7$ x H_2O)	Sigma-Aldrich, St. Louis, MO, USA
CryoSure-DMSO	WAK-Chemie Medical GmbH, Steinbach, Germany
CTL Wash 10x	C.T.L Europe, Bonn, Germany
D-Biotin	Sigma-Aldrich, St. Louis, MO, USA
Di-Sodium hydrogen phosphate dihydrate (Na_2HPO_4 x 2 H_2O)	Sigma-Aldrich, St. Louis, MO, USA
Dubecco's Phosphate-buffered saline (DPBS)	Gibco by Thermo Fisher Scientific, Carlsbad, CA, USA
EDTA	Carl Roth GmbH, Karlsruhe, Germany
Ethanol	Carl Roth GmbH, Karlsruhe, Germany
HCL (35-37 %)	Sigma-Aldrich, St. Louis, MO, USA
Human serum albumin (HSA) 20 %	Octapharma, Lachen, Switzerland
Isopropanol	Carl Roth GmbH, Karlsruhe, Germany
LB Agar (Lennox)	Carl Roth GmbH, Karlsruhe, Germany
LB Broth (Lennox), granulated	Carl Roth GmbH, Karlsruhe, Germany
LB Medium (Lennox)	Carl Roth GmbH, Karlsruhe, Germany
L-Glutamine	Thermo Fisher Scientific, Waltham, MA, USA

MaxCyte® Electroporation Buffer	Cytiva, Marlborough, MA, USA
Pancoll human	PAN Biotech GmbH, Aidenbach, Germany
PeqGREEN	Peqlab, Erlangen, Germany
Phenylmethylsulfonylfluorid (PMSF)	Sigma-Aldrich, St. Louis, MO, USA
Sodium acetate	Merck, Darmstadt, Germany
Sodium azide	Carl Roth GmbH, Karlsruhe, Germany
Sodium butyrate	Sigma-Aldrich, St. Louis, MO, USA
Sodium hydroxide (NaOH)	Carl Roth GmbH, Karlsruhe, Germany
Sodium hydroxide (NaOH) 1M	Chemsolute® Th.Geyer, Renningen, Germany
Sodium pyruvate	c.c. pro, Oberdorla, Germany
Sodiumchloride (NaCl)	Carl Roth GmbH, Karlsruhe, Germany
Tris(hydroxylmethylaminomethan)	Carl Roth GmbH, Karlsruhe, Germany

3.1.4 Buffers and Solutions

Name	Components
1x TAE	20 mL 50 x TAE 980 mL H_2O
50x TAE, pH 8.3	242 g Tris 57.1 mL Acetic acid 100 mL EDTA 0.5 M, pH 8.0 Ad 1 L MilliQ H_2O
ActiPro™	ActiPro™ 1 x HT supplement 8 mM GlutaMax
ActiPro™ + G418	ActiPro™ 1 x HT supplement 8 mM GlutaMax 1 mg/mL Geneticin (G418)
ActiSM™	ActiSM™ 1 x HT supplement 8 nM GlutaMax
Ampicillin	2.4 g Ampicillin 24 mL MilliQ H_2O

CD CHO	CD CHO
	1 x HT supplement
	8 mM GlutMax
	0.1 % Pluronic
CDM4CHO™	CDM4CHO™
	1 x HT supplement
	0.1 % Pluronic
CDM4PerMAb™	CDM4PerMAb™
	1 x HT supplement
	8 mM GlutaMax
ClonaCell™-CHO CD	ClonaCell™-CHO CD
	1 x HT supplement
	8 mM GlutaMax
CTL Wash	5 mL CTL Wash (10 x)
	95 mL H_2O
D-Biotin	77.9 mg D-Biotin
	3.2 ml 200 nM Tris-Base
EDTA 0.5 M, pH8.0	29.2 g EDTA
	200 mL H_2O
	NaOH (for pH adjustment)
Elution Buffer (Capture column)	17.7 g Citric acid monohydrate (84.4 nM)
	5,6 g Di-Sodium hydrogen phosphate dihydrate (31.2 nM)
	Ad 1 L H_2O
	Sterile filtered
FACS Buffer (PBS, 1% BSA, 2 mM EDTA)	5 g BSA
	500 mL PBS
	2 mL EDTA 0.5 M, pH 8.0
HyCell CHO	HyCell CHO
	6 mM GlutaMax
Injection Buffer HLA Refolding	MilliQ H_2O
	Guanidine-HCL 3M
	Sodium acetate 10 mM
	EDTA 10 nM
LB Agar (Lennox)	35 g LB Agar
	1 L H_2O
LB Broth	20 g LB Broth
	1 L H_2O
LDH-Assay Medium	RPMI 1640 without phenol-red
	10 % human serum, heat-inactivated

	1 x GlutaMax
	1 x Penicillin/Streptomycin
Medium D	RPMI 1640 without phenolred
	11.5 % Human serum albumin
Medium E	RPMI 1640 without phenolred
	11.5 % Human serum albumin
	20 % DMSO
NaOH 0.5 M	500 mL 1M NaOH
	500 mL H_2O
SEC Running Buffer (TBSA)	MilliQ H_2O
	20 mM Tris base pH 8
	150 mM sodium chloride
	0.02 % sodium azide
	Sterile filtered and degassed
Sodium azide, 10 %	10 g Sodium azide
	100 mL H_2O
Sodium butyrate 1 M	110,09 g
	1 L H_2O
TCM	RPMI GlutaMax
	10 % human serum, heat-inactivated
	1 % Penicillin/Streptomycin
	20 µg/mL Gentamycin
	1 % Sodium pyruvate
Tris-Base 200 mM	2.4 g Tris-Base
	100 mL MilliQ H_2O
Wash Buffer (Capture column)	1.5 g Tris (25 mM)
	0.73 g NaCl
	Ad 400 mL H_2O
	HCl (35-37 %) pH 7.1
	Ad 500 mL H_2O
	Sterile filtered

3.1.5 General Laboratory Devices

Name	Manufacturer
AE2000 Microscope	Motic, Barcelona, Spain
Äkta Pure	Cytiva, Marlborough, MA, USA
BioMAT 2	Contained Air Solutions Ltd, Middleton, UK
Cellgard ES Class II	NuAire, Plymouth, MN, USA

Centrifuge 5424 R	Eppendorf AG, Hamburg, Germany
ChemiDoc™ XRS+	Bio-Rad, Hercules, CA, USA
CoolCell FTS30	BioCision LLC, San Rafael, CA, USA
ED-13 stirred water bath	Julabo GmbH, Seelbach, Germany
EMB 3000-1	Kern®, Balingen, Germany
MACSQuantX	Miltenyi Biotec, Bergisch Gladbach, Germany
MaxCyte STx/ATx	MaxCyte, Gaithersburg, MD, USA
MEGA STAR 3.0R	VWR International, Radnor, PA, USA
MicroPulser™	Bio-Rad, Hercules, CA, USA
Microwave	Sharp, Osaka, Japan
Minitron incubation shaker	Infors GmbH, Sulzemoos, Germany
MS3 basic	IKA®, Staufen im Breisgau, Germany
Multi-Application Cell Sorter MA900	Sony Biotechnology Inc, San José, CA, USA
Multipette M4	Eppendorf AG, Hamburg, Germany
Multitron incubation shaker	Infors GmbH, Sulzemoos, Germany
NanoDrop™ 8000	Thermo Fisher Scientific, Waltham, MA, USA
Nucleo Counter NC-250	Chemometec, Allerød, Denmark
Octet HTX	Sartorius, Goettingen, Germany
Pipetboy	INTEGRA Biosciences GmBH, Biebertal, Germany
Pipet-Lite XLS 0.1-2 µL	Mettler-Toledo Rainin, Oakland, CA, USA
Pipet-Lite XLS 0.5-10 µL	Mettler-Toledo Rainin, Oakland, CA, USA
Pipet-Lite XLS 10-100 µL	Mettler-Toledo Rainin, Oakland, CA, USA
Pipet-Lite XLS 20-200 µL	Mettler-Toledo Rainin, Oakland, CA, USA
Pipet-Lite XLS 2-20 µL	Mettler-Toledo Rainin, Oakland, CA, USA
PowerPac Basic	Bio-Rad, Hercules, CA, USA
ProfiLine Frigde & Freezer	Liebherr, Biberach an der Riß, Germany
RH basic 2 magnetic stirrer	IKA®, Staufen im Breisgau, Germany
SevenExcellence Multiparameter	Mettler-Toledo Rainin, Oakland, CA, USA
Sorvall Lynx 6000	Thermo Fisher Scientific, Waltham, MA, USA
Spectral Analyzer SA3800	Sony Biotechnology Inc, San José, CA, USA

SpectraMax ix3	Molecular devices, San José, CA, USA
SU1550	Sustainable Lab Instruments, Mannheim, Germany
Sub-Cell® GT	Bio-Rad, Hercules, CA, USA
Sub-Cell® Model 192	Bio-Rad, Hercules, CA, USA
ThermoMixer C	Eppendorf AG, Hamburg, Germany
Ultrafiltration stirred cell 8400	Merck Millipore, Burlington, MA, USA
ViCell™ XR	Beckman Coulter, Brea, CA, USA
Vortex Genie 2	Scientific Industries Inc. Bohemia, NY, USA

3.1.6 Consumables

Name	Manufacturer
10 µL BioClean Ultra	Mettler-Toledo Rainin, Oakland, CA, USA
10 mL culture tube round bottom	Carl Roth GmbH, Karlsruhe, Germany
10 mL Stripette	Corning Incorporated, Corning, NY, USA
100 mL Reagent Reservoir	Corning Incorporated, Corning, NY, USA
1000 mL non-baffled polycarbonate Erlenmeyer Shake Flask with vented cap	Corning, Corning, NY, USA
1200 µL BioClean Ultra	Mettler-Toledo Rainin, Oakland, CA, USA
125 mL non-baffled polycarbonate Erlenmeyer Shake Flask with vented cap	Corning, Corning, NY, USA
15 mL High-Clarity tube	Falcon by Corning Incorporated, Corning, NY, USA
175 cm² Cell culture flask	GreinerBio-One GmbH, Frickenhausen, Germany
2 mL 96-well deepwell plate	Thermo Fisher Scientific, Waltham, MA, USA
2 mL Serological pipet	Falcon by Corning Incorporated, Corning, NY, USA
200 µL BioClean Ultra	Mettler-Toledo Rainin, Oakland, CA, USA
25 cm² Cell culture flask	GreinerBio-One GmbH, Frickenhausen, Germany

25 mL Stripette	Corning Incorporated, Corning, NY, USA
250 mL non-baffled polycarbonate Erlenmeyer Shake Flask with vented cap	Corning, Corning, NY, USA
300 µL BioClean Ultra	Mettler-Toledo Rainin, Oakland, CA, USA
5 mL Stripette	Corning Incorporated, Corning, NY, USA
50 mL Reagent Reservoir	Corning Incorporated, Corning, NY, USA
50 mL Stripette	Corning Incorporated, Corning, NY, USA
500 mL non-baffled polycarbonate Erlenmeyer Shake Flask with vented cap	Corning, Corning, NY, USA
75 cm^2 Cell culture flask	GreinerBio-One GmbH, Frickenhausen, Germany
96-well plates flat bottom	Greiner Bio-One, Kremsmuenster, Austria
96-well plates U-bottom	Greiner Bio-One, Kremsmuenster, Austria
Amicon 15-Ultra centrifugal filter device	Merck Millipore, Burlington, MA, USA
CellStar 12 Well Cell Culture Plate	Greiner Bio-One, Kremsmuenster, Austria
CellStar 48 Well Cell Culture Plate	Greiner Bio-One, Kremsmuenster, Austria
CellStar 96 Well Cell Culture Plate	Greiner Bio-One, Kremsmuenster, Austria
CellStar Cellreactor Tube, 50 mL	Greiner Bio-One, Kremsmuenster, Austria
CellStar Tube, 50 mL	Greiner Bio-One, Kremsmuenster, Austria
Costar 96 Well Cell Culture Plate	Corning Incorporated, Corning, NY, USA
Cryo.s 2 mL vial	Greiner Bio-One, Kremsmuenster, Austria
Disposal Bags	Carl Roth GmbH, Karlsruhe, Germany
HiLoad 26/600 Superdex 75 pg	GE Healthcare, Chicago, IL, USA
Injekt® single use syringe (luer lock)	B. Braun Deutschland GmbH & Co. KG, Melsungen, Hessen
Inoculation loop	Carl Roth GmbH, Karlsruhe, Germany
Kimtech Purple Nitrile Xtra Gloves	Kimtech, Roswell, GA, USA
Kimwipes	Carl Roth GmbH, Karlsruhe, Germany
Moisture Barrier Seal 24	4titute Ltd by Brooks Life Sciences, Chelmsford, MA, USA

Moisture Barrier Seal 96	4titute Ltd by Brooks Life Sciences, Chelmsford, MA, USA
OC-100x2 Electroporation cuvette	MaxCyte, Gaithersburg, MD, USA
OC-25x3 Electroporation cuvette	MaxCyte, Gaithersburg, MD, USA
OC-400 Electroporation cuvette	MaxCyte, Gaithersburg, MD, USA
Parafilm PM-996	Bemis, Neenah, WI, USA
PCR Plate	Carl Roth GmbH, Karlsruhe, Germany
Petri dish sterile	GreinerBio-One GmbH, Frickenhausen, Germany
Safe-Lock Tubes 0.5 mL	Eppendorf, Hamburg, Germany
Safe-Lock Tubes 1.5 mL	Eppendorf, Hamburg, Germany
Safe-Lock Tubes 2.0 mL	Eppendorf, Hamburg, Germany
Safe-Lock Tubes 5 mL	Eppendorf, Hamburg, Germany
Scale pan	Carl Roth Carl Roth GmbH, Karlsruhe, Germany
Sterican® single use canula, blunt	B. Braun Deutschland GmbH & Co. KG, Melsungen, Hessen
Stericup® and Steritop®	Merck Millipore, Burlington, MA, USA
Sterile syringe filter Puradisc 0,22 μm	Cytiva, Marlborough, MA, USA
Toyopearl AF-rProteinL-650F	Tosoh Bioscience, Tokio, Japan
Ultrafiltration membrane 30 kDa	Merck Millipore, Burlington, MA, USA
Wide-mouth bottle	Thermo Scientific Nalgene by Thermo Fisher Scientific, Waltham, MA, USA

3.1.7 Kits

Name	Manufacturer
CytoTox 96 Non-Radioactive Cytotoxicity Assay Kit	Promega, Madison, WI, USA
MACSPlex Cytotoxic T/NK Cell Kit, human	Miltenyi Biotec, Bergisch Gladbach, Germany

NucleoBond® Xtra Maxi EF	Macherey-Nagel, Dueren, Germany
NucleoBond® Xtra Midi EF	Macherey-Nagel, Dueren, Germany
NucleoSpin® Gel and PCR Clean-up	Macherey-Nagel, Dueren, Germany
Phire Tissue Direct PCR Master Mix	Thermo Fisher Scientific, Waltham, MA, USA
QIAprep® Spin MiniPrep Kit	Qiagen, Hilden, Germany
QIFIKIT®	Dako Denmark ApS, Glostrup, Denmark
SartoClear Dynamics	Sartorius AG, Goettingen, Germany

3.1.8 Bacteria Strain

Name	Manufacturer
E.coli **TOP10**	Thermo Fisher Scientific, Waltham, MA, USA

3.1.9 Enzymes

Name	Manufacturer
BirA ligase	Avidity LLC, Aurora, CO, USA
EcoRI	New England Biolabs, Ipswich, MA, USA
Flp	Miltenyi Biotec, Bergisch Gladbach, Germany
Leupeptin	Roche, Basel, Switzerland
NheI	New England Biolabs, Ipswich, MA, USA
Pepstatin	Roche, Basel, Switzerland
Phusion® Polymerase	New England Biolabs, Ipswich, MA, USA
PvuI	New England Biolabs, Ipswich, MA, USA
T4 DNA Ligase	Thermo Fisher Scientific, Waltham, MA, USA

3.1.10 Antibodies

Name	Manufacturer
APC anti-human CD69	BioLegend, San Diego, CA, USA
APC/Cyanine7 anti-human CD8a	BioLegend, San Diego, CA, USA
Biotin anti-human IgG Fc (Clone HP6017)	BioLegend, San Diego, CA, USA

Brilliant Violet 421™ anti-human CD56 (NCAM)	BioLegend, San Diego, CA, USA
CD28 antibody [9.3]	University of Tuebingen, Tuebingen, Germany
eBioscience™ Anti-Hu Vb5.1 TCR APC (Clone LC4)	eBioscience, by Thermo Fisher Scientific, Waltham, MA, USA
FITC anti-human CD4	BioLegend, San Diego, CA, USA
Mouse anti-human CD8-Biotin	BD Pharmingen, San Diego, CA, USA
PE anti-human CD25	BioLegend, San Diego, CA, USA
PE/Cyanine7 anti-human CD3	BioLegend, San Diego, CA, USA
Purified anti-human CD3 antibody [OKT3]	BioLegend, San Diego, CA, USA
Streptavidin, Alexa Fluor™ 647 conjugate	Invitrogen by Thermo Fisher Scientific, Waltham, MA, USA
Streptavidin, Allocyanin, crosslinked conjugate	Invitrogen by Thermo Fisher Scientific, Waltham, MA, USA
Streptavidin, R-phytoerythrin conjugate [SAPE]	Invitrogen by Thermo Fisher Scientific, Waltham, MA, USA

3.1.11 Vectors

Name	Source/Reference
pJD1	Dilchert unpublished
pJD4	Dilchert unpublished
pJD5	Dilchert unpublished
pMH1	Hofmann unpublished

3.1.12 Plasmids

Name	Source
11581_alpha_pMH1	GeneArt by Thermo Fisher Scientific, Waltham, MA, USA
11581_pJD1	GeneArt by Thermo Fisher Scientific, Waltham, MA, USA
11594_alpha_pMH1	GeneArt by Thermo Fisher Scientific, Waltham, MA, USA

11594_pJD1	GeneArt by Thermo Fisher Scientific, Waltham, MA, USA
11611_alpha_pMH1	GeneArt by Thermo Fisher Scientific, Waltham, MA, USA
11611_pJD1	GeneArt by Thermo Fisher Scientific, Waltham, MA, USA
11614_alpha_pMH1	GeneArt by Thermo Fisher Scientific, Waltham, MA, USA
11614_beta_pMH1	GeneArt by Thermo Fisher Scientific, Waltham, MA, USA
11614_pJD1	GeneArt by Thermo Fisher Scientific, Waltham, MA, USA
11623_alpha_pMH1	GeneArt by Thermo Fisher Scientific, Waltham, MA, USA
11623_beta_pMH1	GeneArt by Thermo Fisher Scientific, Waltham, MA, USA
11623_pJD1	GeneArt by Thermo Fisher Scientific, Waltham, MA, USA
7435_alpha_pMH1	GeneArt by Thermo Fisher Scientific, Waltham, MA, USA
7435_beta_pMH1	GeneArt by Thermo Fisher Scientific, Waltham, MA, USA
7435_pJD1	GeneArt by Thermo Fisher Scientific, Waltham, MA, USA
7445_alpha_pMH1	GeneArt by Thermo Fisher Scientific, Waltham, MA, USA
7445_beta_pMH1	GeneArt by Thermo Fisher Scientific, Waltham, MA, USA
7445_pJD1	GeneArt by Thermo Fisher Scientific, Waltham, MA, USA
7467_alpha_pMH1	GeneArt by Thermo Fisher Scientific, Waltham, MA, USA
7467_beta_pMH1	GeneArt by Thermo Fisher Scientific, Waltham, MA, USA
7467_pJD1	GeneArt by Thermo Fisher Scientific, Waltham, MA, USA
7475_alpha_pMH1	GeneArt by Thermo Fisher Scientific, Waltham, MA, USA
7475_beta_pMH1	GeneArt by Thermo Fisher Scientific, Waltham, MA, USA
7475_pJD1	GeneArt by Thermo Fisher Scientific, Waltham, MA, USA
7480_alpha_pMH1	GeneArt by Thermo Fisher Scientific, Waltham, MA, USA
7480_beta_pMH1	GeneArt by Thermo Fisher Scientific, Waltham, MA, USA
7480_pJD1	GeneArt by Thermo Fisher Scientific, Waltham, MA, USA
DuoFc_pJD5	GeneArt by Thermo Fisher Scientific, Waltham, MA, USA
Flpe_pMH1	Cloned with inserts ordered from GenScript, Piscataway Township, NJ, USA
GFP_pJD1	Cloned with inserts ordered from GenScript (Piscataway Township, NJ, USA)
HC-scTv_pJD5	GeneArt by Thermo Fisher Scientific, Waltham, MA, USA
LC-scTv_pJD5	GeneArt by Thermo Fisher Scientific, Waltham, MA, USA

RFP_pJD1	Cloned with inserts ordered from GenScript (Piscataway Township, NJ, USA)
ScFc_pJD5	GeneArt by Thermo Fisher Scientific, Waltham, MA, USA
scTv_pJD5	GeneArt by Thermo Fisher Scientific, Waltham, MA, USA
TCER_pJD1	GenScript, Piscataway Township, NJ, USA
TCER_pJD5	GeneArt by Thermo Fisher Scientific, Waltham, MA, USA

3.1.13 PCR Primer

Primers were ordered from Sigma Aldrich (Sigma-Aldrich, St. Louis, MO, USA) at a concentration of 100 µM and stored at -20 °C.

Name	Sequence (5'-3')
A03_head_forw	GGAGTCTATGTATGTGCAC
A03_tail_rev	GTCGAAGCGGCGGC
Flpe_forw_NheI	GAAGCTGGCTAGCGCCGCCACCATGAGCCAGTTCGACATCC
Flpe_rev_EcoRI	CTGGATATCTGCAGAATTCTCAGATCCGCCTATTGATATAG
GFP_forw	CTGGCTAGCGCCGCCACCATGGTGTCCAAGGGAGAGG
GFP_rev	TCTGCAGAATTCCACTTATACAGCTCATCCATGC
HiAff#1_TLA_forw	GCACGGCGAGGAACGG
HiAff#1_TLA_rev	CCGCCTTGGTCATTGTCG
JD057	CAGCGCCTACTCTGAGG
JD059	GCTGGATATCTGCAGAATTCC
JD061	GACACGAAGCTGGCTAG
JD065	CTTGCTGGCAGAAGTAGG
RFP_forw	ACGAAGCTGGCTAGCGCCGCCACCGCCTCCAGCGAGGACG
RFP_rev	CTGGATATCTGCAGAATTCTCAAGCGCCGGTGC
RFP_TLA_forw	GAGGCCTCTACAGAGAG
RFP_TLA_rev	CAGCTTGGCTGTCTGG

3.1.13.1 Sequencing Primers

Name	Sequence (5'-3')
GFP forward (SP54)	GGCAAGCTGACACTGAAG
GFP reverse (SP55)	CCTCTTCTCGTTTGGGTC
RFP forward (SP17)	CAGTACGGCTCCAAGGC
RFP reverse (SP18)	CCATTGTCTTCTTCTGCATCAC
TCER Chain 1 reverse (SP60)	GAGATAGTCAGGGTATAGTC
TCER Chain 2 reverse (SP59)	CTTCACTTCTGGGTCCTC

3.1.14 Peptide Sequences

	Sequence at peptide position*								
	1	2	3	4	5	6	7	8	9
PRAME	S	L	L	Q	H	L	I	G	L
Similar 1	.	x	.	.	x	.	.	x	x
Similar 2	.	.	x	x	.	.	x	.	.
Similar 3	.	.	x	.	.	.	x	x	x
Similar 4	.	.	.	x	x	.	.	x	.
Similar 5	.	.	.	x	.	.	x	x	.
Similar 6	.	.	.	.	.	x	.	x	.
Similar 7	.	.	.	.	x	x	x	x	.
Similar 8	.	.	x	.	x	.	x	.	x
Similar 9	.	x	.	x	x	.	.	.	x
Similar 10	x	.	.	x	.	x	.	.	.
Similar 11	x	x	x	x	.	.	.	x	x

* with "x" representing a variation to the PRAME peptide and "." representing a wt residue

3.1.15 Software Programs

Name	Manufacturer
Cell Sorter Software 3.2.0	Sony Biotechnology Inc, San José, CA, USA
FlowJo Software (10.7.1)	Becton Dickinson, Franklin Lakes, NJ, USA
Geneious Prime (2020.2.5)	Biomatters Ltd, Auckland, New Zealand
GraphPad Prism (9.2.0)	GraphPad Software, San Diego, CA, USA
HT Software 12.0	Sartorius, Goettingen, Germany

Image Lab 5.2.1	Bio-Rad, Hercules, CA, USA
Microsoft Office 365	Microsoft Cooperation, Redmond, USA
Quantify Software 2.13.2	Miltenyi Biotec, Bergisch Gladbach, Germany
SA3800 Software 2.0.4.13263	Sony Biotechnology Inc, San José, CA, USA
SoftMax Pro 7	Molecular devices, San José, CA, USA

3.2 Methods

3.2.1 Cell Culture

3.2.1.1 Tumor Cells

All tumor cell lines were cultured at 37 °C, 5 % CO_2, 80 % relative humidity (rH) and were passaged when more than 80 % confluent. For adherent cells cell culture medium was removed and cells were washed once with 1x PBS and detached using 0.05 % Trypsin/EDTA or Accutase. Cells were incubated at 37 °C until the cells were completely detached. The culture medium was used to inactivate the detaching enzyme and cells were centrifuged for 5 min at 300 g. Afterwards cells were resuspended in the respective culture medium and counted via the ViCell XR device. The desired cell number was split into a new cell culture flask with the respect volume of culture medium. Suspension cell lines were counted via the ViCell XR device and the respective cell number was centrifuge at 300 g for 5 min and resuspended in the desired volume of culture medium.

Table 1: Cell Lines Overview

Cell Line	Type	Medium	Seeding Density
A375	Adherent	DMEM high glucose + 10 % FCS	0.14-0.042 mio/mL
HS695T	Adherent	DMEM high glucose + 10 % FCS	0.112-0.14 mio/mL
SET2	Suspension	RPMI 1640 + 20 % FCS	0.7-1.12 mio/mL
T98G	Adherent	DMEM high glucose + 10 % FCS + 1 x MEM NEAA	0.028-0.056 mio/mL
UACC257	Adherent	RPMI 1640 + 15 % FCS	0.042-0.07 mio/mL

3.2.1.2 CHO Cells

3.2.1.2.1 Routine Culture

CHO cells were cultured at 37 °C, 5 % CO_2, 70 % rH at 95 (flasks) or 145 (tubes) rotations per minute (rpm) and were passaged three times a week. Cells were counted with the ViCell XR device and seeded at 0.25 mio/mL for two days and at 0.1 mio/mL for three days. The desired cell number was directly transferred into a new culture tube or flasks when the needed volume was smaller than 3 ml or was centrifuged for 5 min at 300 g and resuspended into new medium when the volume was above that. Depending on the resistance status cells were either cultivated in ActiPro without G418 or with 1mg/mL G418. Cells with a culture volume under 20 mL were incubated in 50 mL cell culture tubes and cell cultures with larger volumes in respective Erlenmeyer flasks.

3.2.1.2.2 Single Cell Culture

Single cells after single cell sorts were cultured in 100 µL CD-CHO with 1:20 InstiGRO CHOPLUS and were incubated for 10-14 days without shaking in a 96-Well flat bottom plate with a gas permeable adhesive film at 37 °C, 5 % CO_2, and 80 % rH. Monoclonal cultures were then expanded in 1-2 mL ActiPro with 1 mg/mL G418 in culture tubes at 37 °C, 5 % CO_2, 70 % rH and were treated as routine culture afterwards.

3.2.2 Peripheral Blood Mononuclear Cells (PBMCs)

3.2.2.1 Isolation and Freezing

Leukaphereses from healthy HLA-A*02:01 positive donors were obtained from the Deutsches Rotes Kreuz Mannheim for the isolation of PBMCs via density gradient separation. The leukapheresis product was diluted at a 1:1 ratio with PBS and carefully layered over 15 mL Pancoll. The samples were centrifuged at 800 g at room temperature (RT) for 20 min without brake. The formed PBMC layer was carefully transferred into a new 50 mL tube and washed once with PBS by centrifugation at 300 g at RT for 10 min. The supernatant was discarded, the pellet resuspended and pooled in PBS with 1 % HSA. The cells were counted with the ViCell™ XR device. The cells were centrifuged again and resuspended in the appropriate volume of medium D.

$$Medium\ D/E = \frac{Total\ cell\ count}{Frozen\ cell\ concentration\ [x10e6/mL]} x2$$

The calculated volume of Medium E was added dropwise while swirling the tube. The cell suspension was transferred into 2 mL cryotubes, put into a CellCool FTS30 container, and stored in a -80 °C freezer for at least 3 days before transferring the cells into liquid nitrogen storage.

3.2.2.2 Thawing

Cryotubes were thawed in a 37 °C water bath until only a small lump of ice remained. The cells were resuspended in CTL Wash with 0.1 % Glutamine and 50 U/mL Benzonase and centrifuged at 300 g at RT for 10 min. Afterwards cells were resuspended in T cell medium (TCM) with 10 U IL-2 and counted via the ViCell™ XR device. Cells were adjusted to a density of 5 mio/mL and transferred into a cell culture flask followed by incubation over night at 37 °C, 5 % CO_2, and 80 % rH.

3.2.3 Co-culture

When using adherent target cells, these were plated one day before co-culture start. Therefore, the target cells were harvested by discarding the medium, rinsing the flask with PBS and adding Accutase. The cells were incubated at 37 °C until they detached from the flask. The reaction was stopped by adding culture medium with subsequent centrifugation at 300 g for 5 min. Hereafter, the supernatant was discarded, cells were resuspended in culture medium, and counted using the ViCell™ XR. The cell density was adjusted to 0.1 mio/mL and 100 µL was added to each well of a 96-Well flat bottom plate according to the experimental setup. The plates were put on an orbital shaker for 30 sec at 450 rpm to evenly distribute the cells in the well. The plates were incubated over night at 37 °C, 5 % CO_2, and 80 % rH. At the same day the effector cells (PBMCs) were thawn as described above in the section *PBMC – Thawing* (3.2.2.2). The next day the medium from the adherent target cell line was removed and 50 µL/well LDH-AM with 10 U/mL Interleukin-2 (IL-2) was added. When working with suspension cells, they were harvested at 300 g for 5 min. The supernatant was discarded and cells were resuspended in LDH-AM with 10 U/mL IL-2. The cell density was determined using the ViCell™ XR and adjusted to 0.2 mio/mL to apply 10 000 target cells per well when adding

50 µl of the cell suspension to each well of a 96-Well round bottom plate according to the plate setup (Figure 8). Hereafter, serial dilutions of the TCER® molecules were performed in LDH-AM with 10 U/mL IL-2 with the threefold of the starting concentration, since it was diluted 1:3 with effector and target cells. 50 µL of each dilution was added to the respective well of the 96-Well plate according to the plate set-up. The control wells were all filled up with LDH-AM with 10 U/mL IL-2 to reach a final volume of 150 µL after adding the effector cells. The effector cells were transferred into a 50 mL tube and centrifuged at 300 g for 5 min. The supernatant was discarded and the cells were resuspended in LDH-AM with 10 U/mL IL-2. Cells were counted using a ViCell™ XR and the density was adjusted to 2 mio/mL to apply 100 000 effector cells in each well when pipetting 50 µL of the cell suspension into each well according to the plate setup.

3.2.4 Lactatdehydrogenase (LDH)-Release Assay

The LDH-release assay was performed using the CytoTox 96® non-radioactive cytotoxicity assay kit. After performing the co-culture 15 µL of the 10x lysis solution was added to the maximum LDH release (Target cells + Lysis) and the volume correction control (Medium + Lysis) (Figure 8). The plates were incubated for 30 sec at 450 rpm on an orbital shaker and spun down for 1 min at 300 g. The plates were put in an incubator for 48 h at 37 °C, 5 % CO_2, and 80 % rH. All conditions were plated as triplicates.

	1	2	3	4	5	6	7	8	9	10	11	12
A	PBS			PBMCs (Effector spontaneous release)			Medium (Medium background control)			Medium + Lysis (Volume correction control)		
B	Target cell line + PBMCs + TCER 1						Target cell line + PBMCs + TCER 2					
C	10 nM	1 nM	100 pM	10 pM	1 pM	0.1 pM	10 nM	1 nM	100 pM	10 pM	1 pM	0.1 pM
D												
E	Target cell line + PBMCs + TCER 3						Target cell line + PBMCs + TCER 4					
F	10 nM	1 nM	100 pM	10 pM	1 pM	0.1 pM	10 nM	1 nM	100 pM	10 pM	1 pM	0.1 pM
G												
H	PBS			Target cells (Target spontaneous release)			Target cells + PBMCs (Negative control)			Target cells + Lysis (Maximum release)		

Figure 8: Plate layout for the LDH release assay. Target cell line and PBMCs were inserted into the respective wells of a 96- Well flat bottom plate. TCER® molecules were assessed as triplicates in serial dilutions from 10 nM – 0.1 pM. Lysis solution was added to the labelled wells to measure the maximum of LDH release of the target cells.

On the day of the readout the assay buffer was thawn in a water bath at 37 °C 1-2 h before harvesting of the supernatant. Subsequently the substrate mix and the assay buffer were brought to RT protected from light. Cells were centrifuged at 300 g for 4 min and 50 µL supernatant was transferred into a new 96-Well flat bottom plate. Now the assay buffer and the substrate mix were reconstituted and 50 µL of the reagent was added per well. The plate was incubated for 30 min at RT in the dark and 50 µL stop solution was added after the incubation period. The absorbance was measured within 1 h at 490 nm and 650 nm in a SpectraMax i3x. The cytotoxicity (%) was calculated as followed and X was defined as:

$X = \Delta A490 - 650$:

a) $Xcorr = X - Mean\ X\ (Medium\ Background\ Control)$

b) $X\ (Max\ release) = Mean\ X\ (Max\ release) - Mean\ X\ (Volume\ correction\ control)$

c) $\%\ Cytotoxicity = \frac{Xcorr - Mean\ X\ (Effector\ sponanteous) - Mean\ X\ (Target\ spontaneous)}{X\ (Max\ release) - Mean\ X\ (Target\ spontaneous)} * 100$

3.2.5 Activation Assay

Activation of different cell populations after co-culture was detected using the following staining panel: CD3-PE/Cy7 (1:200), CD4-FITC (1:20), CD8-APC/Cy7 (1:50), CD25-PE (1:25), CD56-BV421 (1:50), CD69-APC (1:50). Dead cells excluded from the analysis by staining with Fixable Viabilit Dye eFlour™ 506 (1:100). Cells were washed with MACSQuant running buffer between the staining steps. Staining was performed 20 min in the dark at 4 °C shaking (450 rpm) for live/dead and 30 min in the dark at 4 °C shaking for the antibody mix. The read out was performed on a MACSQuantX device.

3.2.6 Cytokine-release Assay

Cytokine release assays were performed using the MACSPlex cytotoxicity T/NK cell kit following the manufacture's instruction. Analysis was performed using the express mode in the MACSQuantify Software (version 2.13.2). OKT CD3 antibody and a CD28 antibody were used for positive controls. The measurement was performed via a MACSQuantX device.

3.2.7 Flow Cytometry

3.2.7.1 Staining for Analyses

All steps were performed with chilled reagents and buffers. Incubation and centrifugation were done at 4 °C and in the dark. A least 1×10^5 cells were pelleted by centrifugation at 300 g for 3 min. Analysis were performed in a 96-Well round bottom plate. Cells were washed with FACS Buffer (PBS, 1 % BSA, 2 mM EDTA) and centrifuged again. The applied staining solution and the following handling depends on the desired analysis method. Detection of monomer binding was performed by resuspending the cells in 50 µL staining solution containing biotinylated PRAME pHLA complexes and incubating them for 30 min at 4 °C in the dark. After the incubation time cells were washed twice and resuspended in 50 µL of a second staining solution containing streptavidin coupled fluorescent dyes. In order to detect tetramer binding cells were resuspended in 50 µL staining solution containing 10 nM of fluorescently labelled pHLA tetramers. For the detection of the expression level an anti-Vβ5.1-APC antibody was used. After the incubation cells were washed once and resuspended in 70 µL FACS Buffer and binding was measured using a Sony Spectral Analyzer. Dead cells and doublets were excluded from the measurement by gating.

3.2.7.2 Sorting after RMCE

All steps were performed with chilled reagents and buffers under a laminar flow hood. Incubation and centrifugation were done at 4 °C and in the dark. In order to enrich cells with a correctly exchanged locus, they were sorted regarding the expression of the GOI in the tagged locus. For the detection of fluorescent proteins like red fluorescent protein (RFP) or green fluorescent protein (GFP) cells were washed only once with FACS Buffer and then directly applied to sorting. Cells expressing a non-fluorescent protein from the tagged locus were stained with biotinylated pHLA monomers and subsequently with fluorescent coupled streptavidin for 30 min in the dark at 4 °C. Cells were washed twice between the first and the second staining solution by centrifugation and resuspended in FACS Buffer. After the last staining step cells were resuspended in FACS Buffer to achieve a sorting rate of 200-2000 events per second at a moderate sample flow rate using Sony MA900 in targeted mode with a 100 μm sorting chip. Dead cells and doublets were excluded by gating. Cells were collected in a 15 mL tube and afterwards resuspended in the culture medium and incubated at 37 °C, 5 % CO_2, 145 rpm, and 70 % rH in a 50 mL tube with vented cap.

3.2.7.3 Library Sorting with Target and Off-target Staining

All steps were performed with chilled reagents and buffers under a laminar flow hood. Incubation and centrifugation were done at 4 °C and in the dark. Libraries including a GOI with a specificity for a pHLA complex were stained using a staining solution that contained the biotinylated pHLA complex along with off-target peptides as fluorescently labelled tetramers. Incubation was performed for 30 min in the dark at 4 °C. After the incubation cells were washed twice and stained with a streptavidin-coupled fluorescent dye. Cells were once again incubated for 30 min in the dark and washed afterwards. The resuspension volume was chosen the way that a flow rate of around 2000 events per second for bulk sorts or 200 events per second for single cell sorts (SCS) at a moderate sample flow rate was achieved. A Sony MA900 was used in targeted mode with a 100 μm sorting chip. Dead cells and doublets were excluded by gating.

3.2.8 Plasmid Preparation

3.2.8.1 Transformation

One Shot™ TOP10 electrocompetent *Escherichia coli* (*E.coli*) cells were transformed by electroporation according to the manufacturer's instruction. Single clones were picked and expanded for plasmid DNA isolation in LB broth containing 100 µg/mL Ampicillin.

3.2.8.2 Small Scale Plasmid DNA Isolation

In order to check for the correct plasmid DNA in single clones, each clone was expanded in 5 mL LB broth containing 100 µg/mL Ampicillin at 37 °C and 170 rpm for 7-12 h. Afterwards the plasmid DNA was isolated using the QIAspin® Miniprep Kit following the manufacturer's instruction. DNA concentration was estimated using a NanoDrop 8000 via absorbance measurements at 260 nm. The ratio$_{260/280}$ was used to estimate the purity of the sample. DNA was further analyzed via sequencing.

3.2.8.3 Large Scale Plasmid DNA Isolation

Plasmid DNA isolation was performed using the NucleoBond® Xtra Midi or Maxi EF Kit following the manufacturer's instructions. The obtained DNA was heated for 20 min at 95 °C and handled sterile afterwards. DNA concentration was measured using the NanoDrop 8000 via absorbance measurements at 260 nm. The ratio$_{260/280}$ was used to estimate the purity of the sample.

3.2.9 Sequencing

Samples for sequencing were send to MicroSynth Seqlab GmbH, Göttingen Germany. Primers for sequencing were synthesized and stored at MicroSynth.

3.2.10 Transfection of CHO Cells

CHO cells were cultured in ActiPro Medium and were splitted the day before the transfection to a density of 1.5 mio/mL and cultured as described for the *Routine Culture* (3.2.1.2.1). At the day of the transfection the required cell number was harvested and washed once with the MaxCyte® Electroporation Buffer. Afterwards cells were resuspended in the required volume of Electroporation Buffer to obtain a cell density of 200 mio/mL.

3.2.10.1 Transient Transfection

For transient transfection both plasmids encoding each one of the two TCER® chains were added (1.5 µg/mio) to the cells and mixed. The mixture was transferred into an OC-400 electroporation cuvette and electroporated using the CHO program of the STx Maxcyte system. Afterwards cells pulsed with the same DNA was pooled and rested in a 25 cm^2 cell culture flasks at 37 °C, 70 % rH, and 5 % CO_2 for 40 min. After resting the cells were transferred into shake flasks with a density of 4 mio/mL and incubated for 24 h. The next day a temperature shift from 37 °C to 32 °C was performed and Sodium butyrate was added to the culture to a final concentration of 1 mM. The cells were fed on day 4, 6, and 8 with Cell Boost 7A and 7B, 5 % and 0.5 %, respectively. Cells were harvested either when the cell viability was below 70 % or after day 11. The supernatant was filtered using the SartoClear Dynamics® Lab V. Afterwards, Sodium azide was added to a final concentration of 0.1 %. The supernatant was stored at 4 °C until it was purified using a Äkta Pure 25.

3.2.10.2 Stable Transfection

For stable transfection the plasmid DNA was linearized and added at a final concentration of 1 µg/mio cells to the CHO cells. The DNA/cell mixture was transferred into an electroporation cuvette and pulsed using the CHO-2 program of the STx/ATx MaxCyte system. After the electroporation the cells were rested for 40 min at 37 °C, 70 % rH, and 5 % CO_2 without shaking. Next, the cells were transferred into ActiPro™ at a density of 4 mio/mL and incubated for 24 h at 37 °C, 70 % rH, and 5 % CO_2 at 95 rpm. The next, day cells were transferred into culture medium with selection pressure (1mg/mL G418) and expanded.

3.2.10.3 RMCE

For RMCE the donor vector was added to the desired cell number to achieve a final concentration of 1 µg/mio cells. The RNA encoding the recombinase (Miltenyi Biotec) was added with a final concentration of 4 µg/mio cells. The cell/DNA/RNA mixture was transferred into an electroporation cuvette and pulsed using the CHO-2 program of the STx/ATx MaxCyte system. Afterwards, cells were rested for 40 min at 37 °C, 70 % rH, and 5 % CO_2 without shaking. The cells were then transferred into a shake flask with a cell density of 4 mio/mL in ActiPro™ Medium. On the next day, the cells were centrifuged and resuspended with a cell density of 0.25 mio/mL or 0.1 mio/mL into ActiPro™ containing 1 mg/mL G418 for 2 or 3 days,

respectively. After expansion cells were sorted or analyzed as described in *Sorting after RMCE* (3.2.7.2).

3.2.10.4 Stable Cell Line Generation

The aim was to obtain a stable CHO cell line expressing a GOI stably from a single copy locus. Therefore, a GFP encoding vector was added as linearized DNA. The stable transfection was performed as described in *Stable Transfection* (3.2.10.2). After cultivation for two weeks two rounds sorting the top 2 % of GFP expressing cells were performed. The top 2 % of the cells underwent a RMCE step exchanging GFP against RFP as described in *RMCE* (3.2.10.3). Cells were single cell sorted for RFP only expressing cells to increase the chance of having only cells expressing the GOI from a single copy landing pad. Cells expressing GFP or GFP and RFP were discarded. The single cells were expanded as described in *Single Cell Culture* (3.2.1.2.2). The monoclonal cell cultures were screened for high long-term RFP expression and selected clones were sent for Targeted Locus Amplification (TLA) analysis to Cergentis B.V. described in de Vree et al.[155]. Cells with multicopy integrations were discarded and a single copy clone with a reusable landing pad was expanded as the master cell line.

3.2.11 Protein Purification

Soluble proteins were purified via Tandem purification using an Äkta Pure 25 with a ProteinL and Size-Exclusion Column. Elution of protein-L bound proteins was performed at pH 2.8. Monomeric fractions were pooled and concentrated using an Amicon Ultra-15. The concentrated proteins were sterile filtered (0.22 µm) and the concentration was estimated using a NanoDrop 8000 using a specific extinction coefficient based on the primary amino acid sequence.

3.2.12 Biolayer Interferometry

The affinity of TCER® molecules for different pHLA complexes was measured on an Octet HTX system using kinetic or steady state binding analysis. All analytes or ligands were diluted to their final concentration in kinetics buffer (PBS, 0.1% BSA, 0.05% Tween-20). HIS1K biosensors with immobilized Penta-His were hydrated for at least 10 min in kinetics buffer before use. Loadings and measurements were performed in 384 tilted well plates with 60 µL

sample volume at a 3 mm sensor offset. Plate temperature was set to 30°C and shaker speed to 1000 rpm. To allow inter-step correction, baseline before association phases and the following dissociation phase were performed in the same well. All sensograms were analyzed using the Octet system software data analysis HT 12.0. Raw sensor data was aligned at the Y axis by adjusting the data to the end of the baseline step. Alignment of the start of the dissociation to the end of the association phase was done via inter-step correction. Savitzky-Golay filtering was applied to smooth the obtained data. The resulting sensograms were fitted using a 1:1 Langmuir kinetics binding model.

3.2.13 DNA Amplification

3.2.13.1 Genomic PCR

To check for a correct exchange of the landing pad genomic PCR was performed using the Phire Tissue Direct PCR Master Mix following the instructions for the Dilution & Storage Protocol of the manufacturer. Primers were designed so that one of them binds in the adjacent genomic part and one in the GOI in the landing pad. The following two primer pairs were tested: A03_head_forw and RFP_TLA_rev/HiAff#1_TLA_rev as well as A03_tail_rev and RFP_TLA_forw/HiAff#1_TLA_forw. The primer for the GOI was adapted for either the fluorescent expression marker (RFP) or the introduced TCER®molecule. The obtained product was analyzed via Gel Electrophoresis.

The clonal DNA sequence of the TCER® library was obtained with the following primers for the TCR alpha chain JD061 and JD065 and JD057 and JD059 for the TCR beta chain. The obtained products were sent for sequencing.

3.2.13.2 Plasmid PCR

For the amplification of plasmid DNA templates, the 2x MasterMix of the Phusion® High-Fidelity Polymerase was used following the instructions of the manufacturer.

3.2.14 Cloning

3.2.14.1 Cloning Strategy RFP_pJD1 and GFP_pJD1

The sequences of RFP and GFP were amplified with the primer pair RFP_forw/RFP_rev. and GFP_forw and GFP_rev, respectively. The amplicons and the vector pJD1 were digested with NheI and EcoRI and cloned into pJD1 resulting in RFP_pJD1 and GFP_pJD1.

3.2.14.2 Cloning Strategy Flpe_pMH1 and Cre_pMH1

The vectors expressing the recombinases Flpe and Cre were generated by the amplification of the templates ordered from GenScript using the primer pairs Flpe_forw_NheI/Flpe_rev_EcoRI and Cre_forw_NheI/Cre_rev_EcoRI, respectively. The amplicons and pMH1 were digested with NheI and EcoRI and inserted into pMH1 resulting in Flpe_pMH1 and Cre_pMH1.

3.2.15 Vector Linearization

The vectors containing the landing pad for stable integration were linearized in the AmpR sequence using the PvuI enzyme. Cre_pMH1 or Flpe_pMH1 were linearized using AvrII. After incubation of the reaction for 8 h the DNA was precipitated with NaOAc (1/10 of the volume) and mixed thoroughly. Then cold ethanol absolute (2.5 x of the volume) was added and mixed carefully. The mixture was incubated for at least 2 h at -20 °C. The DNA was centrifuge at 4 °C for at least 30 min at 16 000 g. The supernatant was discarded and the DNA pellet was washed twice with 70 % ethanol by centrifugation. Afterwards, the pellet was dried for 10-15 min and dissolve in H_2O.

3.2.16 Gel Electrophoresis and Extraction

For the separation of DNA products, a 1 % Agarose gel was produced in 1 x TAE Buffer. 1 µL peqGREEN was added per 100 mL gel volume. When the gel was cooled down, samples were loaded and the DNA was separated applying an electric field so that the negatively charged DNA move through the matrix and was separated by size. The size was estimated by the usage of a DNA ladder. The gel was examined in a ChemiDoc™ XRS+ under UV-light. If a gel extraction and following clean-up was to be performed the needed bands were cut out and collected in a 1.5 mL Eppendorf tube. For the clean-up of DNA fragments from gel electrophoresis the NucleoSpin® Gel and PCR Clean-up Kit was used following the

manufacturer's instructions. After the clean-up the DNA concentration was estimated by absorbance measurement at 260 nm using a NanoDrop 8000. The ratio$_{260/280}$ was used to estimate the purity of the DNA samples.

3.2.17 DNA Concentration Measurement

For the absorbance measurement at 260 nm a NanoDrop 8000 was used applying the following formula for estimation:

Concentration (µg/mL) = (A$_{260}$ reading-A$_{320}$ reading) x dilution factor x 50 µg/mL

3.2.18 HLA Complex Production

3.2.18.1 Inclusion Body Production, Purification, and Refolding

HLA molecules were generated as inclusion bodies in *E.coli* and purified as described in Garboczi *et al.*[156]. The refolding reaction was also performed as described by Garboczi *et al.* with minor changes. The HLA chains and the β$_2$m molecule diluted in HLA injection buffer were transferred into HLA refolding buffer via syringe usage. The PRAME peptide or a UV light sensitive peptide was added a final concentration of 30 µM. The refolding reactions were stirred at 10 °C for 2-4 days and concentrated via stirred ultrafiltration cells with a 30 kDa membrane. The obtained concentrate was further purified via SEC chromatography with TBSA running buffer using a HiLoad 26/600 75 pg column on an AKTAprime plus system. The pooled monomere fractions were complimented with protease inhibitor PSMF, leupeptin, and pepstatin and adjusted to a final concentration of 2000 µg/mL via an Amicon Ultra-15 centrifugation unit and biotinylted via a BirA biotin-protein ligase overnight at 27°C following the manurfacturer's instruction. The pHLA was gel-filtered again before concentrated and aliquoted.

3.2.18.2 Peptides Synthesis

All peptides used in this work were produced in house using standard Fmoc chemistry via a Syro II peptide synthesizer. Obtained peptides were subsequently applied to HPLC analysis. UV-light sensitive peptides were generated with a 2-nitrophenylamino acid residue as part of

a light-sensitive building block. Peptides were solved in 10 % DMSO + 0.5 % TFA at a final concentration of 10 mg/mL before use and stored at -20 °C until further usage.

3.2.18.3 UV-Exchange and Tetramerization

The exchange of UV-light-cleavable peptides was performed as described by Rodenko and colleagues[157]. Desired peptides were mixed with a biotinylated UV-light-sensitive pHLA complex at a molar ratio of 100:1 and exposed to UV-light (366 nm) for 1 h.

3.2.18.4 Tetramerization of Monomers

Biotinylated pHLA monomers were tetramerized with different fluorochrome-coupled streptavidin. Streptavidin-conjungate and monomers were mixed in a 1:4 ratio. The monomer streptavidin mixture was incubated at 4 °C and 1500 rpm in a thermomixer C for 30 min in the dark. The total volume of streptavidin coupled fluorochrome was added in three steps every 30 min. After the final incubation Biotin is added to reach a final concentration of 25 μM to saturate possibly unconjugated streptavidin binding sites.

3.2.19 Statistical Analysis

All *in vitro* values are shown as mean with the corresponding standard deviation. EC_{50} values were calculated via four parameter logistic sigmoidal non-linear regression. Subsequent significance analyses requested for some results could not be performed due to lack of access to Immatics' proprietary data.

3.2.20 Software

3.2.20.1 Statistical Analysis and Data Plotting

Data plotting was performed using GraphPad Prism (Version 9.2.0). Flow Cytometry Data

Flow cytometry data was analyzed using the FlowJo software (Version 10.4 and 10.7).

3.2.20.2 Sequence Analysis

Sequence analysis and construct planning was performed via the Geneious Prime software (Version 2020.2.5).

4 Results

4.1 Clonal Outgrowth of Single Cell-Sorted CHO cells

The ability to grow CHO cells derived from a single cell sorting process is a prerequisite for establishing a mammalian cell display technology. To identify optimized conditions for growth of single CHO cells different media and media supplements were tested for CHO culture.

As shown in Figure 9, usage of different media compositions led to larger differences in the clonal outgrowth of single cell-sorted CHO cells. From the four media tested, the best performance was observed for CD-CHO medium leading to an outgrowth rate ranging from 34.4 – 66.7 % dependent on the applied supplement. Among the 3 tested supplements, the InstiGROPLUS showed the best performance in combination with 3 out of the 4 tested media while no outgrowth was observed without media supplementation. CD-CHO cell medium with InstiGROPLUS supplement resulted in the highest outgrowth rate of 66.7 %, which is an excellent result given the technical difficulty of growing single CHO cells. This media composition was therefore used throughout this study for clonal outgrowth of CHO cells.
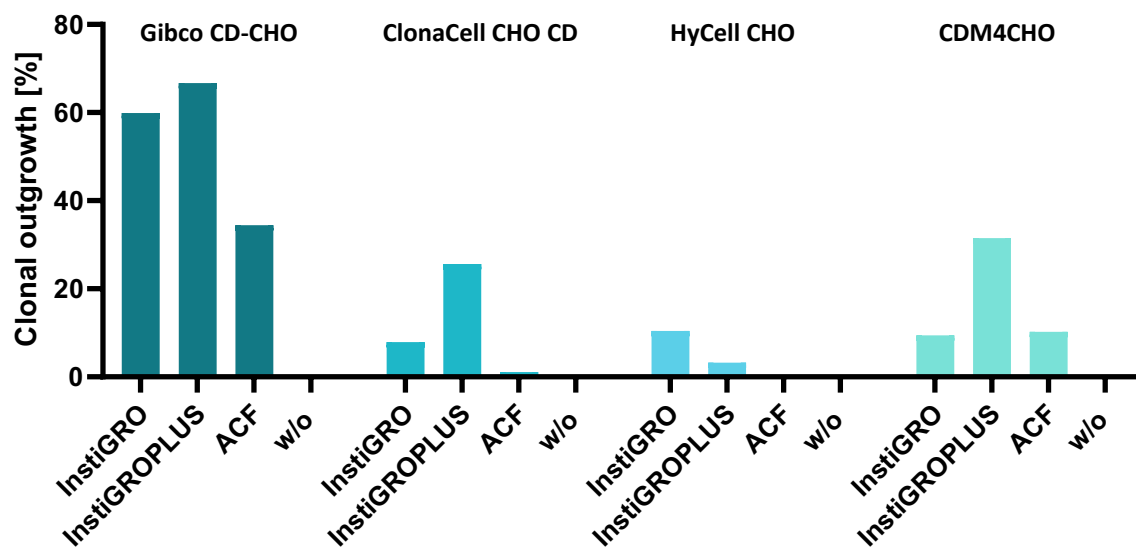

Figure 9: Clonal outgrowth after single cell sorting depending on culture media. CHO cells were sorted into 100 μL of different culture media and the percentage of outgrowing clones was obtained after 10 -14 days of incubation. n=1

4.2 Generation of CHO Cell Line with 1ˢᵗ Generation Landing Pad

4.2.1 Vector Design

As depicted in Figure 10 A-C, two vectors were designed for the generation of a landing pad-contained CHO cell line, both encoding a neomycin resistance and FRT-flanked fluorescence markers GFP (pJD1_GFP) or RFP (pJD1_RFP). The vector pJD1_GFP was used for stable integration of the landing pad into the CHO genome and contained a human cytomegalovirus (hCMV) promotor driven GFP cassette flanked by FRT and FRT F3 3' and 5', respectively. The design of the RMCE donor vector pJD1_RFP was identical to pJD1_GFP with exception of using an RFP fluorescence marker instead of GFP. RMCE of the GFP to RFP cassette was induced by addition of Flp recombinase (see process in Figure 10 C).
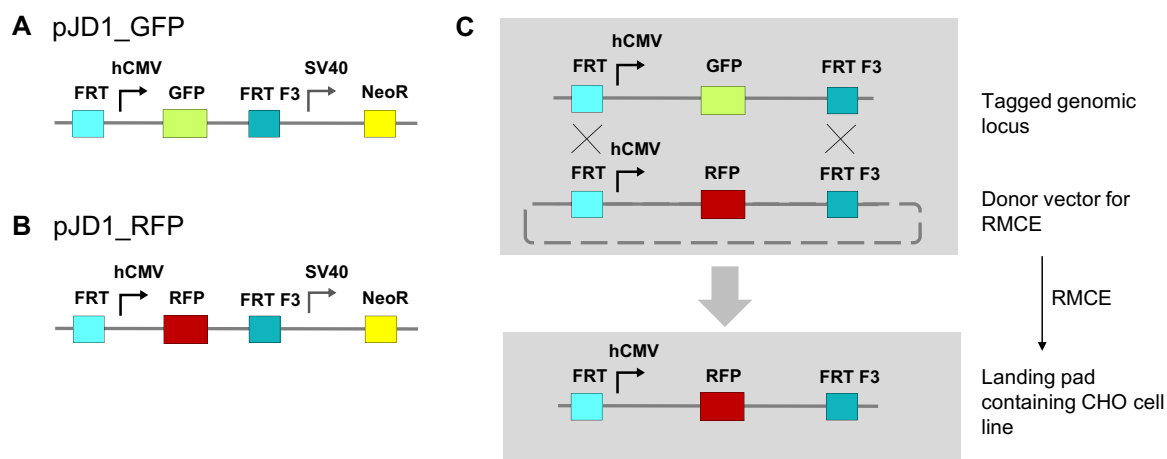
Figure 10: Vector design and process overview for the generation of a landing pad containing CHO cell line. A) pJD1_GFP contains a FRT recombination site (light blue), a hCMV promotor for the expression of the *gfp* gene (green), a FRT F3 site (petrol), and a SV40 promotor for the expression of the Neomycin resistance (yellow). B) pJD1_RFP contains a FRT recombination site (light blue), a hCMV promotor for the expression of the *rfp* gene (red), a FRT F3 site (petrol), and a SV40 promotor for the expression of the Neomycin resistance (yellow). C) During the RMCE process the FRT flanked cassette in the tagged genomic locus is exchanged against a FRT flanked cassette of a donor vector. The exchange is executed by the Flp recombinase. After the exchange RFP is expressed from the genomic locus.

4.2.2 Selection of High GFP Expressing CHO Clones

After electroporation of CHO cells with the GFP encoding vector pJD1_GFP and subsequent culturing for 14 days under selection pressure with G418, about 2 % of cells with the highest GFP expression were sorted (Figure 11). This led to an enrichment of CHO cells expressing GFP at a high level as indicated by the increase in the mean fluorescence intensity (Figure 11 A). Highest GFP expression was observed after two sorting rounds (Figure 11 B).
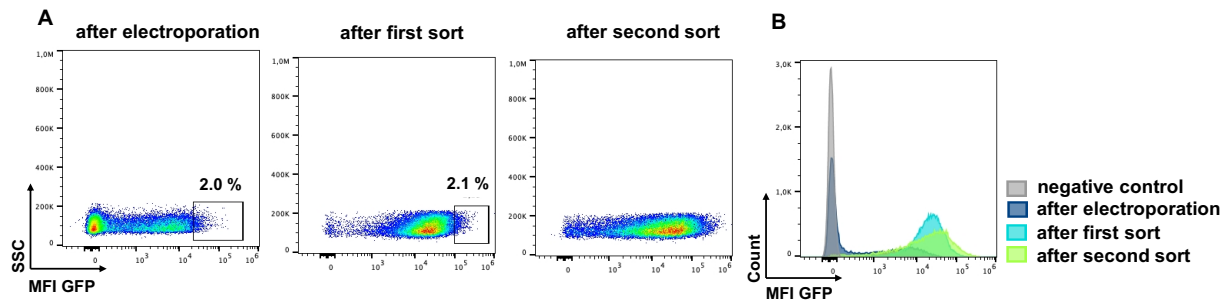
Figure 11: Flow cytometric analysis of CHO cells during landing pad integration. A) Gating strategy of the enrichment of high expressing GFP cells. The top 2 % of the GFP expressing cells were sorted two times. B) The histogram plot indicates the GFP expression levels of the different sorting rounds in comparison to non-transfected CHO cells (negative control).

4.2.3 Exchange of GFP and RFP Cassettes

CHO cells with stable GFP expression were subjected to the first RMCE step exchanging GFP with RFP via transfection with the donor vector and addition of Flp recombinase (Figure 12). RFP-positive cells could be detected after RMCE reactions with DNA-encoded Flp as well as RNA-encoded Flp. The exchange with Flp DNA resulted in 2.9 % exchange rate (GFP-negative/RFP-positive) cells while the reaction with Flp RNA led to a higher rate of 5.4 %. As depicted in Figure 12 C, a small RFP-positive CHO cell population of 0.3 % could also be detected in the absence of Flp recombinase indicating some level of random integration of the linearized donor vector into the CHO genome.
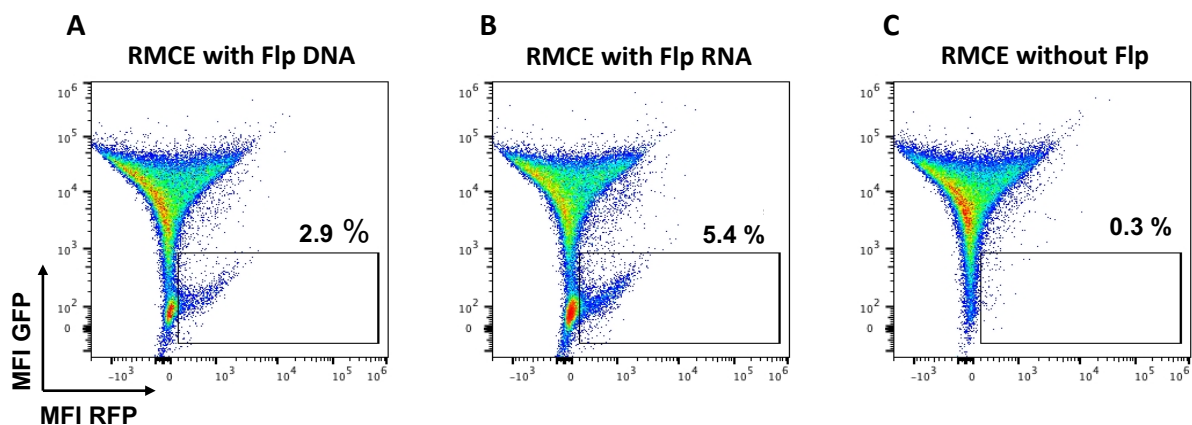
Figure 12: Landing pad exchange of 1st generation system exchanging GFP with RFP. A) RMCE reaction with DNA-encoded Flp recombinase. B) RMCE reaction with RNA-encoded Flp recombinase C) RMCE reaction without adding Flp recombinase.

4.2.4 Exchange of RFP with TCER® Cassettes

In a next step, a second RMCE reaction was performed to exchange the RFP cassette with a cassette encoding for a bispecific TCER® molecule targeting an HLA-A*02-binding peptide derived from the tumor-specific antigen PRAME. The TCER® molecule with about 100 kDa size is composed of two polypeptide chains as depicted in Figure 13. For visualization of the exchange, the CHO cells were incubated with biotinylated PRAME pHLA monomer and stained with Streptavidin-APC. As shown in Figure 14, about 0.5 % TCER®-expressing CHO cells were detected when Flp was supplied as DNA while this proportion increased to 2.5 % when RNA-encoded Flp was added. Again, as observed for the exchange of the RFP cassette, about 0.4 % of TCER®-positive CHO cells were detected in absence of Flp recombinase, which can only be explained by a background level of random integration into the CHO cell genome. Overall, the presented results suggest that the RFP locus can be used for a repeated exchange step with an even larger insert of ~6900 bp encoding a functional TCER® molecule. Further the results support that an RNA-based Flp application seems the most favorable option for an efficient exchange.
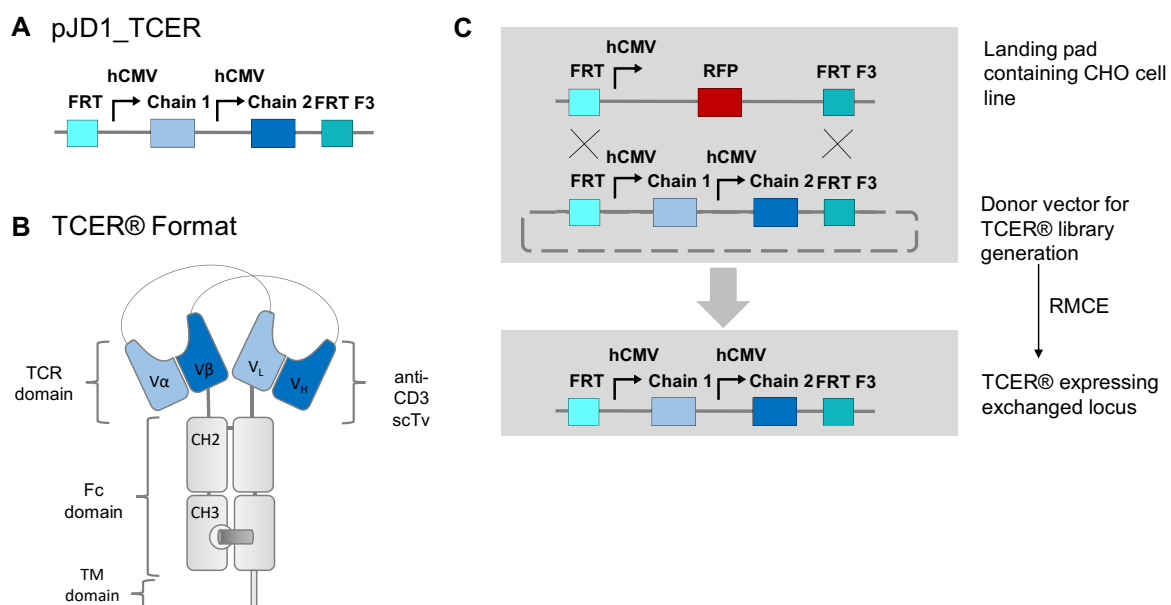
Figure 13: Vector design and process overview for the generation of RMCE-based TCER® library. A) pJD1_TCER contains a FRT recombination site (light blue), a hCMV-driven TCER chain 1 (light blue), a hCMV-driven TCER® chain 2 including a TM domain (dark blue), and a FRT F3 site (petrol). B) Structure of the TCER® molecule when expressed on the CHO surface with knob-into-hole mutations[23,158] (for details see chapter 4.4) to enforce heterodimerization of TCER chain 1 and 2. C) During the RMCE process the FRT flanked RFP-encoding cassette in the tagged genomic locus is exchanged against a FRT flanked TCER®-encoding cassette of the different pJD1_TCER vectors encoding all library sequences. The exchange is executed by the Flp recombinase.
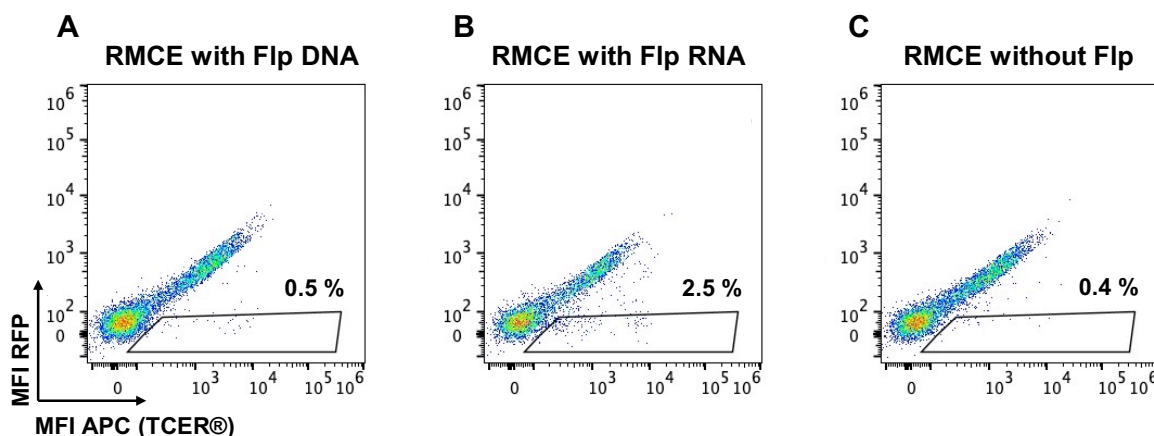
Figure 14: Landing pad exchange replacing RFP with a PRAME pHLA binding TCER®. A) RMCE was performed with DNA-encoded Flp recombinase. B) RMCE was conducted with RNA-encoded Flp recombinase. C) RMCE reaction without Flp recombinase. The y-axis shows the mean fluorescent intensity (MFI) of RFP and the x-axis the MFI of APC of the stained TCER® molecules. The shown gates indicate the sorted cells.

4.2.5 Landing Pad Validation by Targeted Locus Amplification

TLA analysis was performed to identify an RFP- or TCER®-expressing CHO clone whose expression is driven by a single copy cassette integration at a defined genomic locus. Therefore, eight CHO clones from different RMCE steps and different expression levels were analyzed regarding their landing pad integration side and copy number. Four RFP-expressing clones (A03 and G06 with high RFP expression; A02 and A06 with low RFP expression) were obtained from the GFP/RFP exchange mediated by RNA-encoded Flp (Figure 15 A). Additionally, four TCER®-expressing clones (E06 and D11 with high TCER® expression; C06 and A11 with low TCER® expression) were obtained from the RFP/TCER® exchange mediated by RNA-encoded Flp and in absence of Flp (Figure 15 B). The different expression levels of the selected clones could be related to expression from different loci and/or copy numbers, which was therefore investigated by TLA analysis.
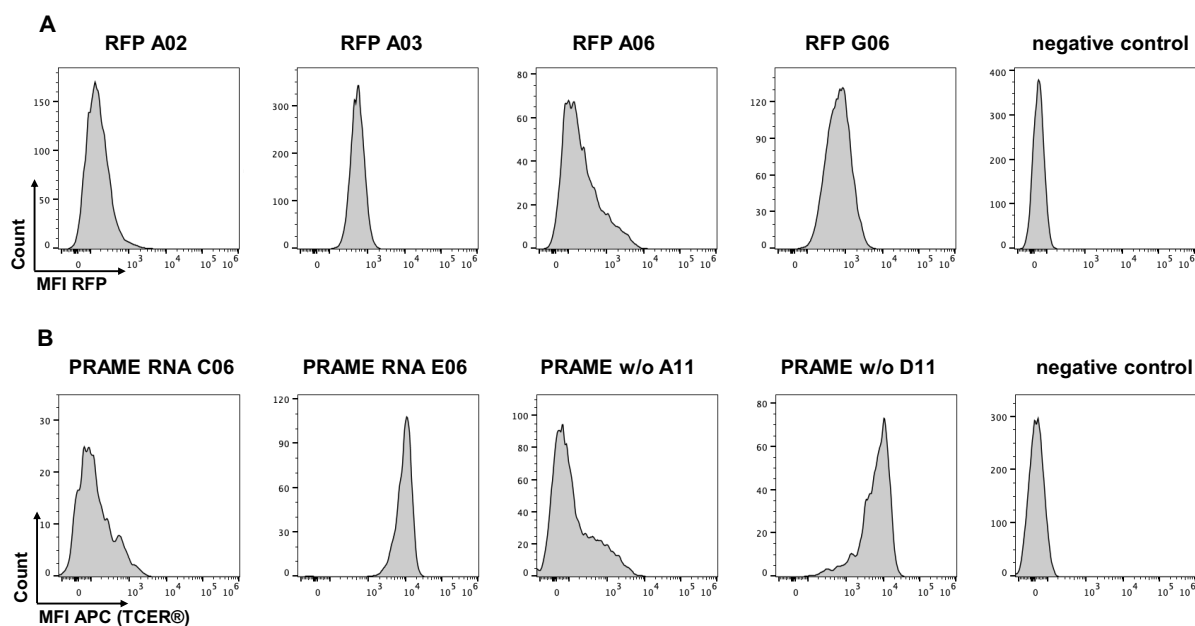
Figure 15: Histograms of selected single cell clones for TLA analysis. A) Clones RFP A02, RFP A03, RFP A06, and RFP G06 were obtained from a SCS after the first RMCE. Non-transfected CHO cells served as a negative control. B) Clones PRAME RNA C06, PRAME RNA E06 were sorted from a second RMCE step exchanging RFP against a PRAME pHLA specific TCER®. Clones PRAME w/o C06, PRAME w/o D11 were sorted from a population of PRAME pHLA binding cells after exchange of RFP without the addition of Flp. Non-transfected cells served as negative control.

TLA analysis revealed that RPF-expressing clones A02, A03, and A06 had only one integration site while clone G06 harbored three integration sites. Further, only the high RFP-expressing clone A03 contained a single copy integration of RFP while the remaining clones had multiple RFP integrations. Among the TCER®-expressing clones, the high expressing clones E06 and D11 contained a single copy integration at a single integration site while the other two clones had multiple copies. From the 3 high expressing, single site and single copy clones A03, E06, and D11, only the RFP_A03 clone presented a breakpoint in the *ampicillin resistance* gene of the vector backbone in line with the anticipated linearization site of the first GFP containing landing pad vector. Therefore, clone RFP_A03 was selected as an interesting candidate for the master cell line generation and was further analyzed regarding stable long-term expression and reusability of the landing pad.

Table 2: TLA results of selected clones (1st Generation)

Name	No. of Integration site	Copy Number	Breakpoint
RFP A02	1	10-15	NeoR; ColE1 Ori
RFP A03	1	1	AmpR
RFP A06	1	90-140	PolyA Tail
RFP G06	3	4-22	AmpR
PRAME RNA C06	1	3-15	NeoR, hCMV
PRAME RNA E06	1	1	FRT site
PRAME w/o A11	1	35-60	TCER® C_H2 chain
PRAME w/o D11	1	1	ColE1 Ori

4.2.6 Stability of RFP Expression of RFP_A03 Clone

CHO clone RFP_A03 was further analyzed by flow cytometry to confirm long-term expression of RFP without any G418 selection pressure. During the long-term culture period of 135 days, RFP_A03 showed high and stable RFP expression for both, the expression level and the proportion of RFP-positive CHO cells (Figure 16) supporting the suitability of RFP_A03 for the landing pad-containing CHO cell line.
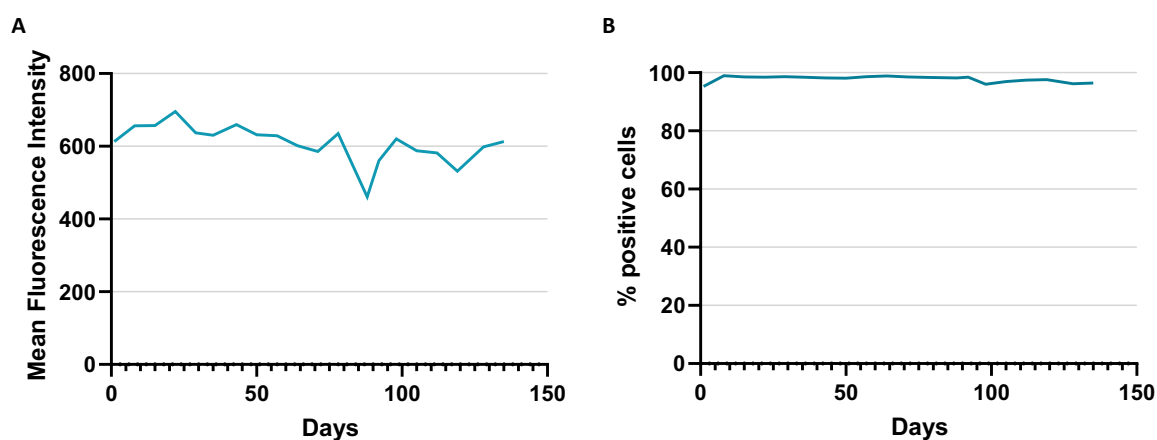
Figure 16: Results of the long-term analysis of RFP_A03. A) MFI values of flow cytometry-based analyses over 135 days. B) Frequent of parent values of the long-term monitoring of RFP_A03.

4.2.7 Molecular Confirmation of Targeted Integration Process

In a last step, a combined analysis using flow cytometry and PCR was performed to check if the tagged genomic locus can be targeted repeatedly and to confirm undirected background integration. To achieve this, GFP-expressing CHO clones were generated by RMCE using RFP-expressing clone A03 as starting point. 27 different GFP-expressing clones were generated via RMCE with RNA-encoded Flp recombinase via single-cell sorts and subsequent expansion. Also, different GFP-expressing cells from RMCE without Flp recombinase were single cell sorted but only one clone could be grown out of these cells. As shown in Figure 17 and Table 3, GFP expression could be confirmed for 26 out of 27 clones generated with RNA-encoded Flp recombinase and for the single clone generated without Flp recombinase. Using PCR analysis, a targeted integration of the GFP cassette could be confirmed for 23 out of the 26 GFP-positive clones generated with Flp recombinase RNA while three clones did not show the correct PCR band (Figure 18 and Table 3). As expected, the only GFP-expressing clone derived from RMCE process without Flp recombinase also did not show a correct PCR band supporting the concept of a given level of undirected integration of GFP from the donor vector in the CHO genome observed for the 1st generation landing pad CHO cell line.

A

B

C
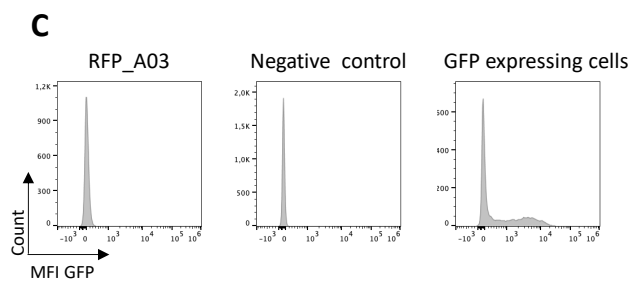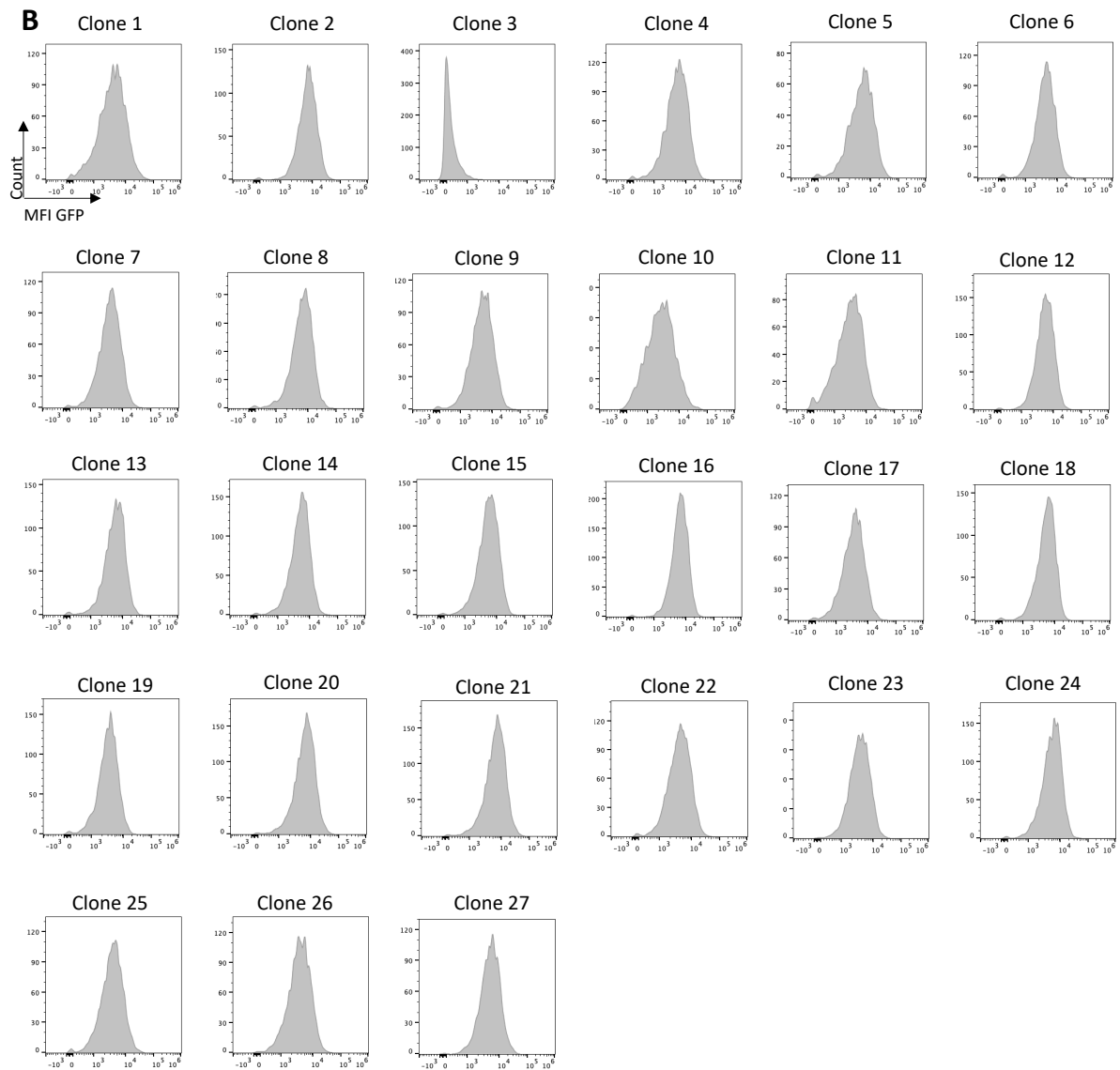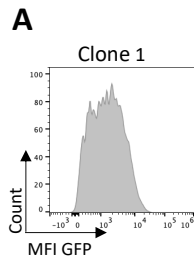
Figure 17: Histograms of GFP expressing clones. Flow cytometry-based analysis of GFP expressing cells after RMCE. A) Histogram of clone 1 from RMCE without Flp. B) Histograms of clone 1-27 from RMCE with Flp RNA. C) Histograms of control measurements. RFP_A03 expressed RFP from the tagged locus. Non-transfected CHO cells served as negative control. GFP expressing cells with GFP expressed from a different locus served as positive control.

A

B
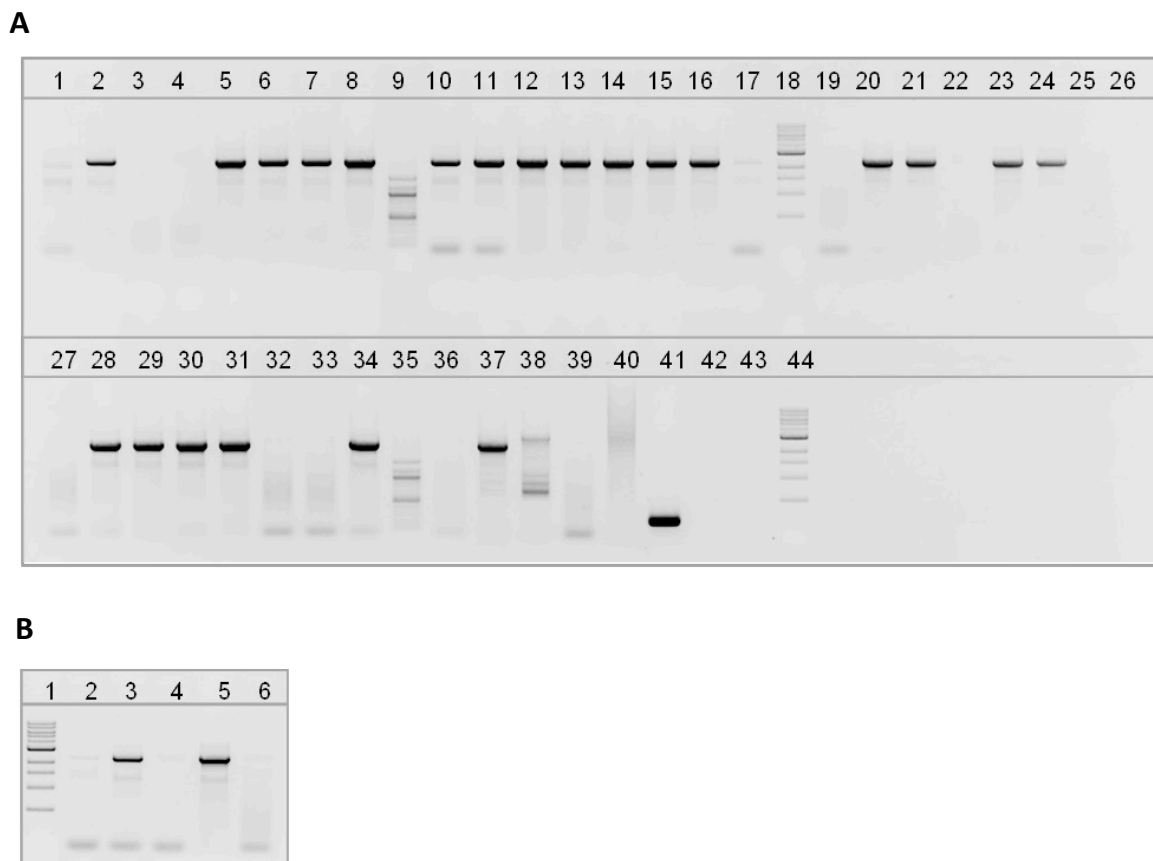
Figure 18: PCR amplification results of GFP expressing clones. The reaction amplifying the tagged locus with GFP resulted in a ~2300 bp amplicon. Lane 1: Clone 1 RMCE without Flp; Lane 2-8: clone 1-7 RMCE with Flp RNA; Lane 9: 100 bp DNA ladder; Lane 10-17: Clone 8-15 RMCE with Flp RNA; Lane 18: 1 kbp DNA ladder; Lane 19-24: Clone 16-21 RMCE with Flp RNA; Lane 25: empty; Lane 26: Clone 22 RMCE with Flp RNA; Lane 27: empty; Lane 28-31: Clone 23-26 RMCE with Flp RNA; Lane 32-33: empty; Lane 34: Clone 27 RMCE with Flp RNA; Lane 35: 100 bp DNA ladder; Lane 36: empty; Lane 37: RFP containing master cell line clone amplified with RFP specific primers; Lane 38: non-transfected CHO cells; Lane 39: cells expressing GFP from a different locus; Lane 40: negative control; Lane 41 positive control; Lane 42-43: empty; Lane 44; 1 kbp DNA ladder. B) Lane 1: 1 kb DNA ladder; Lane 2-6: Clone 2, 3, 16, 19, 23 RMCE with Flp RNA.

Table 3: Phenotypic and genotypic characteristics of different RMCE populations

Population	GFP expression	Correct PCR band
RMCE with Flp DNA	20/24 (83 %)	14/24 (58 %)
RMCE with Flp RNA	26/27 (96 %)	23/26 (89 %)
RMCE without Flp	1/1 (100 %)	0/1 (0 %)

4.3   Generation of CHO Cell Line with 2nd Generation Landing Pad

4.3.1   Vector Design

To avoid background signals from undirected integration the donor vector design was modified moving the FRT site downstream of the hCMV promotor and the SV40 promotor upstream of the FRT F3 site. This change should prevent the expression of the GOI if not correctly integrated into the landing pad since the donor vector does not contain a promotor for the GOI expression anymore.

A pJD4_GFP

B pJD5_RFP
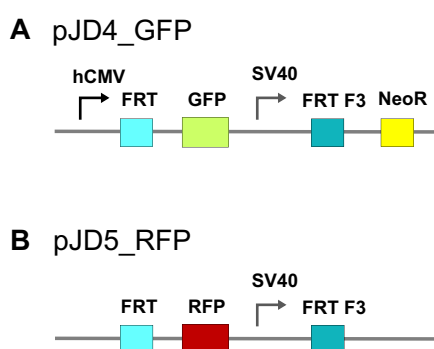
Figure 19: Schematic overview of the 2nd generation vector designs. A) pJD4_GFP contains a hCMV promotor driven expression of the *gfp* gene, a FRT site (light blue), a SV40 driven *Neomycin resistance* gene (yellow) expression, a FRT F3 site (petrol). B) pJD5_RFP contains a FRT site (light blue), the *rfp* gene, a SV40 promotor, and a FRT F3 site (petrol).

4.3.2   Selection of High GFP Expressing CHO Clones and RFP Cassette Exchange

Similar to the approach used to generate the 1st generation landing pad, flow cytometry assisted sorting was performed to sort about 2 % of high GFP expressing cells after applying G418 selection pressure for two weeks. Sorting of the highest GFP expressing cells resulted in an increase of the GFP expression level with the highest expression achieved after two sorting rounds (Figure 20). In a next step, the GFP cassette was exchanged to RFP by transfecting the cells with the RFP containing donor vector together with Flp recombinase encoded by DNA or RNA. As shown in Figure 21, about 1 % RFP positive CHO cells were detected with DNA-encoded Flp recombinase while this proportion increased to 3.9 % with RNA-encoded Flp. Notably, no RFP-positive CHO cells were detected in the RMCE reaction without Flp recombinase supporting that background signals from undirected integration events could successfully be suppressed with the 2nd generation landing pad approach.
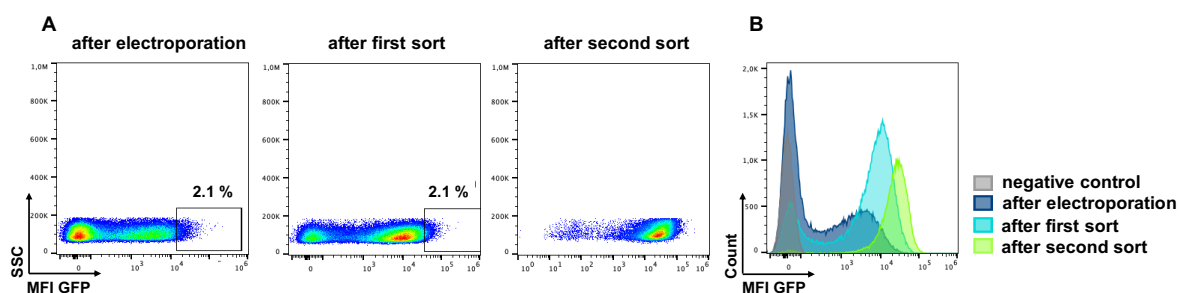
Figure 20: Flow cytometric analysis of CHO cells during landing pad integration. A) Gating strategy of the enrichment of high expressing GFP cells. About the top 2 % of the GFP expressing cells were sorted two times. B) The histogram plot indicates the GFP expression levels of the different sorting rounds in comparison to non-transfected CHO cells (negative control).
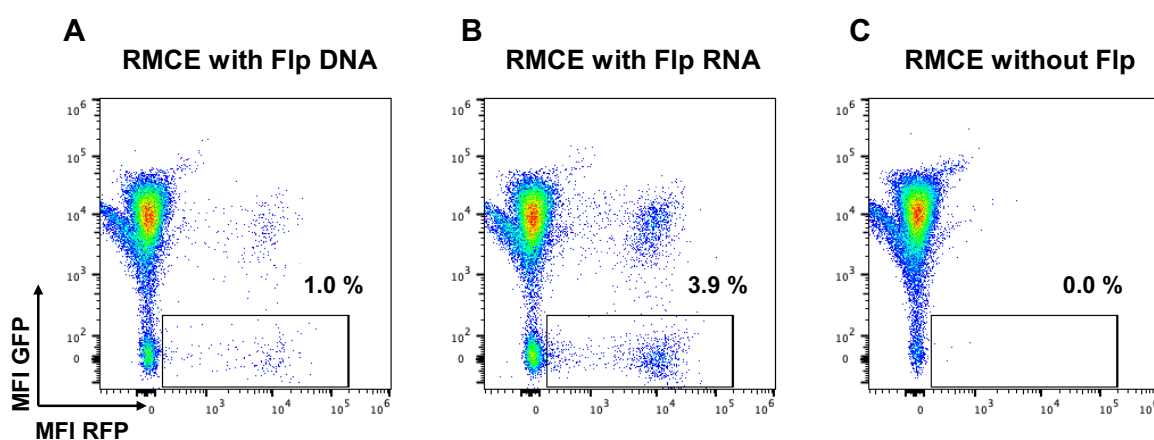
Figure 21: Landing pad exchange of 2nd generation system exchanging GFP with RFP. A) RMCE reaction with DNA-encoded Flp recombinase. B) RMCE reaction with RNA-encoded Flp recombinase C) RMCE reaction without adding Flp recombinase.

4.3.3   Landing Pad Validation by Targeted Locus Amplification

For the identification of a single copy clone, nine RFP-expressing CHO clones from the 2nd generation approach were selected for TLA analysis. In contrast to the 1st generation approach, only high RFP expressing clones were selected (Figure 22). To identify at least one clone with a single copy integration at a defined genomic site, four and five CHO clones obtained from single cell sorting of the RFP-positive population generated via RMCE approach with Flp DNA and Flp RNA, respectively, were selected. The TLA analysis revealed two integration sites for the majority of analyzed clones together with multiple copies of the RFP insert (Table 4). Only two clones (DNA Clone 13 and RNA Clone 9) were found to harbor a single copy integration of the landing pad in the CHO cell genome. Since DNA Clone 13 and RNA Clone 9 also showed an expected breakpoint in the *ampicillin resistance* gene, the two clones were selected for analysis of the RFP long term expression stability.
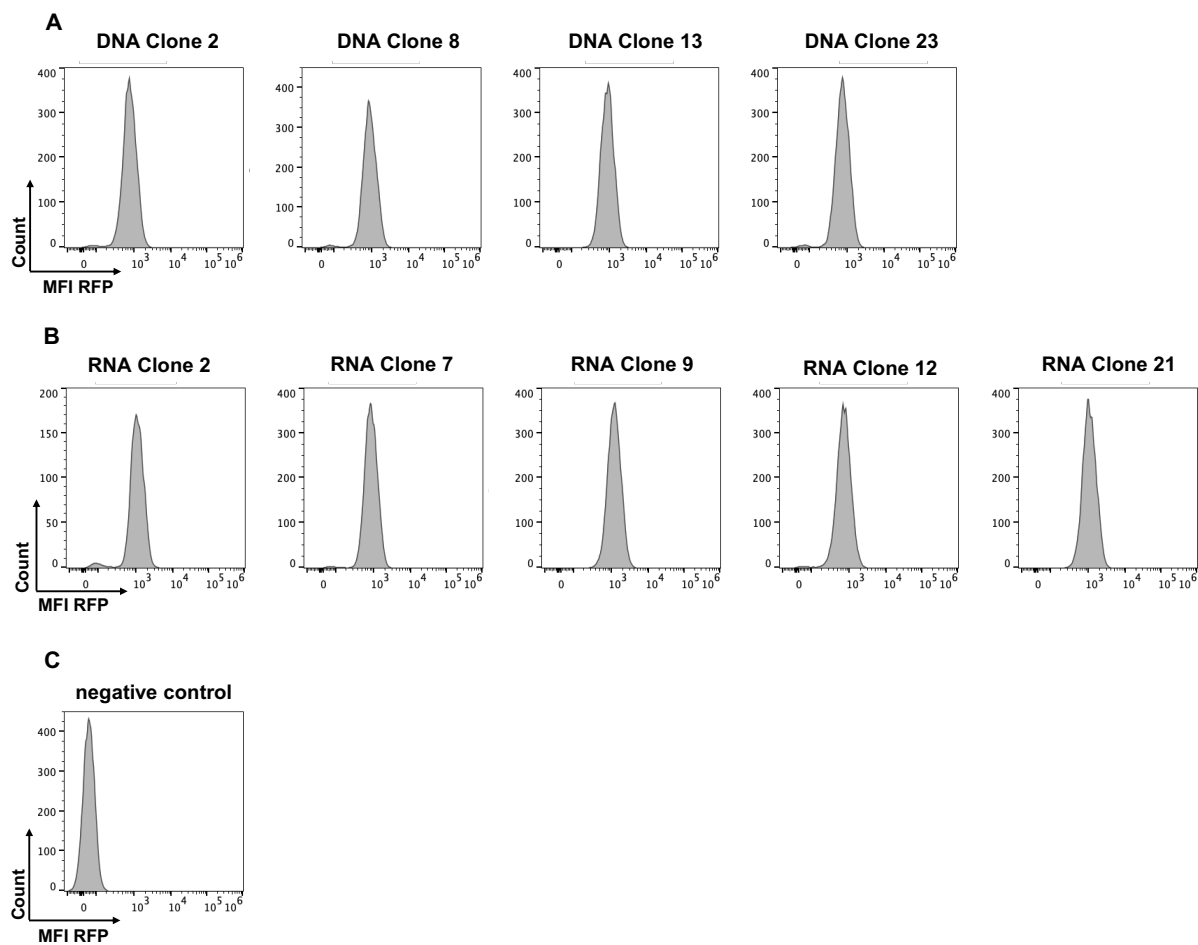
Figure 22: Histograms of the selected single cell clones for TLA analysis. A) Clones obtained from the RMCE reaction with Flp DNA. B) Clones obtained from the RMCE reaction with Flp RNA. C) Non-transfected negative control cells.

Table 4: TLA results of selected clones (2nd Generation)

Name	No. of Integration site	Copy Number	Breakpoint
DNA Clone 2	2	6-7	AmpR
DNA Clone 8	2	3-5	AmpR
DNA Clone 13	1	1	AmpR
DNA Clone 23	2	3-5	AmpR
RNA Clone 2	2	6-20	AmpR
RNA Clone 7	2	3-6	AmpR
RNA Clone 9	1	1	AmpR
RNA Clone 12	2	3-5	AmpR
RNA Clone 21	2	2-16	AmpR

4.3.4 Stability of RFP Expression of DNA Clone 13 and RNA Clone 9

Long-term expression of RFP was analyzed for the two clones with a single copy landing pad, DNA Clone 13 and RNA Clone 9. Flow cytometric analysis of the two clones, cultured without G418 selection pressure, revealed high and stable expression of RFP and a constant RFP-positive population close to 100% expressing RFP over a time period of 36 days (Figure 23). Driven by the slightly higher RFP signals over time, RNA Clone 9 was chosen as CHO master cell line for the 2nd generation landing pad approach.
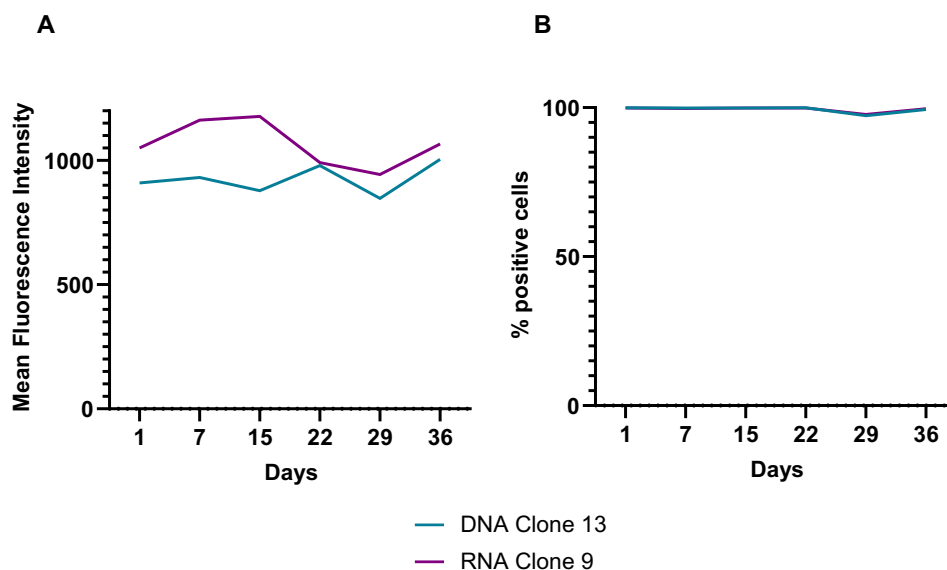
Figure 23: Long-term stability of possible 2nd generation landing pad containing CHO clones. A) MFI values of flow cytometry-based analyses over 36 days. B) Frequent of parent values of the long-term monitoring of DNA Clone 13 and RNA Clone 9.

4.4 Evaluation of Different TCR Format in CHO Display

Successful maturation of TCRs is strongly dependent on the ability to express these receptors on the surface of cells or particles used for the display approach. Therefore, six different TCR formats based on a PRAME-specific model TCR including the bispecific TCER® format were evaluated in CHO display regarding their expression level, target binding, and off-target recognition. With the exception of the bivalent DuoFc-scTv format all formats used a monovalent TCR domain for target binding. The formats can be subdivided into two Fc-based ones (Figure 24 A): A DuoFc-scTv format and a ScFc-scTv format. The DuoFc-scTv is formed by the homodimerization of an IgG Fc part fused to an TM domain and a PRAME-binding scTv. The ScFc format is composed of an scTv fused to an IgG Fc part anchored in the cell membrane by an TM domain. Figure 24 B shows the Fab fragment-based formats. On the one hand, the HC-scTv format comprised of an scTv N-terminally linked to the heavy chain of an IgG Fab fragment. On the other hand, the LC-scTv with the scTv N-terminally linked to the light chain of an IgG Fab fragment. Both Fab-based formats are anchored by a TM domain linked to the heavy chain of the Fab fragment. The third category is a single scTv (Figure 24 C) linked to an TM domain for anchoring. Figure 24 D shows the last tested format namely the TCER® made up of two individual chains. The first chain is composed of an anti-pHLA scTv α chain linked to the variable light chain of an hUCHT1 antibody fused to a silenced IgG1 Fc part with a knob-

72

forming mutation fused to an TM domain. The second chain compromises the variable heavy chain of the hUCHT1 antibody linked to the β chain of the anti-pHLA scTv and the silenced Fc part with a hole-forming mutation. The knob-into-hole structure was introduced to enforce heterodimerization of TCER chain1 (knob) and chain 2 (hole) and was achieved by inserting several point mutations into the C_H3 domains. These compromise the mutations T336W and S354C for knob formation and T366S, L368A, Y407V, Y349C for hole formation[158]. Additionally, a C_H3-C_H3 disulfide bridge[23] was introduced. The Fc part was further modified to abolish interactions with Fcγ receptors and C1q of the complement system by introducing E233P, L234V, delG236[159,160], P331S[159], and N297Q[161] (sequence numbering according to EU-scheme) mutations. Furthermore, deletion of the c-terminal glycine-lysine residues of the human IgG1 heavy chain was performed to avoid c-terminal heterogeneity.
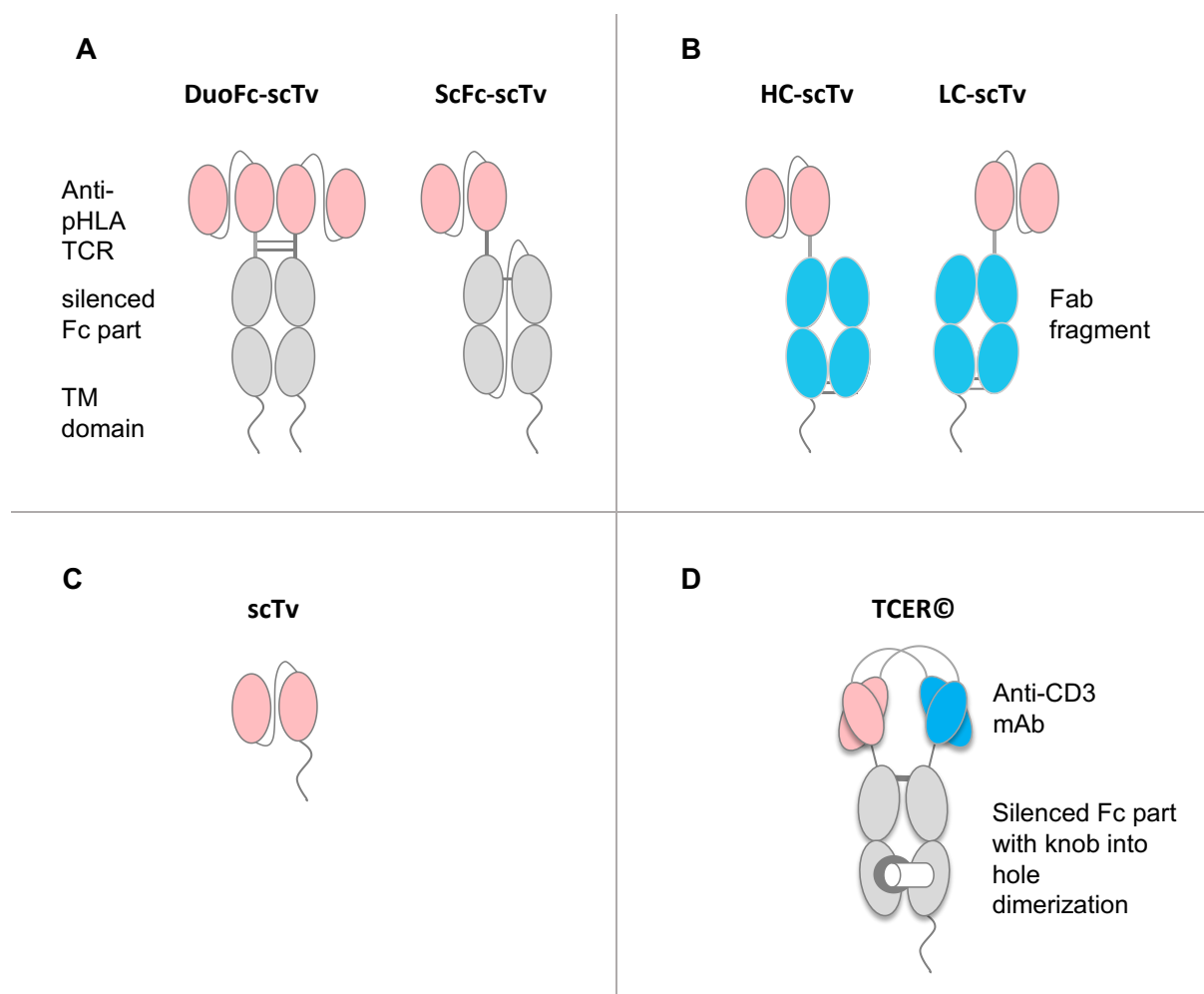
Figure 24: Structure of the evaluated formats for CHO surface display. A) Two Fc-based formats. DuoFc-scTv is composed of an IgG1 homodimerizing Fc chain (light grey) with an N-terminal scTv (rose) resulting in a bivalent format anchored by two TM domains. ScFc-scTv is a monovalent format made of an N-terminal scTv (rose) bound to one Fc chain followed by a linker and a second Fc chain (light grey) anchored by a TM domain. B) Two Fab fragment-based formats. HC-scTv is comprised of a heavy chain Fab fragment (blue) coupled N-terminally to a scTv (rose) dimerizing with a light chain Fab fragment (blue). The

construct is anchored by a TM domain fused to the heavy chain of the Fab fragment. LC-scTv is composed of a heavy chain Fab fragment (blue) linked to a TM domain dimerizing with a light chain Fab fragment (blue) linked N-terminally with a scTv (rose). C) scTv (rose) fused to a TM domain. D) Molecular structure of a TCER® molecule. TCER® chain 1 encodes for the variable TCR alpha chain (V_α), the variable light chain (V_L) of an hUCHT1 anti-CD3 antibody followed by IgG1 constant domains CH2 and CH3 modified with specific mutations to ablate Fc gamma receptor binding and complement activation as well as knob-forming mutations. TCER® chain 2 encodes for the variable heavy chain (V_H) of the anti-CD3 antibody and the variable TCR beta chain (V_β) followed by IgG1 constant domains CH2 and CH3 modified with specific mutations to ablate Fc gamma receptor binding and complement activation as well as hole-forming mutations. All formats contain a PRAME pHLA binding scTv as their target binding moiety.

4.4.1 Expression and Binding Analysis of Different scTv Formats

All formats of interest could be successfully expressed on the CHO membrane from the tagged locus of the landing pad containing CHO cell line clone (RNA Clone 9) as indicated by the binding of an V_β-specific antibody (Figure 25 A). The DuoFc-scTv format showed the highest expression signal in line with the two binding sites for the anti-V_β antibody. The ScFc-scTv, HC-scTv, and the LC-scTv format were expressed at a similarly high level whereas the scTv and the TCER® formats were expressed at a lower level. Figure 25 B shows the binding of all formats to the PRAME pHLA. The expression of the different TCR formats resulted in functional binding of the target PRAME pHLA of almost 100 % at a target concentration of 316 - 3.16 nM (Figure 25 B). A slow decrease in the binding is seen from 1 - 0.0316 nM target concentration. The formats with a stronger, target binding could be discriminated by the first detectable binding signal with DuoFc-scTv and HC-scTv being the most sensitive with a binding at 0.001 nM followed by the LC-scTv, scTv format, and the TCER® format at concentrations of 0.00316 nM and 0.01 nM, respectively. Besides, binding to the target pHLA the binding specificity was analyzed by using monomeric or tetrameric pHLA complexes from 11 peptides exhibiting a high degree of sequence similarity to the PRAME peptide. All formats showed a comparable degree of off-target binding with the more sensitive detection using an avidity-driven pHLA tetramer approach compared to a pHLA monomer one. The highest binding is observed for 3 out of 11 similar peptides with the strongest recognition of similar peptides 10 and 11 displaying a sequence similarity in 6 of 9 and 3 of 9 positions, respectively. Similar peptide 9 which was also bound strongly displays an equal sequence in 5 out of 9 positions. Similar peptides 5 was only bound in the avidity-driven approach with 6 identical positions, by every format except for the TCER®. The DuoFc-scTv also showed binding to similar peptide 6 tetramers with 7 identical positions in line with its two binding moieties targeting the pHLA. There are only small differences between the different formats regarding their off-target

binding with the DuoFc-scTv being the less specific one which might be useful for the identification of off-target recognition of the underlying TCR and the TCER® format being the most specific one. Interestingly, all but one of the detected similar peptides show a high degree of sequence similarity with the target peptide with more than 5 identical positions except for similar peptide 11 only displaying 3 equal positions arguing for an important role of the c-terminal peptide stretch for the TCR binding motive.

A

B

concentration PRAME pHLA monomer

C

peptide HLA tetramer

D

peptide HLA monomer
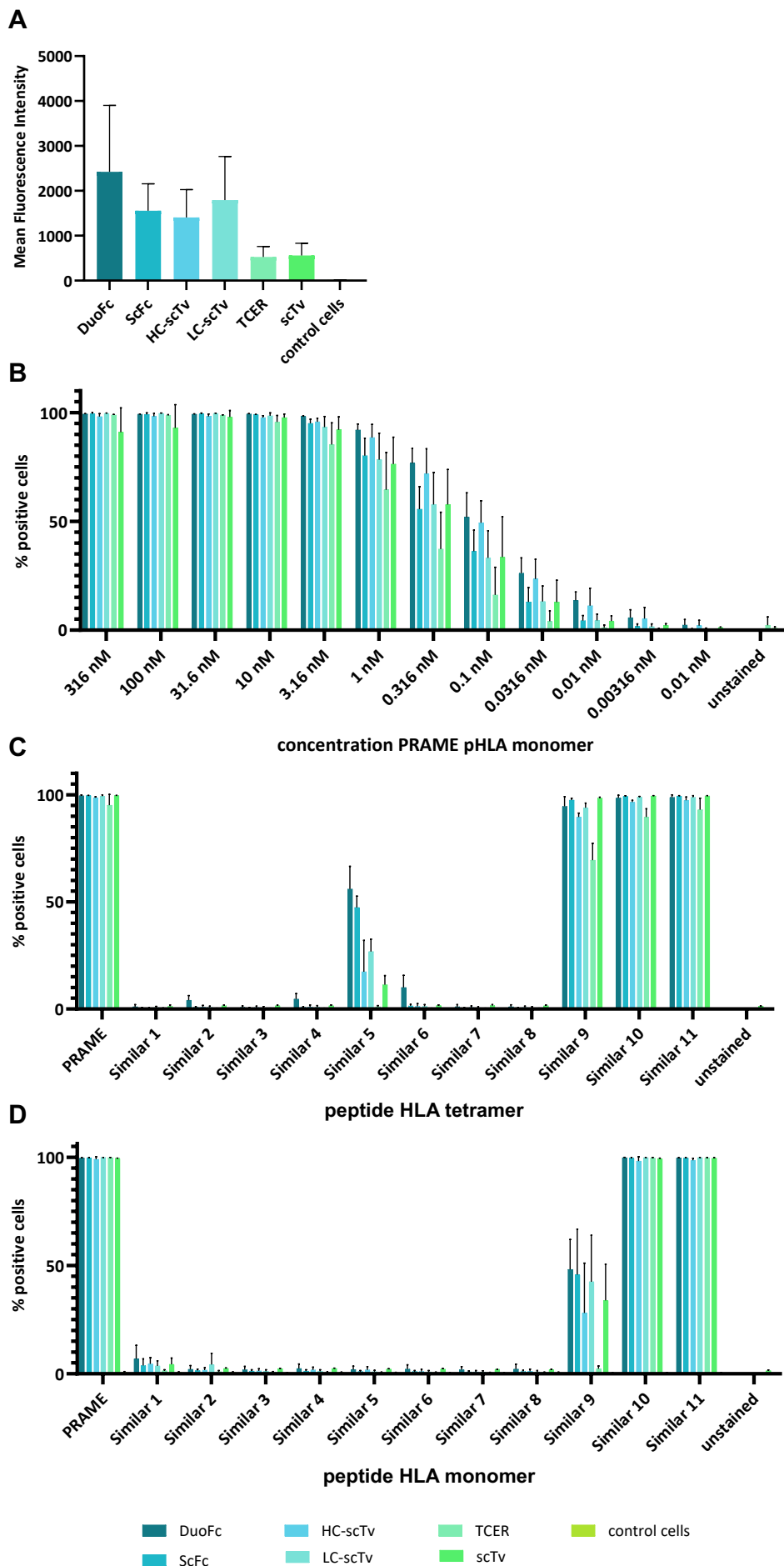
Figure 25: Results of flow cytometry-based analysis of different display formats. A) Surface expression of the display formats detected with a Vβ antibody. Non-transfected CHO-S cells served as a negative control. B) Binding of display formats of PRAME pHLA target titration (316 nM - 0.001 nM). C) Binding of UV-exchanged similar peptide-HLA tetramers. The analysis was performed with 10 nM fluorochrome-labeled tetramers. PRAME pHLA was used as a positive control of the UV-exchange reaction. D) Binding of UV-exchanged similar peptide-HLA monomers at 10 nM. PRAME pHLA was used as a positive control of the UV-exchange reaction. Results are shown as means of three independently performed experiments with error bars indicating the SD.

4.5 TCR Maturation using CHO Display of TCER® Molecules

4.5.1 Generation and Selection of PRAME-specific TCER® Library

In order to demonstrate the applicability of the established CHO display for TCR maturation a library containing previously identified CDR sequences was generated. The library contained two CDRα1, six CDRα2, 16 CDRα3 and six CDRβ1, 16 CDRβ2, and two CDRβ3 stabilized high affinity sequence variants of a PRAME-specific model TCR (Table 5). The library was generated via RMCE exchange into the 1st generation landing pad containing cell line clone RFP_A03. The chosen library design allowed the expression of TCER® molecules containing every possible combination resulting in a library size of 36,864 different variants allowing the identification of optimal CDR combinations.

Table 5: CDR sequences for the CDR combinatorial screening library.

CDRα1	CDRα2	CDRα3	CDRβ1	CDRβ2	CDRβ3
DRGSQS	YSNGDKE	DNAHGGM	SGHRS	EHGLER	CASSPWDSPNVQY
DRGSQL	YQEGDKE	DNDQGGI	EGHRA	FSETQR	CASSPWDSPNEQY
	YQTGDKE	DNDVGGI	PGHKA	IHGEER	
	YQAGDKE	DNEQGGM	PGHRA	IHGQER	
	YPQGDKK	DNKAGGI	PGHRS	IHGVER	
	YSQGDKE	DNPAGGI	QGHRA	VHGAER	
		DNPRGGM		VHGEER	
		DNPVGGP		VHGIER	
		ENKPGGP		VHGKER	
		GNAQGGM		VHGLER	
		GNDLGGI		VHGMER	
		NNPSGGM		VHGNER	
		PNPPGGK		VHGQER	
		PNTHGGP		VHGRER	
		SNFGNEK		VHGVER	
		TNIAGGS		VHGYAR	

For enrichment of high binding clones the library was applied to three selection rounds including a final single cell sort according to a selection and counterselection principle (Figure 26). The first sorting round was performed with 100 nM PRAME pHLA monomer without counterselection. The second and third sorting was done with 31.6 and 10 nM PRAME pHLA, respectively with simultaneous counterselection to maintain binding specificity of the TCER® clones. The counterselection was conducted with 10 nM pHLA tetramers of the 11 similar peptides. The final single cell sort resulted in the identification of 171 individual TCER® clones compromising 39 unique TCR variable domain sequences.

Based on the highest abundance of sequences and the highest binding strength towards the PRAME pHLA 10 clones (Table 6) were chosen for further analysis. The wt TCR sequence refers to the CDRs of a non-maturated TCR sequence as identified from a healthy donor. Among the 10 selected TCER® variants 3 to 5 modified CDRs were observed with a stringent effect

observed for CDRβ2 displaying only one possible variant (VHGEER) indicating an important role in the improvement of the TCER® affinity for PRAME pHLA. The observed variance in the CDRα3, CDRα2, CDRβ1, and CDRβ3 regions with 9, 8, 7, and 5 TCER® variants, respectively, cannot clearly be discriminated from a random distribution. Therefore, a contribution of these CDRs to an affinity improvement cannot clearly be demonstrated based on these findings. No sequence variation was detected for CDRα1 only displaying the wt sequence. An impact of this CDR on the affinity maturation process is therefore unlikely.
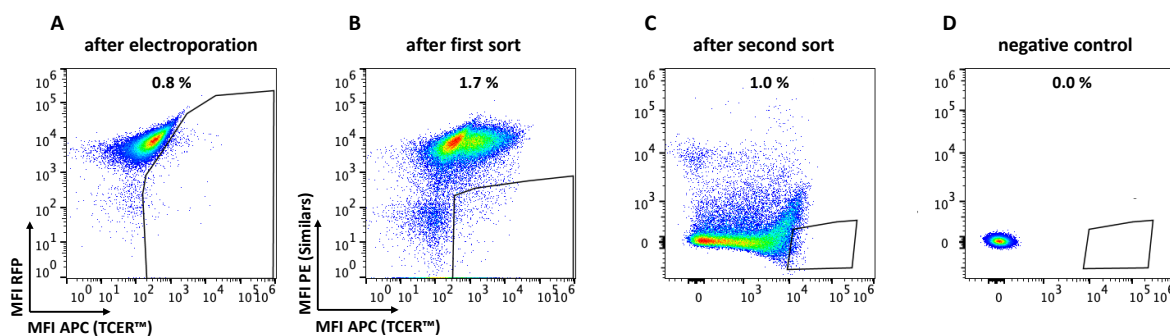
Figure 26: Sorting of PRAME pHLA binding TCER® library. A) In the first selection round PRAME pHLA binding cells were enriched using 100 nM PRAME pHLA and were subjected to a second sorting round. B) The second sorting round was conducted with 31.6 nM PRAME pHLA and 10 nM of each 11 UV-exchanged tetrameric similar peptides. C) The final single cell sort was performed with 10 nM PRAME pHLA and 10 nM of each of 11 UV-exchanged tetrameric similar peptides. D) Non-transfected CHO cells were used as a negative control. Dead cells and doublets were excluded by gating.

Table 6: Sequence information of selected clones of the CDR combinatorial screening approach.

Clone	CDRα1	CDRα2	CDRα3	CDRβ1	CDRβ2	CDRβ3
wt TCR	DRGSQS	YSNGDKE	SNFGNEK	SGHRS	FSETGR	CASSPWDSPNEQY
CL-7435	DRGSQS	YQAGDKE	GNDLGGI	SGHRS	VHGEER	CASSPWDSPNEQY
CL-7445	DRGSQS	YSNGDKE	DNPRGGM	QGHRA	VHGEER	CASSPWDSPNEQY
CL-7467	DRGSQS	YQAGDKE	GNAQGGM	PGHRA	VHGEER	CASSPWDSPNVQY
CL-7475	DRGSQS	YPQGDKK	DNPAGGI	SGHRS	VHGEER	CASSPWDSPNVQY
CL-7480	DRGSQS	YQEGDKE	SNFGNEK	PGHRA	VHGEER	CASSPWDSPNEQY
CL-11581	DRGSQS	YSQGDKE	DNPRGGM	PGHRS	VHGEER	CASSPWDSPNVQY
CL-11594	DRGSQS	YSNGDKE	DNEQGGM	PGHRS	VHGEER	CASSPWDSPNVQY
CL-11611	DRGSQS	YQEGDKE	NNPSGGM	QGHRA	VHGEER	CASSPWDSPNEQY
CL-11614	DRGSQS	YSQGDKE	DNPAGGI	SGHRS	VHGEER	CASSPWDSPNEQY
CL-11623	DRGSQS	YSQGDKE	NNPSGGM	PGHRS	VHGEER	CASSPWDSPNVQY
Proportion of possible variants	1/2	5/6	7/16	4/6	1/16	2/2

4.5.2 Evaluation of TCER® Expression and Binding in CHO Display

The selected 10 TCER® candidates (Table 6) were analyzed to assess their expression level and binding specificity profile. All candidates could be expressed and detected on the CHO surface with CL-7435 showing the weakest expression and CL-7467, CL-7475, and CL-11594 the highest expression (Figure 27 A). Binding analysis with PRAME pHLA monomers revealed strong target binding for six out of 10 selected variants as indicated by the low level of 0.1 nM pHLA required for staining the TCER® expressing CHO cells. The remaining four variants (CL-7435, CL-7475, CL-7480, and CL-11614) showed weaker PRAME pHLA binding (Figure 27 B). Additionally, to the binding strength also the specificity was assessed using 11 similar peptides exhibiting a high degree of sequence similarities to the PRAME peptide. As seen previously for the different formats, strong to moderate binding of similar peptides 9, 10, and 11 (Figure 27 C) was observed arguing for no detectable gain in the specificity compared to the model TCR sequence used previously for the format testing.

A

B

C
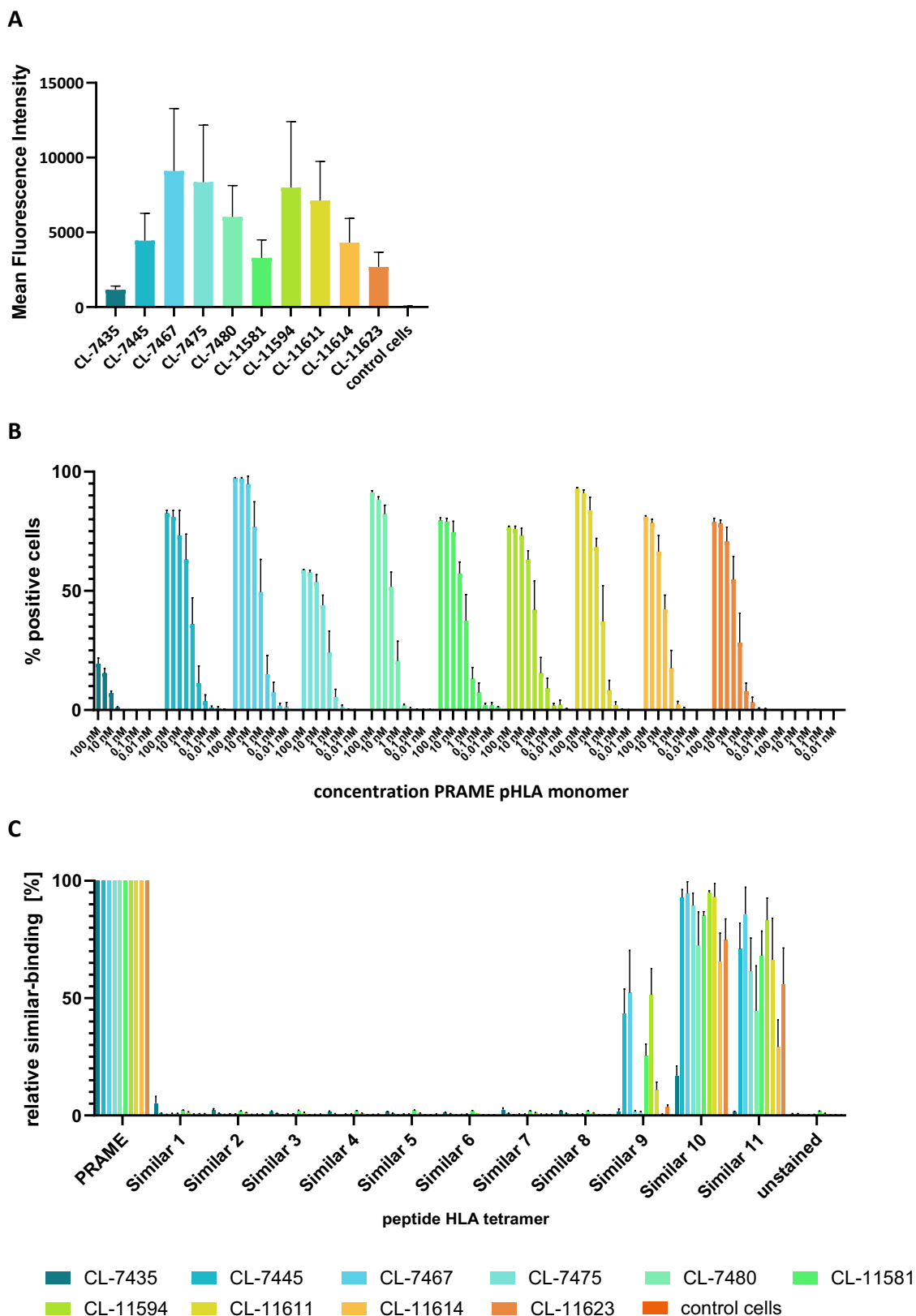
Figure 27: Flow-cytometric analysis of PRAME and similar peptide binding of CHO-displayed TCER® candidates. A) Surface expression of selected candidates detected with an anti-Vβ antibody. B) Target binding was analyzed with PRAME pHLA monomer used at concentrations from 100 nM - 10 pM. C) Binding of TCER® candidates to 10 nM similar peptide tetramers of each of 11 different similar peptides in relation to 10 nM PRAME pHLA tetramer. Each data point represents the mean of triplicate measurements with the respective SD.

4.5.3 Affinity Determination for Solubly Expressed TCER® Candidates

For further functional testing, the 10 selected TCER® candidates were expressed as soluble proteins in CHO cells and the affinity of the purified molecules was measured via biolayer interferometry. TCER® candidates CL-7467 and CL-7445 exhibited the highest pHLA affinity towards the PRAME pHLA with K_D values of 3.4 and 3.7 nM, respectively (Table 7). CL-7435, CL-11614, CL-7480, and CL-7475 exhibited the lowest affinities with K_D values ranging from 16.5 nM to 37.4 nM, which is in line with the weaker target binding concluded from a lack of binding signal at a target concentration of 0.1 nM. These data support the conclusion that the CHO display system is well suited for the enrichment of high affinity binding candidates and an early assessment of their potential via a CHO-based binding analysis.

Table 7: Affinity data of selected soluble TCER® candidates

Clone	KD [nM]
CL-7467	3.4
CL-7445	3.7
CL-11581	5.2
CL-11594	6.1
CL-11623	6.6
CL-11611	12.0
CL-7435	16.5
CL-11614	17.8
CL-7480	24.5
CL-7475	37.4

4.5.4 Assessment of TCER®-mediated Killing of Tumor Cells

The TCER® candidates were analyzed regarding their potential to kill PRAME-positive tumor cells. Therefore, LDH release assays with three different target positive cell lines (UACC-257, HS695T, and A375) and human PBMCs as effector cells were performed. The target positive cell lines were chosen to cover a broad range of target densities displayed by the PRAME pHLA copy number per cell (cpc) on their surface. The copy numbers ranged from 1100 cpc for UACC-257, 400-550 cpc for HS695T, and 50 cpc for A375. T98G and SET-2 cells were used as

target negative which lack any detectable PRAME pHLA expression on their surface. As shown in Figure 28 all selected candidates induce pronounced target cell killing in UACC-257 and HS695T cells. The killing potential of the candidates is in line with their measured affinities with CL-7467, CL-7445, CL-11851, CL-11594, and CL-11623, all TCER® candidates with K_D values below 10 nM, mediating the highest target cell killing. The candidates with the lowest affinities CL-7435, CL-7475, CL-7480, and CL-11614 displaying the weakest target cell killing in UACC-257 and HS695T. For the A375 cell line with a very low target cell density (50 cpc) on its surface killing was only detected for higher affinity candidates such as CL-7467, CL-7445, CL-11581, CL-11694, and CL-11623. Killing of the target negative cell line T98G was observed at a high to low level dependent on the affinities of the candidates with CL-7467 and CL-7445 inducing the highest killing and CL-7475 and CL-7480 inducing the weakest killing. In contrast to this no or only weak killing at the highest TCER® concentrations was observed with the SET-2 target negative cell line. The calculated EC_{50} values based on the LDH-release assays are shown in Table 8 pointing to CL-7467 as the candidates with the highest anti-tumor activity which is consistent with its highest target binding affinity.

A
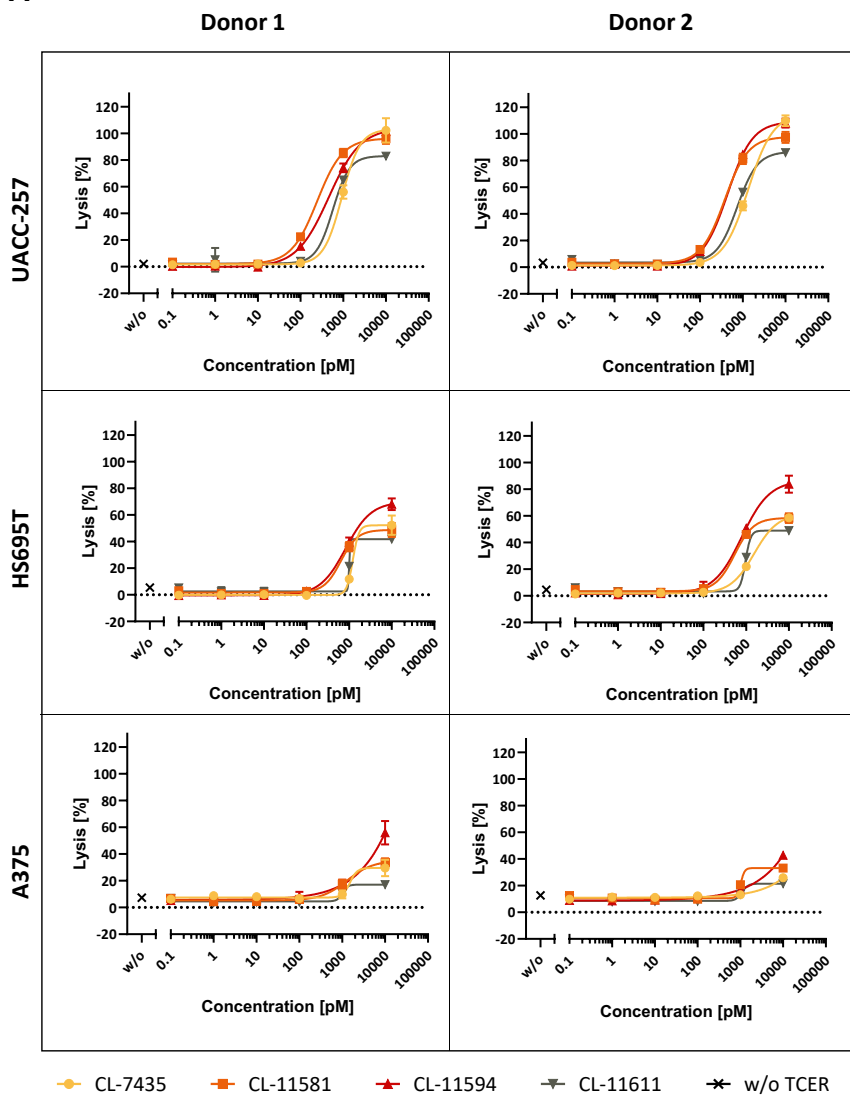
B
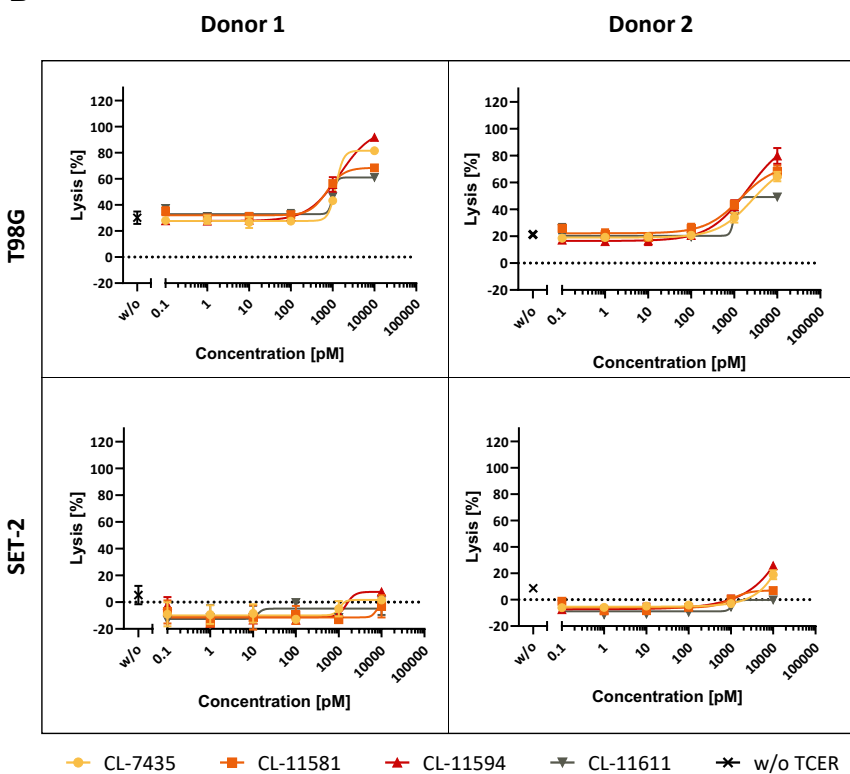
C
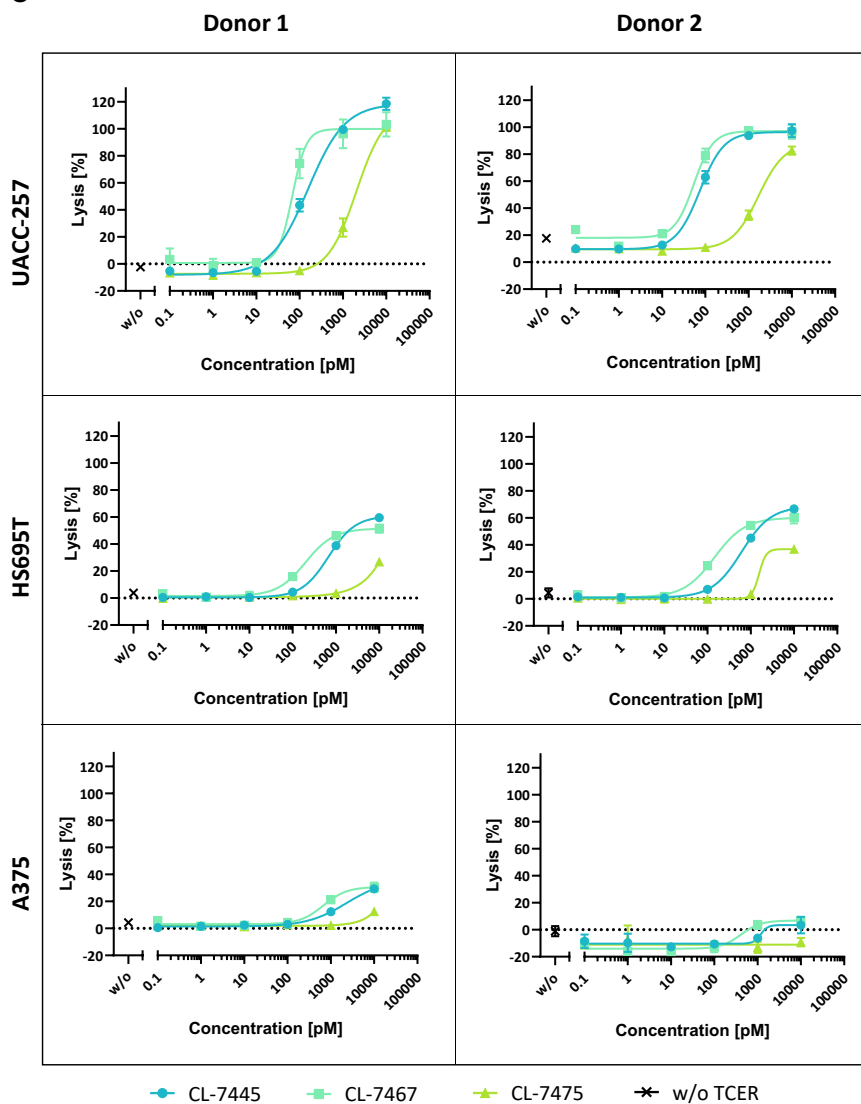
D
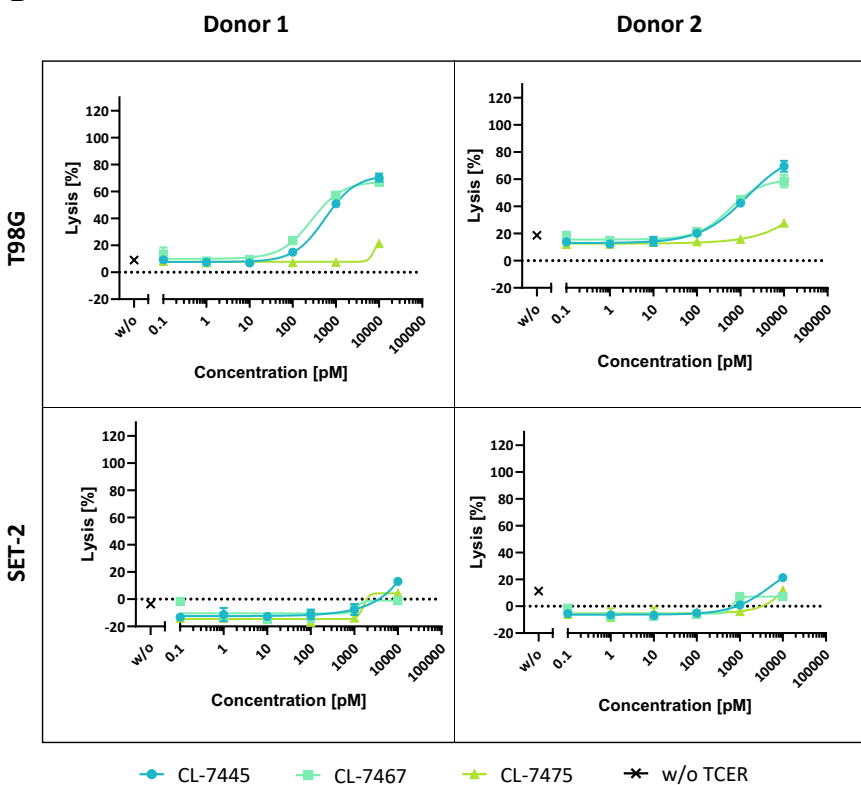
E
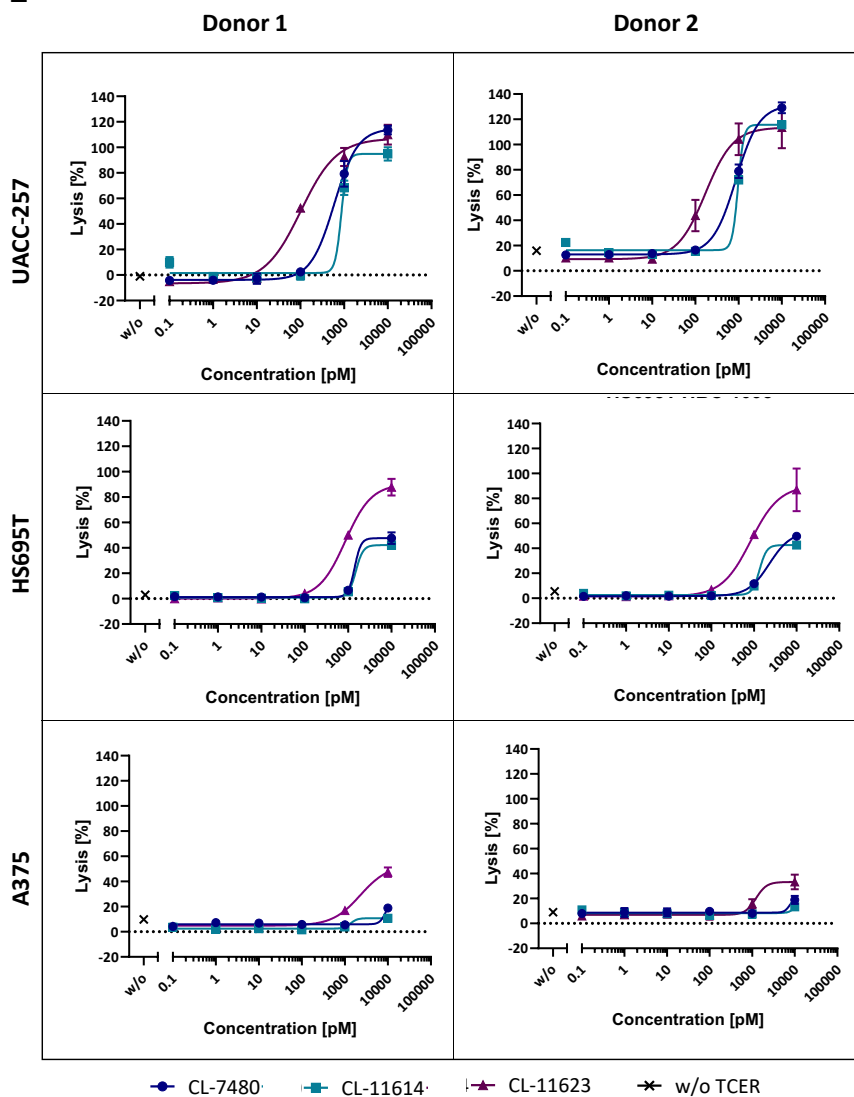
F
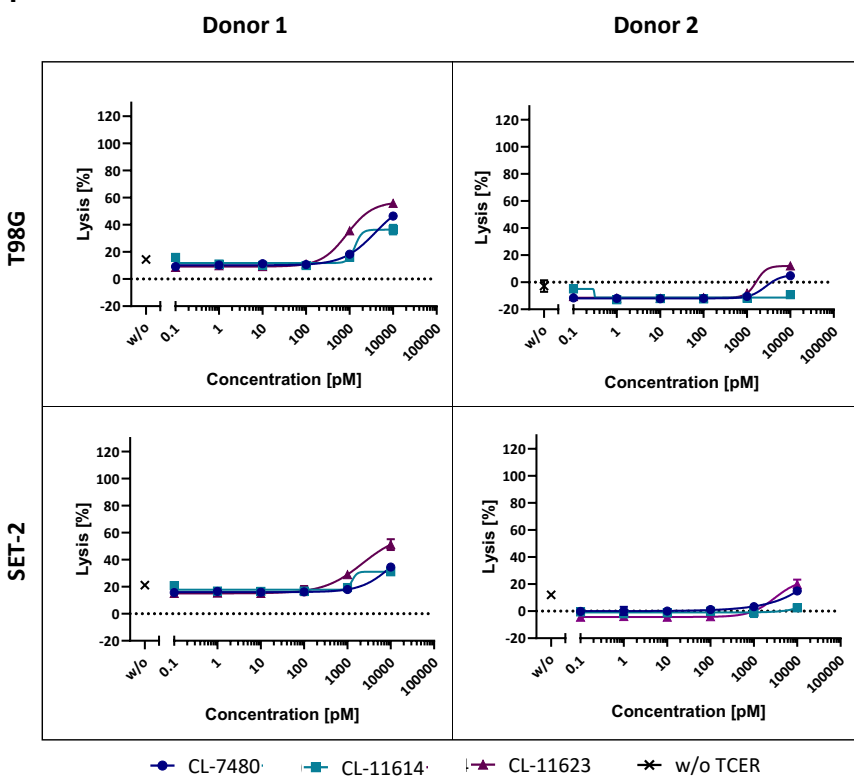
Figure 28: Cytotoxicity assay results of selected candidates. The level of mediated cytotoxicity was determined by LDH release assays for all selected candidates. As target positive cell lines UACC-257 with 1100 copies per cell, HS695T with 400-550 copies per cell, and A375 with 50 copies per cell were used. The copy number per cells refers to the number of PRAME pHLA on the cell surface. T98G and SET-2 cells were used as target negative cell lines without detectable PRAME pHLA on their surface. A) Results for the candidates CL-7435, CL-11594, CL-11581, and CL-11611 with the PBMCs of two different donors on target positive cell lines. B) Results for the candidates CL-7435, CL-11594, CL-11581, and CL-11611 with the PBMCs of two different donors on target negative cell lines. C) Results for the candidates CL-7445, CL-7467, and CL-7475 with the PBMCs of two different donors on target positive cell lines. D) Results for the candidates CL-7445, CL-7467, and CL-7475 with the PBMCs of two different donors on target negative cell lines. E) Results for the candidates CL-7480, CL-11614, and CL-11623 with the PBMCs of two different donors on target positive cell lines. F) Results for the candidates CL-7480, CL-11614, and CL-11623 with the PBMCs of two different donors on target negative cell lines. Each data point represents the mean of a triplicate with the respective SD. Effector:Target ratio 10:1.

Table 8: EC$_{50}$ Values based on cytotoxicity data from selected candidates.

Name	EC$_{50}$ UACC-257 [pM]	EC$_{50}$ HS695T [pM]
CL-7435	1136	1380
CL-7445	115	644
CL-7467	61	172
CL-7475	1864	1556
CL-7480	730	1849
CL-11581	310	587
CL-11594	450	808
CL-11611	656	984
CL-11614	914	1424
CL-11623	136	849

4.5.5 Immune Activation of Selected TCER® Candidates

Further experiments were conducted to assess the ability of the TCER® candidates to activate immune cells capable of mediating an anti-tumor response. The tumor cell lines UACC257 and HS695T and SET-2 as the negative cell line were used. As seen in Figure 31 and Figure 30 all candidates induce a robust to moderate activation of T cells in response to UACC-257 and HS695T cells as measured by the activation marker CD69. For all tested candidates 100 pM and 1 nM TCER® were sufficient to trigger CD4^{+} T cell activation in response to UACC-257 and HS695T, respectively (Figure 29). For CL-7467, the candidate with the highest affinity, CD4^{+} T cell activation was even observed at 10 pM with UACC-257 cells and 100 pM TCER® with HS695T cells. CD4^{+} T cell activation with the target negative cell line SET-2 is only seen at the

highest concentration except for the three candidates with the highest affinity, CL-7445, CL-7467, and CL-11581, also inducing an activation with 1 nM TCER® concentration (Figure 31 C). A similar pattern can be observed for the activation of CD8$^+$ T cells an activation with UACC-257 cells is seen from 1 pM TCER® concentration for higher affinity candidates and from 1 nM with HS695T cells except for CL-7467 already inducing an immune response with 100 pM (Figure 30). Partly TCER® independent activation of CD8$^+$ T cells is seen with SET-2 cells also for lower affinity variants but also TCER® concentration dependent one for concentrations above 1 nM for higher affinity variants (Figure 30 C). Even though T cells were activated in response to the SET-2 cell line this activation did not result in a specific activation associated with the release of perforin as seen in Figure 32. Also measured was NK cell activation observed for higher affinity candidates at concentrations above 100 pM with UACC-257 cells. For NK cell activation with HS695T cells only small effects were seen but the most robust one of these were provoked by the higher affinity variants. No effects were detected with SET-2 cells for any of the tested candidates (Figure 31). In general, these results support the superior role of the higher affinity candidates headed by CL-7467.

A

CD3+ CD56- CD4+ CD69+

B

CD3+ CD56- CD4+ CD69+

Donor 1　　　　　　　　　　　　　　　**Donor 2**
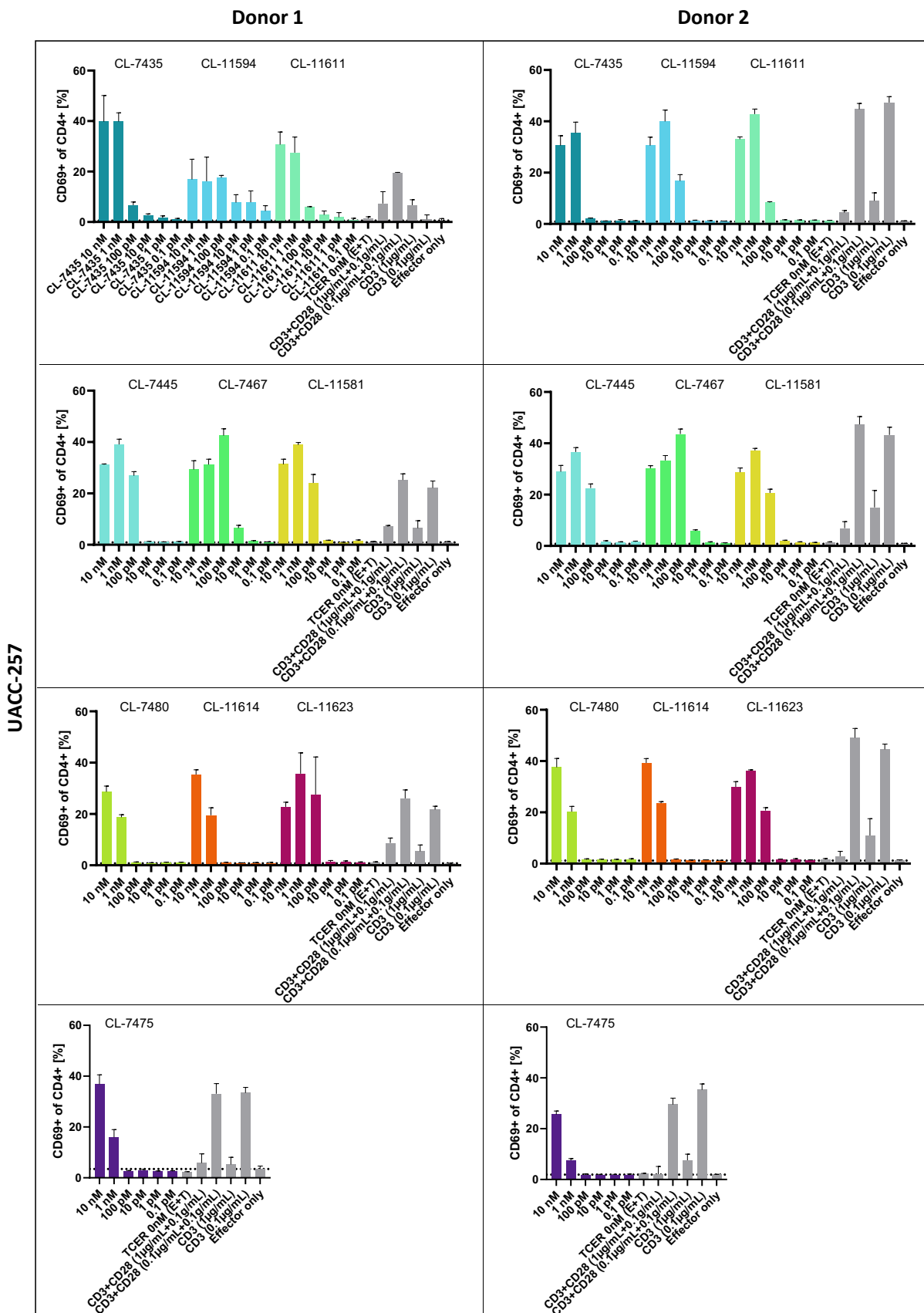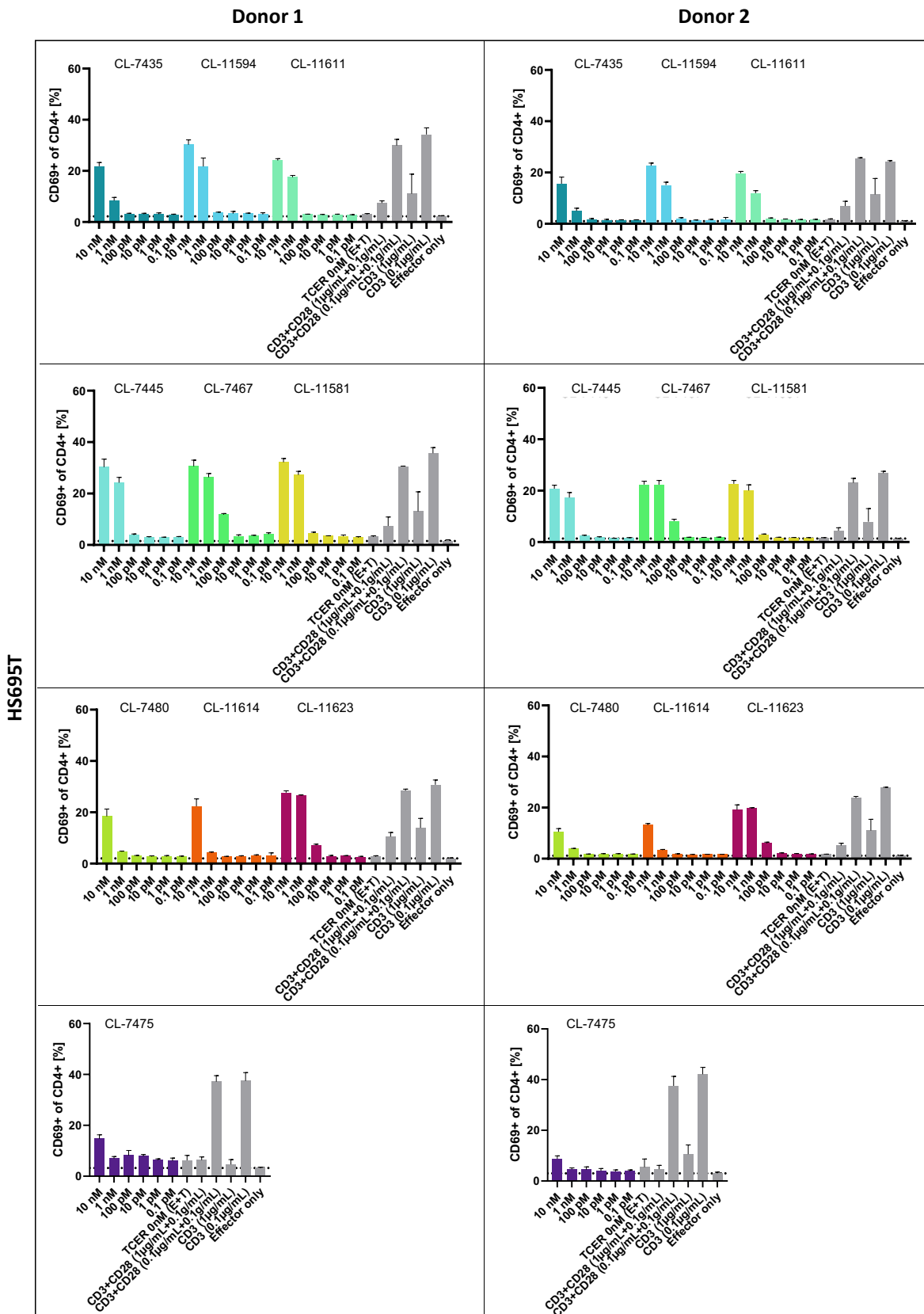
C

CD3+ CD56- CD4+ CD69+
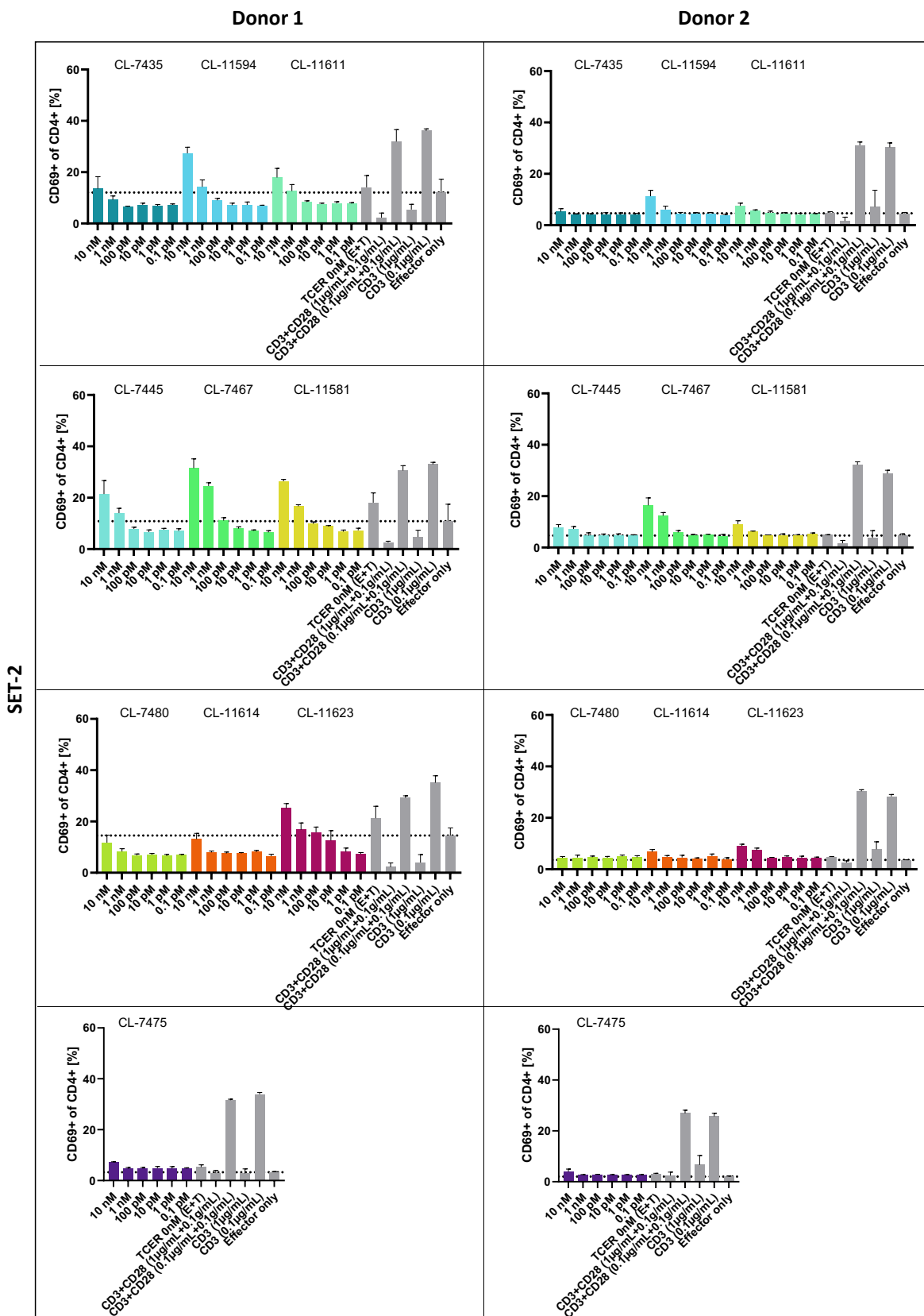
Figure 29: Results of flow cytometry-based activation assays of selected TCER® candidates for CD4+ T cells. The potential to induce an anti-tumor response of the candidates was evaluated via activation assays after co-culture with PBMCs from a

healthy donor and two different tumor cell lines (UACC-257 and HS695T). SET-2 was used as a target negative cell line. Activation was measured using CD69 activation. A) Activation profile of CD4+ T cells after incubation with different TCER® concentrations ranging from 10 nM - 1 pM in response to UACC-257 cells. B) Activation profile of CD4+ T cells after incubation with different TCER® concentrations ranging from 10 nM - 1 pM in response to HS695T cells. C) Activation profile of CD4+ T cells after incubation with different TCER® concentrations ranging from 10 nM - 1 pM in response to SET-2 cells. All experiments were performed with an E:T ratio of 10:1. Each datapoint represents the mean of a triplicate with the respective SD.

A

CD3+ CD56- CD8+ CD69+
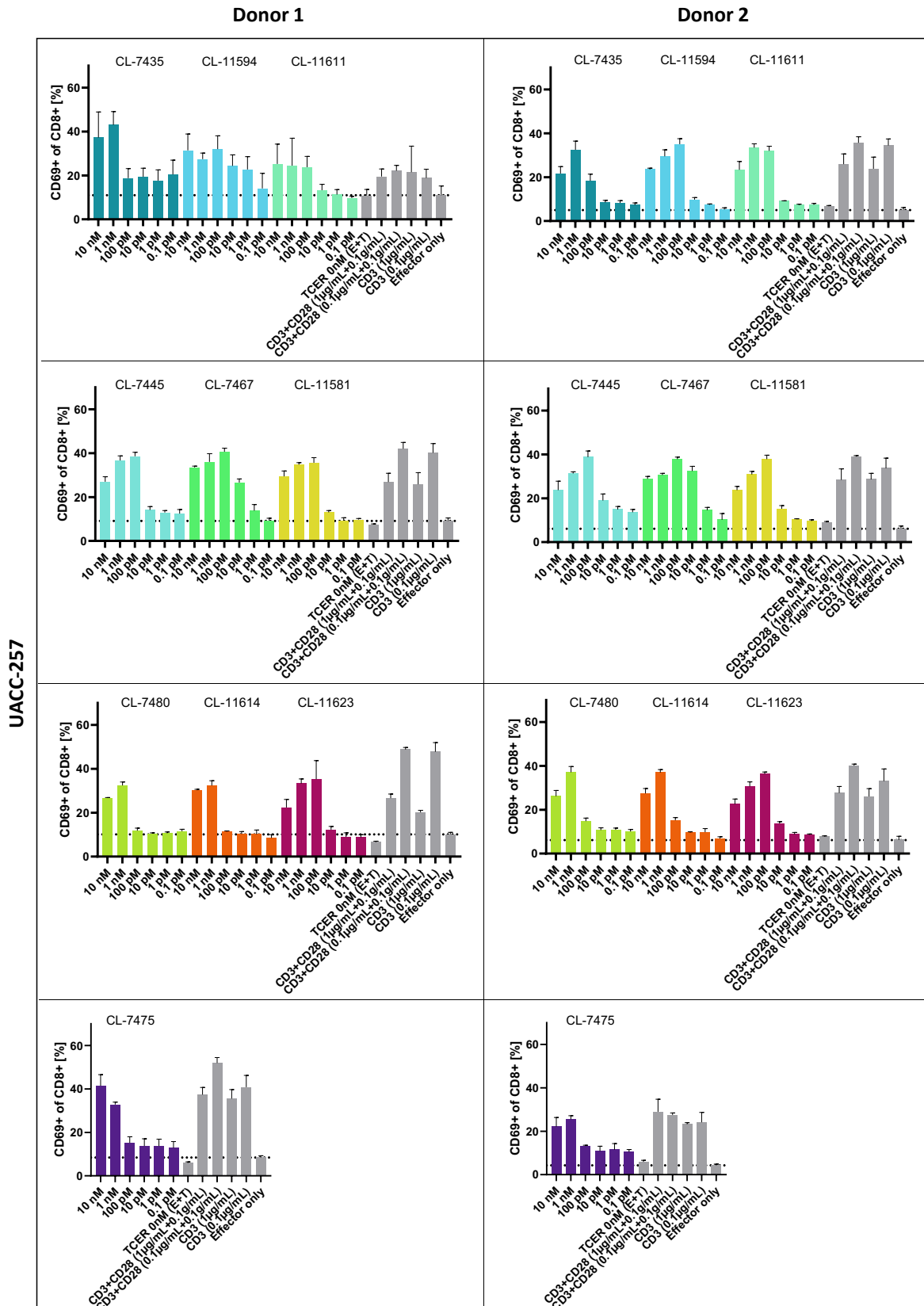
B

CD3+ CD56- CD8+ CD69+
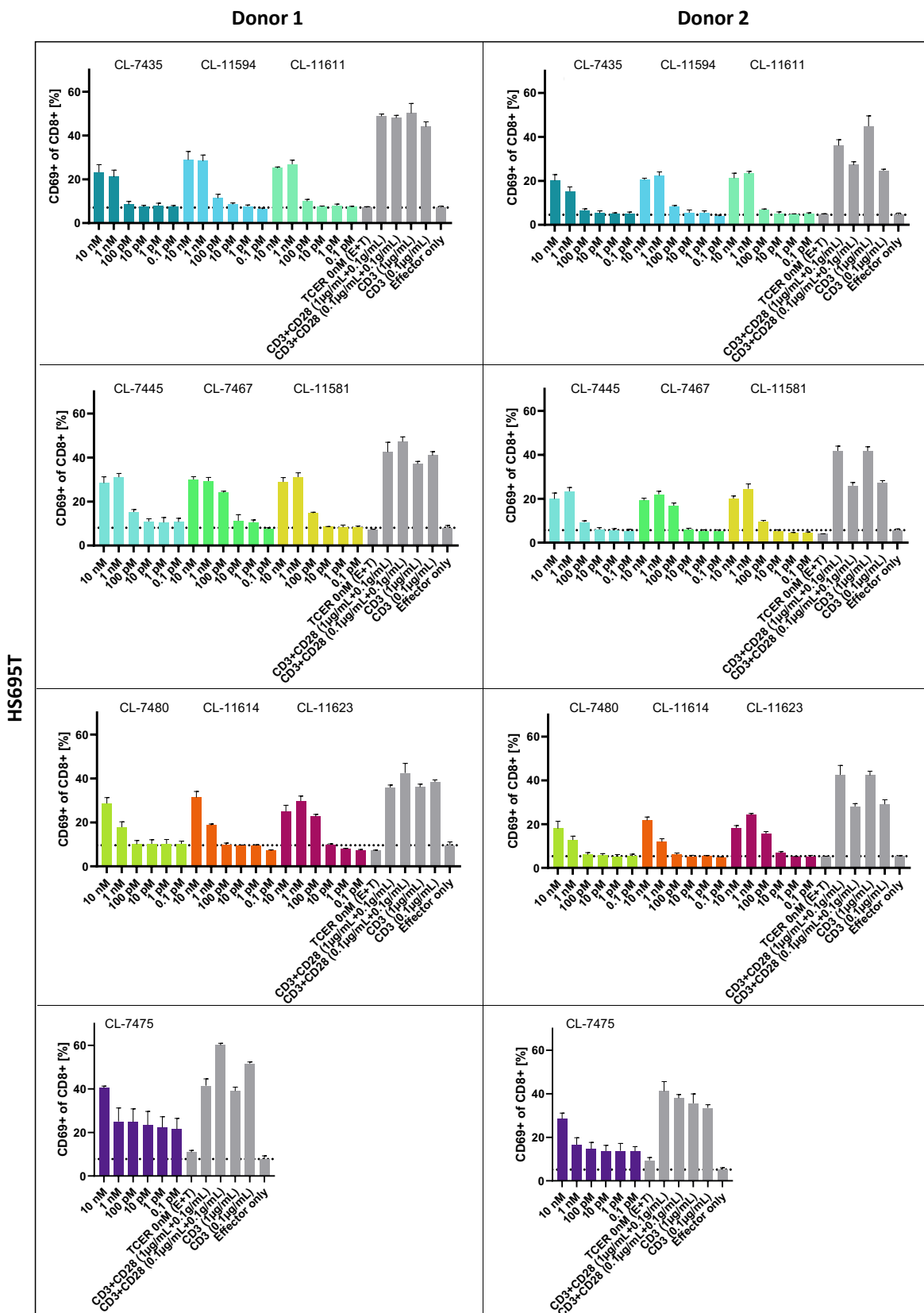
C

CD3+ CD56- CD8+ CD69+
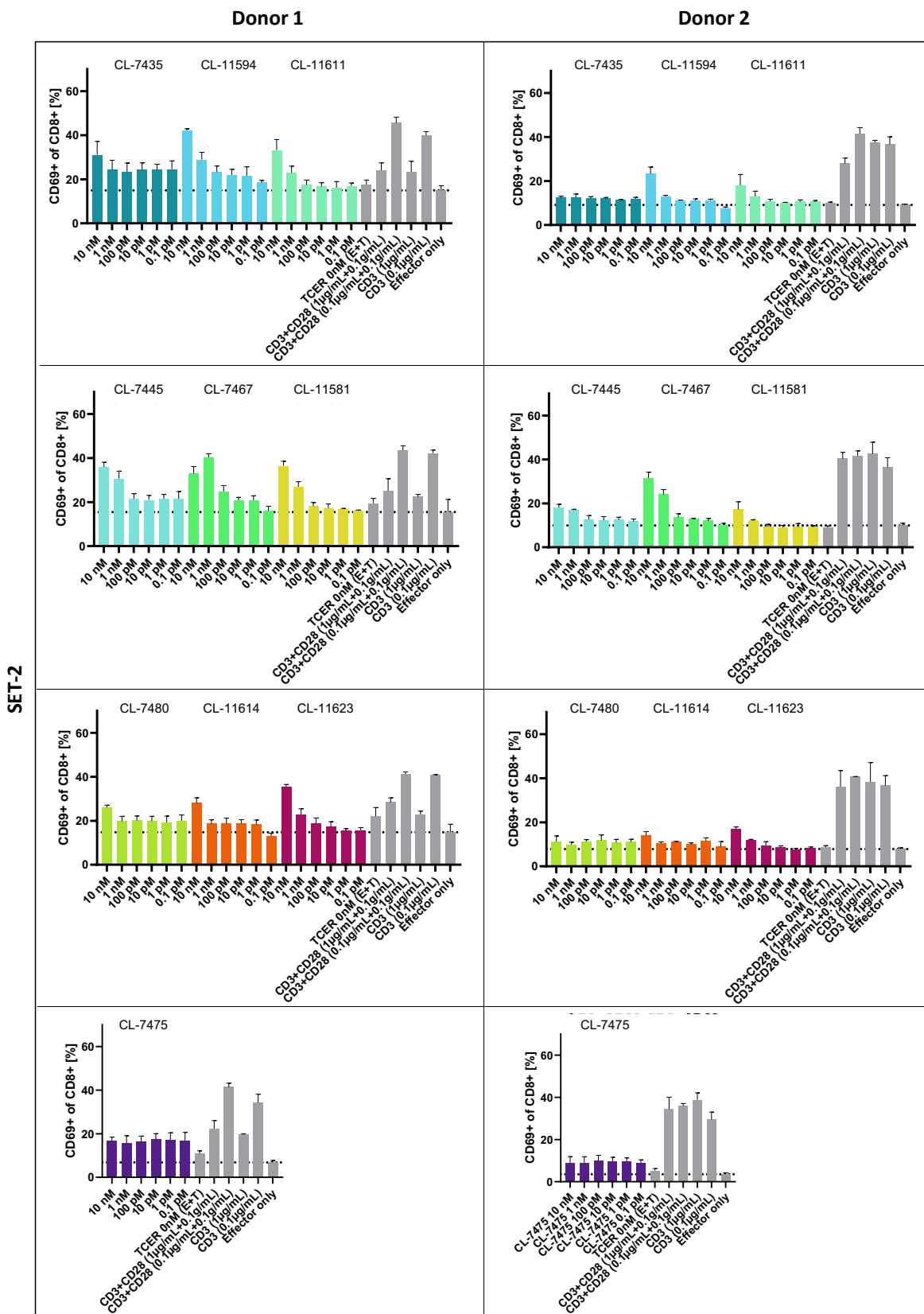
Figure 30: Results of flow cytometry-based activation assays of selected TCER® candidates for CD8+ positive T cells. The potential to induce an anti-tumor response of the candidates was evaluated via activation assays after co-culture with PBMCs

from a healthy donor and two different tumor cell lines (UACC-257 and HS695T). SET-2 was used as a target negative cell line. Activation was measured using CD69 activation. A) Activation profile of CD8+ T after incubation with different TCER® concentrations ranging from 10 nM - 1 pM in response to UACC-257 cells. B) Activation profile of CD8+ T cells after incubation with different TCER® concentrations ranging from 10 nM - 1 pM in response to HS695T cells. C) Activation profile of CD8+ T cells after incubation with different TCER® concentrations ranging from 10 nM - 1 pM in response to SET-2 cells. All experiments were performed with an E:T ratio of 10:1. Each datapoint represents the mean of a triplicate with the respective SD.

CD3- CD56+ CD69+

B

CD3- CD56+ CD69+
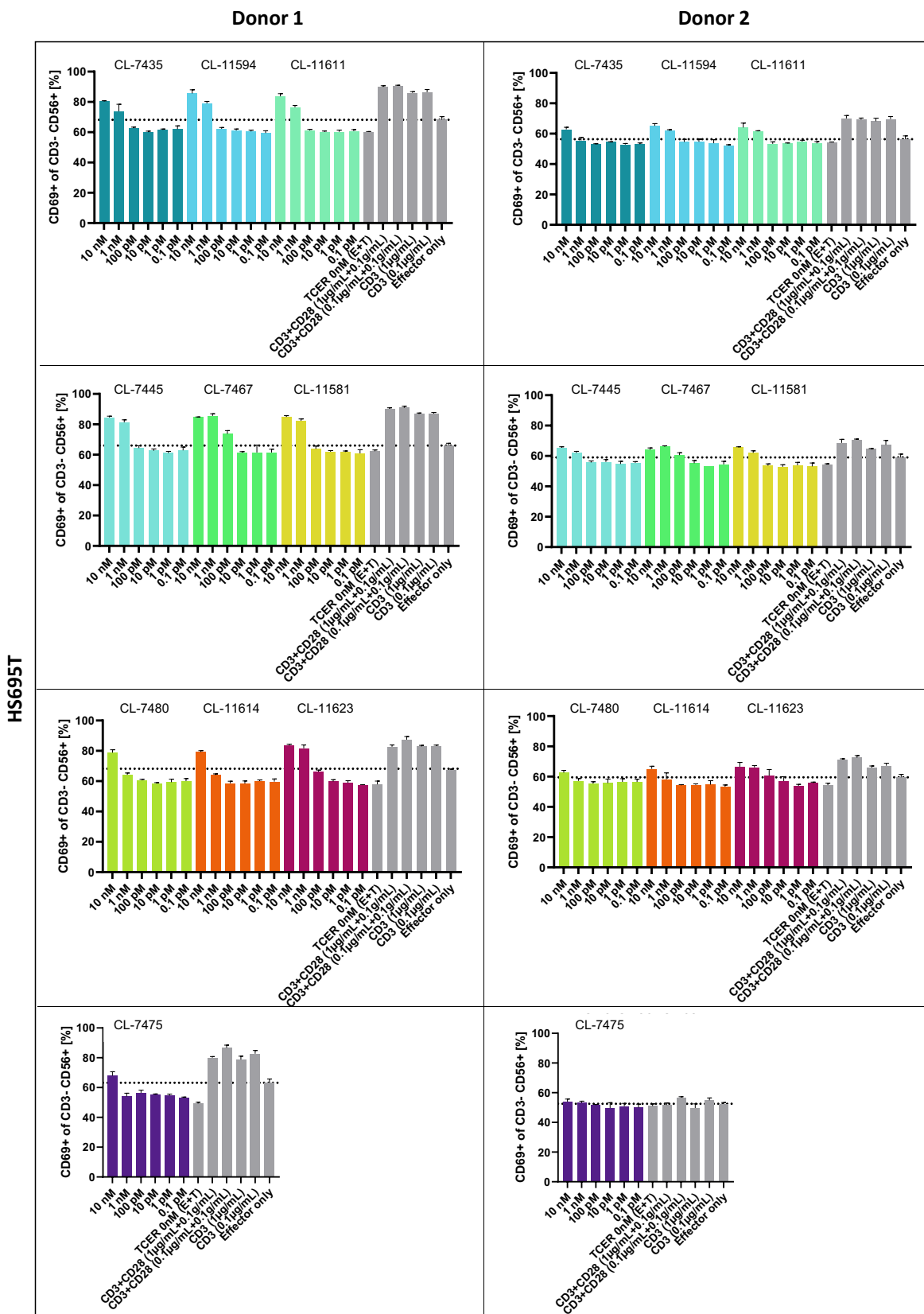
C

CD3- CD56+ CD69+
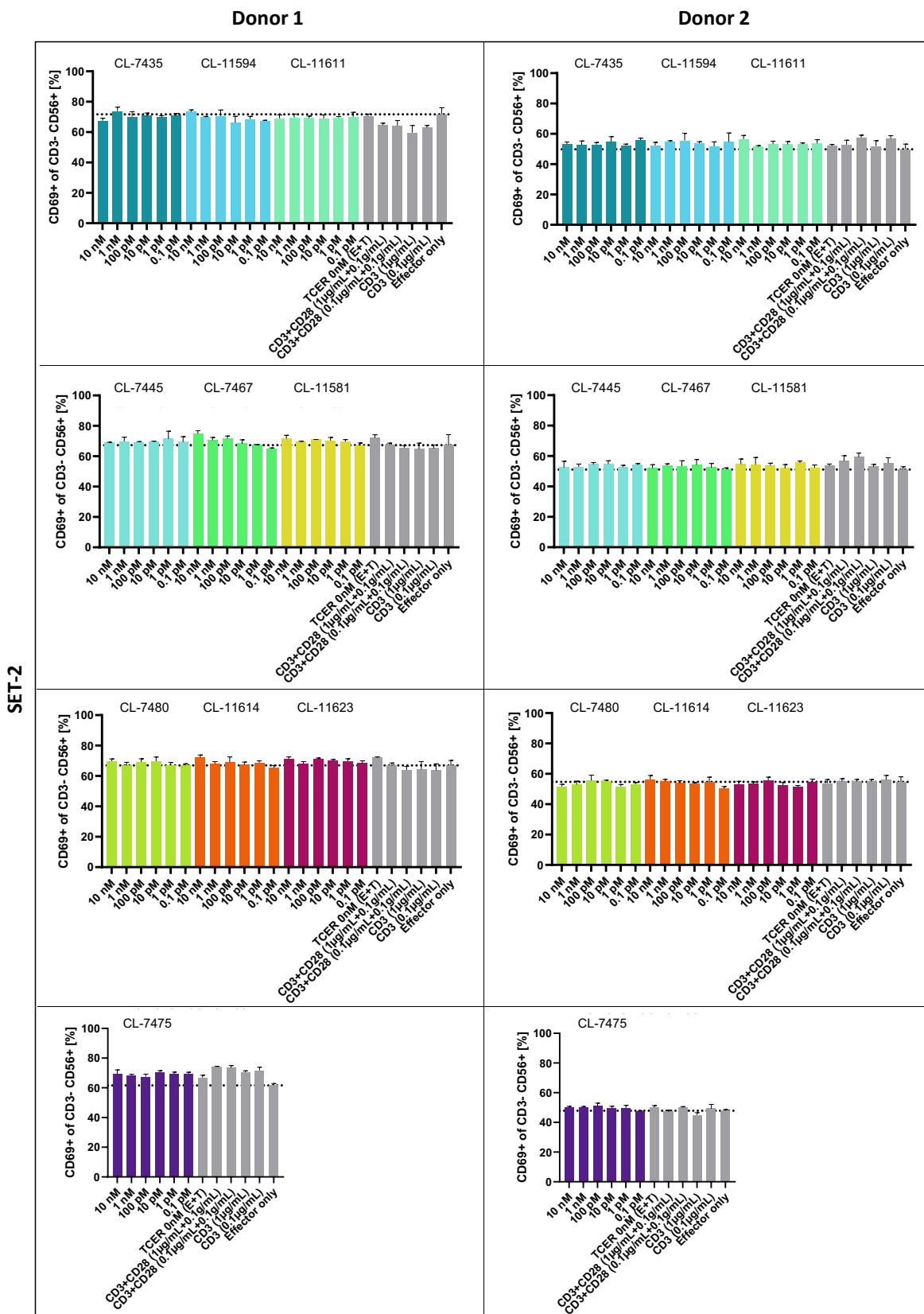
Figure 31: Results of flow cytometry-based activation assays of selected TCER® candidates for NK cells. The potential to induce an anti-tumor response of the candidates was evaluated via activation assays after co-culture with PBMCs from a

healthy donor and two different tumor cell lines (UACC-257 and HS695T). SET-2 was used as a target negative cell line. Activation was measured using CD69 activation. A) Activation profile of NK cells after incubation with different TCER® concentrations ranging from 10 nM - 1 pM in response to UACC-257 cells. B) Activation profile of NK cells after incubation with different TCER® concentrations ranging from 10 nM - 1 pM in response to HS695T cells. C) Activation profile of NK cells after incubation with different TCER® concentrations ranging from 10 nM - 1 pM in response to SET-2 cells. All experiments were performed with an E:T ratio of 10:1. Each datapoint represents the mean of a triplicate with the respective SD.

Cytokine release assays were performed to further assess the immune effects provoked by the three potent TCER® candidates, CL-7445, CL-7467, and CL-11581. All three candidates induced the release of IL-2, perforin, granzyme B, and IFNy from human PBMCs when co-cultured with UACC-257 cells. The most robust response was provoked by CL-7467, the highest affinity candidate also showing superiority in target cell killing and activation of immune cells. CL-7467 triggered the release of perforin, granzyme B, and IFNy already at a TCER® concentration of 100 pM, while an IL-2 release was observed at 1 nM. No or no TCER® dependent cytokine release was measured for any tested candidate in the presence of the target negative cell line SET-2.

A   **UACC-257**
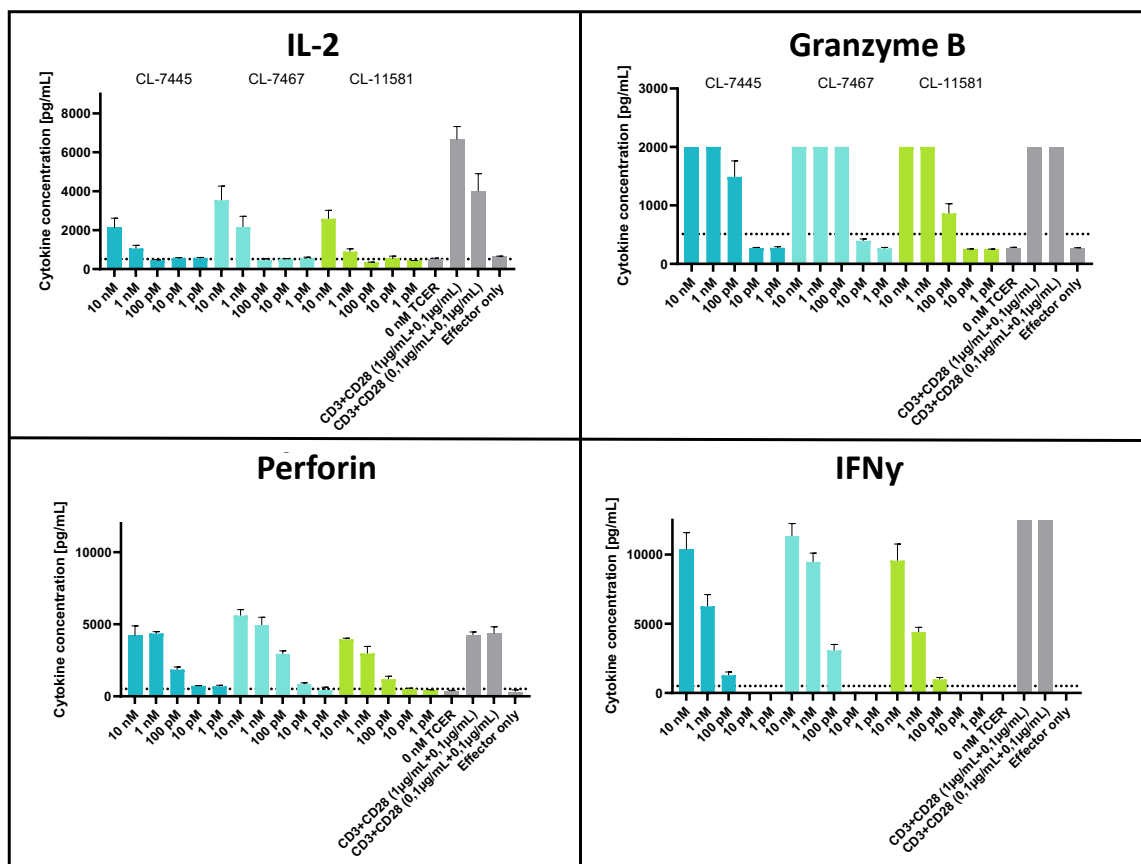
B   **SET-2**
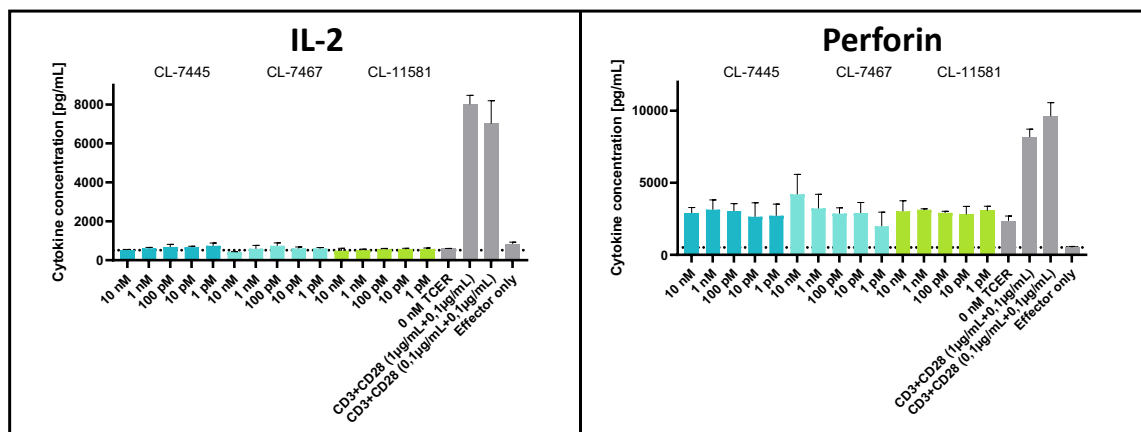
Figure 32: Assessment of TCER®-mediated cytokine release from PBMC in response to tumor cell lines. PBMCs of a healthy human donor were co-cultured with tumor cells at an effector to target ratio of 10:1 and in the presence of increasing TCER® concentrations in the range of 10 nM to 1 pM. CD3 and CD28 antibodies were used as positive control. A) UACC-257 cells (1100 cpc) were used as a PRAME pHLA positive cell line and B) SET-2 as a target negative one. Each datapoint represents the mean of a triplicate with the respective SD.

5 Discussion

5.1 Display Design

5.1.1 Choice of Gene Editing Approach

One of the key features of display technologies for the successful selection of molecules with desired characteristics is the genotype phenotype coupling[76]. For mammalian display this coupling is most reliably achieved by targeted integration since alternative integration technologies through standard transfection, viral transduction, or transposases can lead to random and multiple DNA integrations into one cell[114,122,123], which considerably hamper the selection and isolation of the genomic information[76]. In this work, a targeted integration approach was chosen via the generation of a stable landing pad in CHO cells. The presence of a single copy and stable landing pad was determined carefully to enable a profound coupling of the phenotype to the genotype of each CHO cell. Even though, random integration technologies can also result in single copy integration events via precise titration of DNA or viral particles used[114,122,123], it still has the major downside of variable expression levels of the different library candidates due to unequal transcriptional activity of the different integration sites[76]. Another key aspect to consider for mammalian display is the possible library size. Targeted approaches via CRISPR/Cas9 and TALEN have enabled great advancements in the generation of larger mammalian display libraries, like for monoclonal antibodies with library sizes of 10^5 - 10^7 antibody variants[113,162]. Throughout this work, an RMCE approach was used that, besides freedom to operate aspects, allows for generation of large libraries sizes similar to CRISPR/Cas9- and TALEN-based approaches. RMCE-based systems can also be combined with SHM processes to further increase the library size[117,163]. This feature can easily be integrated in the newly established system since AID activity was also reported to work on TCR sequences[164]. Even without SHM, the display approach established here, has the potential to be scaled up tremendously via flow electroporation protocols allowing electroporation of 1×10^{11} CHO cells in a 30 min cycle and thus theoretically resulting in libraries of about 1×10^9 variants. In summary, the RMCE approach can generate targeted mammalian display libraries in the scale of CRISPR/Cas9 and TALEN-based systems and has the potential to be coupled with SHM technologies. This makes the RMCE-based approach very valuable for biomolecule engineering in mammalian cells, such as CHO cells.

5.1.2 Choice of Recombinase

Following the selection of an RMCE-based approach for CHO display, the choice of the best fitting recombinase had to be made. Many different recombinases can be used for the exchange of genetic information at specific loci. However, all possible recombinases have different characteristics regarding exchange efficiency, specificity, and toxicity. Depending on the needs of a system the choice should be considered carefully.

The exchange efficiency is an important factor when it comes to the generation of larger libraries. Novel gene editing tools like CRISPR/Cas9-dependent systems for targeted integration had a huge impact on the establishment of new mammalian display systems yielding exchange rates of 0.5 % - 1.2 % in HEK 293 cells[113] and with 2.2 % - 5.1 % in CHO cells[120,165]. This is in line with the reported rates of TALEN-based systems ranging between 2.7 % and 5.1 %[113]. Similar exchange efficiencies have been reported for Flp-based systems and an efficiency-enhanced variant of Flp recombinase resulted even in 7.3 % exchange rate in CHO cells[120]. Cre recombinase, that also allows for repeated exchange, showed comparable or even higher rates than Flp recombinase in embryonic stem cells[166] or HEK 293 cells[167], respectively. However, usage of a Dual-RMCE systems with Flp and Cre recombinases did not seem to increase exchange efficiency with yields around 0.3 % in CHO[117]. Highly efficient exchanges have been achieved with ΦC31 recombinase reaching a maximum exchange rate of 13.1 % in CHO cells[119], but the recognized recombination sites do not allow repeated usage and are therefore not suited for the setup of a landing pad-containing cell line. Nevertheless, the exchange rates of 4 - 5 % of the here presented work with a Flp-based RMCE compares favorably with the putative more efficient CRISPR/Cas9- or TALEN-based system and is in line with recombinase efficiencies reported before.

Beyond exchange rate, recombinases can furthermore be judged by their specificity. Different research groups reported the presence of pseudo sites for the ΦC31 recombination sites in the human[148,168] or mouse genome[148]. Pseudo sites are sequences that present a certain similarity to the actual recombination sites leading to off-target activities with their number being estimates to range around 100-1000[148]. These pseudo sites can be beneficial if an unmodified genome should be targeted, but since integration will take place at multiple sites, it undermines a robust single copy integration as needed for a genotype phenotype coupling[118]. The presence of pseudo sites is not only documented for the ΦC31 integrase but also for Cre in mammalian cells. Therefore, it is speculated that these also exist for other

recombinases like Flp[169], but to our knowledge no such sites have been identified. Pseudo sites may appear as possible explanation for the background integration seen for the 1st generation CHO cell line, but this explanation seems unlikely, since no recombinase was added. Hence, random integration into the host genome presents a plausible reason for this background integration events[148]. Even though pseudo sites might exist also for Flp they are most likely not interfering with the established process as Branda and Dymecki concluded that the pseudo sites do not seem to hamper the desired outcome in most of the cases, since for example Cre is often used for genomic rearrangements *in vitro* and *in vivo* without any unwanted effects[142]. Nevertheless, there are reports about unwanted recombination events leading to cell growth arrest or chromosomal aberrations, but in these cases Cre was expressed at very high levels leading to a toxicity due to prolonged presence of high protein levels[170,171]. With no such toxicity reported, Flp seems a good choice for the implementation of the presented CHO display since this recombinase exhibits the highest specificity and lowest cross-reactivity[172]. Moreover, the exchange efficiency might be improved by applying an activity enhanced version, such as Flpe[147]. Besides the type of recombinase, the application form represents an important characteristic. In this work significantly higher exchange rates were observed when RNA-encoded Flp was used compared to DNA-based Flp expression. The increase in the exchange efficiency seen for RNA-encoded Flp might simply be explained by the faster availability of the RNA for translation compared to DNA which first needs to be transcribed. This might lead to a faster and more robust Flp level in the cells and a more efficient exchange reaction when transfected with RNA. Due to this finding, RMCE reactions were all conducted with Flp RNA throughout this work.

5.2 Generation of CHO Cell Line

The generation of a landing pad containing cell line was well demonstrated by Chen and colleagues in the context of maturation of antibodies. In their work, sorting of GFP clones resulted in a pool of high expressing cells as a prerequisite for a robust GOI expression from the tagged locus. In contrast to Chen *et al.*, the landing pad containing line generated in this work carries an RFP expressing cassette instead of Puromycin resistance allowing sorting of RFP positive and GFP negative cells resulting in an enrichment of cells with a putative single integration site[117]. Furthermore, the presence of RPF in non-exchanged cells enables a direct

flow cytometry-based sorting of RFP negative cells as a marker for a successful exchange[173]. The increase of the GFP MFI over the two selection rounds and the constant RFP expression of the landing pad containing clones indicated that the prerequisites of high and stable expression are fulfilled for both clonal candidates. As an important criterion, the single copy integration, was confirmed via TLA analysis and allowed a very detailed insight into the integration site and the copy number. When comparing the TLA data of the 1st and 2nd generation landing pad it appears that the investigated CHO clones of the 1st generation had all different breakpoints while the ones from the 2nd generation exhibited the anticipated breakpoint in the *ampicillin resistance* gene of the donor vector. This difference might be explained by occurrence of random integration events of the RFP-containing donor vector in the 1st generation leading to more diverse integration. In contrast, the presence of only one breakpoint for all clones of the 2nd generation landing pad indicates a clonal relationship[148], most probably originating from linear insertion of the GFP carrying vector and a correct RMCE exchange. These results support the superiority of the 2nd generation vector design, lacking the CMV promotor on the donor vector, over the 1st generation, since random integration events of the donor vector will not lead to RFP expression. Expression of RFP will only occur when integrated correctly into the targeted locus with the integrated hCMV promotor or if by chance integrated in frame behind a promotor of the host genome. Despite its background integration level, the 1st generation landing pad was fully functional while the 2nd generation version additionally prevented expression of randomly integrated target protein copies, which for this generation will likely still occur.

5.3   Evaluation of Different TCR Formats in CHO Display

Different constructs of soluble TCR formats were tested in CHO display using the established landing pad containing cell line with the aim of evaluating the application range of the new system for engineering of TCR-based biomolecules. All formats used the variable domains of a maturated PRAME-targeting model TCR linked in a monovalent fashion with either the N-terminus of an IgG Fc region (ScFc-scTv) or with the heavy (HC-scTv) or the light chain (LC-scTv) of an CD3-binding Fab region. A fourth format (TCER®) used the TCR and CD3 Ab variable domains in a diabody-like design with an Fc region attached. In addition, the TCR was also expressed as monovalent single chain TCR construct (scTv) and as bivalent symmetric Fc

conjugated construct (DuoFc-scTv). All monovalent formats contained only one TM domain for anchoring into the CHO cell membrane to just allow surface expression of heterodimeric TCR constructs. With this setup all TCR formats exhibited detectable expression on the CHO surface with only minor differences. The slightly reduced expression level of the TCER® molecule compared to the Fc- or Fab-based molecules might be due to the more complex structure. The comparable target and off-target binding of all formats can be explained by the fact that they all share the same TCR variable domains of the PRAME-binding model TCR. The only difference is the bivalency of the DuoFc-scTv formats leading to stronger binding due to avidity effects[174], which may also explain the binding to off-targets not recognized by any other format. Therefore, this comparison of different formats has demonstrated that some formats are especially suited to evaluate certain binding characteristics of the underlying TCR like the DuoFc-scTv format for the sensitive detection of potentially relevant off-target peptides. Although the TCER® might not be the optimal format for evaluating the TCR binding characteristics its usage is linked to the huge advantage of maturating the TCR domains in the final therapeutic format and the relevant expression cell line. Recent studies demonstrated that a switch between screening format and therapeutic format can be accompanied by a reduction in affinity also including loss of function. These findings are supported by internal observations when transferring certain yeast display-derived scTv mutations into the TCER® format resulted in unexpected loss of expression or loss of affinity. This might be due to two possible reasons, such as the finding that CHO cells tend to better express molecules matured in a CHO system[117] or the fact that the TCR binding domains are packed very densely with an eight amino acid linker and thus mutations might interfere with the structural setup of the TCER® format allowing only small variations in the angle between α and β domains important for target recognition of TCRs[175]. Minor variations in the structure based on added mutations might lead to changes in the binding behavior due to changed angles of the TCER® domains resulting in reduced or complete loss of target binding. One additional advantages of this system employing the final bispecific TCR format is thus related to the ability to select mutations potentially beneficial for the interdomain stability of the TCER® molecules.

5.4 TCR Maturation Using CHO Display of TCER® Molecules

5.4.1 Generation and Selection of PRAME-specific TCER® Library

PRAME is an attractive target for immunotherapy since its expression is mainly restricted to tumor tissues and germline cells making it a promising target in various cancer entities like metastatic uveal melanoma[176] and sarcoma subtypes[177,178]. The importance of PRAME as a valuable target is shown by various preclinical[179,180] and clinical efforts to generate PRAME-specific therapies[181] reinforcing the significance of this work in maturating a PRAME-specific TCER®. To demonstrate that the established CHO display can achieve this in the context of full TCER® molecules, a CDR combinatorial library was designed based on a PRAME-specific model TCR whose CDR mutations were previously identified from an independent yeast display-based TCR maturation campaign. Different combinations of mutated CDRs can have dramatic impact on the stability and affinity of a TCR, which is supported by internal findings that some combinations of affinity increasing mutated CDRs can also result in decreased binding affinity. The same principle was also previously used in an antibody maturation environment combining smaller CDR libraries selecting optimized scFv candidates for target binding and eliminating non-functional combinations[182]. A systematic screening of all possible combinations of mutated CDRs is therefore beneficial to identify appropriate TCR variants for an increased target binding.

5.4.2 Evaluation of TCER® Expression and Binding in CHO Display

The systematic combination 2, 6, 16, 6, 16, and 2 variants of CDRα1, CDRα2, CDRα3, CDRβ1, CDRβ2, and CDRβ3, respectively, resulted in the identification of 39 unique PRAME TCR sequences, each representing different combinations of the input CDR sequences. The presence of only one out of 16 CDRβ2 input sequences supported the successful selection via the CHO display resulting in TCER® variants with improved PRAME pHLA binding. The mentioned stringency seen for CDRβ2, mainly involved in HLA binding[183], allows the assumption that stabilized binding of the HLA backbone led to a higher affinity binding of the PRAME pHLA. In contrast, the higher diversity of identified CDRα2 and CDRβ1 sequences suggest a minor role of these CDRs in the affinity gain. Peptide binding mainly involves CDRα3 and CDRβ3 but the limited stringency of CDR3 sequences identified after TCR affinity

maturation with a continuous counterselection rather argues against a major role of these CDRs in gaining affinity. Based on the results it can be concluded that the affinity increasement is primarily based on a more stable HLA binding than on an increased and specific target binding. Nevertheless, some small influence of the CDRα3 and CDRβ3 on the affinity can be observed when combining the sequence data with the affinity measurement displaying similarities between the 6 candidates with the lowest K_D values. They all display a methionine at the last position of the CDRα3 while all remaining candidates display a lysine or isoleucine. Therefore, the methionine at this position seems to have a beneficial influence on the affinity of the TCR domain. It can also be noted that the SGHRS motive of the CDRβ1 displayed by three of four of the candidates with the highest K_D values is prompting to a rather negative influence on the binding affinity.

The assumption that the affinity increasement is driven by a stronger binding to the HLA backbone via CDRβ2 would further explain the rather broad off-target recognition of the TCR candidates. The sequence similarities of the recognized similar peptides 9, 10, and 11 point to a C-terminal binding of the PRAME peptide with a predominant role of histidine and isoleucine at positions 5 and 7, respectively. During the maturation process not a single candidate without major off-target recognition could be isolated pointing towards the notion that such off-target recognition represents an inherent property of the parental PRAME TCR used for the affinity maturation rather than being a general weakness of the established system. This assumption is supported by internal observations that few TCRs cannot be satisfactorily matured due to insufficient stability, low starting affinity or due to gain of off-target recognition during maturation, which might be attributed to particular features of the parental TCRs. Nevertheless, this established CHO display system allows the profound selection of high-affinity TCER® candidates while the quality and binding characteristics of the underlying parental TCR strongly influence the final maturation success.

5.4.3 Affinity Determination for Solubly Expressed TCER® Candidates

TCRs in a physiological setting exhibit binding affinities in the micromolar range and maintain a self-tolerance through negative selection in the thymus and high affinity TCRs recognizing tumor targets at quite low copy numbers on tumors are very rare. Therefore, the generation of high affinity TCRs with a significant increase of the affinity in the nanomolar range or lower

via *in vitro* maturation systems is necessary resulting in TCRs recognizing low epitope numbers[184]. The measured affinities of the maturated TCRs were in the single digit nanomolar range demonstrating that the combination of yeast display and mammalian display in this case, can result in the isolation of high affinity TCRs with the potential to recognize sub physiological target pHLA copy numbers. In line with this, first biotherapeutics with high affinity TCR domains[37] showed promising anti-tumor responses in patients resulting in the FDA approval of the gp100-targeting ImmTAC molecule[30]. Even though an increased affinity is associated with the recognition of lower copy numbers this concept cannot be generalized[185] and TCR candidates need a further evaluation of their target recognition potential.

5.4.4 Assessment of TCER®-mediated Killing of Tumor Cells

Functional assessment of the TCER® candidates showed that all selected candidates mediated target cell killing to different extents reflecting two effects already seen in the evaluation of other TCR-based bispecific molecules. This is on the one hand, the copy number dependency of the cytotoxicity resulting in decreased mediated lyses in cell lines with lower target pHLA numbers on the surface[186]. And on the other hand, the dependency of the cytotoxic potential on the affinity of the molecules. The presented results show that the higher affinity candidates with K_D values below or slightly above 10 nM induced target cell killing more efficiently than the remaining ones. Therefore, the TCR affinity is an important criterion for the *in vitro* efficacy of TCR-based bispecifics. The observed lysis rate of 10-50 % in target pHLA positive cell lines with low copy numbers is comparable with the one observed for the gp100-specific ImmTAC even though the experimental setups are not completely comparable. For instance, the ImmTAC molecule was evaluated in the presence of purified cytotoxic CD8$^+$ T cells while the TCER® candidates were incubated with PBMCs. This difference might explain the higher cytotoxicity of the ImmTAC molecule at lower concentrations[74]. When comparing the TCER® candidates with a TCR mimic antibody also targeting a PRAME-derived peptide in an HLA context investigated in a different study, the selected TCER® candidates demonstrate higher cytotoxic potential[180] supporting a TCR-based approach for the targeting of pHLA targets.

Besides efficacy against target-positive tumor cells, also the specificity of the TCER® candidates was evaluated and off-target recognition, visualized via the killing of target-negative T98G cells, could be observed for all candidates at concentrations between 100 pM and 1 nM depending on the K_D values of the candidates. In case of target-negative SET-2 cells such an off-target killing was seen at concentrations above 1 nM. The higher susceptibility for off-target-mediated killing of T98G cells might be explained by the high HLA expression level in T98G resulting in increased off-target pHLA presentation. The off-target reactivity is a key factor for clinical safety and needs to be closely monitored. The importance of this was shown by several examples of unpredicted off-target effects resulting in neurotoxicity after the application of blinatumomab, an anti-CD19/anti-CD3 bispecific antibody,[187] and CD19 chimeric antigen receptors[188]. The application of an enhanced MAGE-A3 targeting TCR even resulted in fatalities of probands due to cross-reactivity to a healthy tissue pHLA[189,190]. The here selected candidates are therefore most probably not suited for further development as therapeutic agents, since unwanted off-target reactivity are observed in target negative cell lines pointing to an insufficient specificity of the underlying TCR and the TCER® candidates.

5.4.5 Immune Activation of Selected TCER® Candidates

In addition to tumor cell killing, the assessment of lymphoid cell activation gives a more detailed insight into the different cell types involved in the anti-tumor response. The superior role of the more affine TCER® candidates especially CL-7467 is further strengthened by the activation profile of CD4$^+$, CD8$^+$, and NK cells inducing robust activation measured via CD69 upregulation. The CD69 marker is one of the earliest activation markers for lymphoid activation detectable on T cells and NK cells acting as a costimulatory molecule for activation and proliferation leading to the production of cytokines including IL-2[191]. Even though newer findings also point to the role of CD69 in the immune escape of tumors via mediating T cell exhaustion[192], the combined data of activation and cytokine release allow the assumption that the tested TCER® candidates specifically mediated effector cell activation also resulting in a profound release of granzyme B, perforin, IL-2, and INFγ. The observed activation of CD3$^-$ NK cell might be explained by a kind of bystander activation induced by high levels of cytokines released from activated T cells during the incubation period. This phenomenon is

known from unspecific T cell activation and was also observed for NK cell in mice in the context of viral infections[193]. The upregulation of CD69 mediated by higher affinity TCER® molecules in the presence of target negative SET-2 cells with no detectable release of relevant cytokines suggest no off-target killing but CD69 upregulation due to other effects mediated by high TCER® concentrations. The affinity dependency of the provoked response also seen throughout the killing assays was in line with the ImmTAC molecules[74].

5.5 Conclusion and Outlook

Throughout the study it was shown that the landing pad containing CHO display system has a great value for the maturation of TCR domains in context of full TCER® molecules, since it has a stable single copy integration ensuring a uniform expression during the maturation campaign. Furthermore, a good correlation between the membrane-bound TCER® candidates and their soluble counterparts was seen with candidates showing more promising functional results like target cell killing, effector cell activation, and cytokine release already standing out in the membrane-bound analysis with first detectable PRAME pHLA binding at 0.1 nM. This enables a profound selection of promising candidates already early in the selection process out of a larger candidate pool without the need of producing all potential candidates as soluble molecules. Even though the maturation of the model TCR targeting PRAME pHLA did not result in the isolation of a candidate suited for further clinical development, the system is well suited for the maturation of an alternative parental TCR with a more specific binding pattern, hopefully resulting in the identification of a TCER® candidate for a potential therapeutic application.

Although the display system is already highly functional, it can be improved via the usage of efficiency enhanced version of the Flp recombinase[147] increasing the exchange rate[120] allowing the generation of larger libraries. Another option to increase the exchange efficiency is the usage of an alternative recombinase reported to mediate exchange rates superior to Flp recombinase, but not suitable for the setup of stable landing pad containing cell line due to non-reusable recombination sites like the ΦC31 recombinase[119]. Moreover, the system can be extended via the coupling with SHM, which is already successfully established for the maturation of antibodies[129,137,194] and TCRs[164,195] allowing repeated cycles of affinity maturation leading to very large libraries with continuous screening of binding and expression

characteristics via flow cytometry. Since the AID enzyme mainly focusses on CDR regions[196], it should be taken into account that also the CD3 binding moiety will be targeted for mutation if complete TCER® molecules are maturated. Besides affinity maturation of the TCR moiety, also the optimization of the TCER® molecules as a whole could be achieved for example via random mutagenesis of the interface region the TCR and CD3 binding domains enabling the isolation of stabilized molecules possibly resulting in enhanced target binding or improved soluble expression. The secretion of soluble proteins directly from the display cells via alternative splicing is likewise a method of interest, allowing a more rapid functional assessment without the need of a separate soluble expression culture[197]. All in all, the here established system is already a valuable tool for the development of TCR-based bispecifics and holds great potential to be extended to display very large libraries and give an even more detailed assessment of developability characteristics.

6 Appendix

6.1 Sequences

6.1.1 DuoFc-scTv

```
ATG AAG TGG GTC ACC TTT ATC AGT CTG CTG TTT CTG TTC TCT AGT GCC TAT TCT CAA
 M   K   W   V   T   F   I   S   L   L   F   L   F   S   S   A   Y   S   Q

AAA GAG GTC GAG CAG AAC AGC GGC CCT CTG TCT GTT CCT GAG GGC GCT ATC GCC TCT
 K   E   V   E   Q   N   S   G   P   L   S   V   P   E   G   A   I   A   S

CTG AAC TGC ACC TAC TCC GAC AGA GGC TCC CAG AGC TTC TTC TGG TAC AGA CAG TAC
 L   N   C   T   Y   S   D   R   G   S   Q   S   F   F   W   Y   R   Q   Y

TCC GGC AAG TCC CCT GAG CTG ATC ATG TCC ATC TAC CAA GAG GGC GAC AAA GAG GAC
 S   G   K   S   P   E   L   I   M   S   I   Y   Q   E   G   D   K   E   D

GGC CGG TTT ACC GCT CAG CTG AAC AAG GCC TCT CAG TAC GTG TCC CTG CTG ATC CGG
 G   R   F   T   A   Q   L   N   K   A   S   Q   Y   V   S   L   L   I   R

GAC TCC CAG CCT TCT GAT TCT GCC ACC TAC CTG TGT GCC GCC GTG ATC GAC AAT GAC
 D   S   Q   P   S   D   S   A   T   Y   L   C   A   A   V   I   D   N   D

CAA GGC GGC ATC CTG ACC TTC GGC ACC GGA ACC AGA CTG ACA ATC ATC CCC AAC ATC
 Q   G   G   I   L   T   F   G   T   G   T   R   L   T   I   I   P   N   I

CAG AAC GGC GGT GGT GGT TCT GGC GGC GGA GGA AGC GGA GGC GGA GGT TCT GGC GGT
 Q   N   G   G   G   G   S   G   G   G   G   S   G   G   G   G   S   G   G

GGT GGT TCT GGC GGC GGA GGA AGC AAA GCT GGT GTC ACC CAG ACA CCT AGA TAC CTG
 G   G   S   G   G   G   G   S   K   A   G   V   T   Q   T   P   R   Y   L

ATC AAG ACC AGA GGC CAG CAA GTG ACA CTG TCC TGC TCT CCC ATT CCT GGC CAC AGA
 I   K   T   R   G   Q   Q   V   T   L   S   C   S   P   I   P   G   H   R

GCC GTG TCC TGG TAT CAG CAG ACA CCA GGC CAG GGC CTG CAG TTT CTG TTC GAG TAT
 A   V   S   W   Y   Q   Q   T   P   G   Q   G   L   Q   F   L   F   E   Y

GTG CAC GGC GAG GAA CGG AAC AAG GGC AAC TTC CCC GGC AGA TTC TCC GGC AGA CAG
 V   H   G   E   E   R   N   K   G   N   F   P   G   R   F   S   G   R   Q

TTC TCC AAC TCC TCC AGC GAG ATG AAC ATC TCC AAC CTG GAA CTG GGC GAC AGC GCC
 F   S   N   S   S   S   E   M   N   I   S   N   L   E   L   G   D   S   A

CTG TAC CTG TGT GCT TCT TCT CCT TGG GAC TCC CCT AAC GTG CAG TAC TTC GGC CCT
 L   Y   L   C   A   S   S   P   W   D   S   P   N   V   Q   Y   F   G   P

GGC ACC AGA CTG ACC GTG ACC GAG GAT CTG AAG AAC GAG CCC AAG TCC TGT GAT AAG
 G   T   R   L   T   V   T   E   D   L   K   N   E   P   K   S   C   D   K

ACC CAT ACA TGC CCA CCT TGT CCA GCT CCA CCA GTG GCT GGC CCT AGC GTG TTC CTG
 T   H   T   C   P   P   C   P   A   P   P   V   A   G   P   S   V   F   L

TTT CCT CCA AAG CCT AAG GAC ACC CTG ATG ATC TCC AGG ACC CCA GAG GTG ACA TGC
 F   P   P   K   P   K   D   T   L   M   I   S   R   T   P   E   V   T   C

GTG GTG GTG GAC GTG AGC CAC GAG GAC CCC GAG GTG AAG TTT AAC TGG TAC GTG GAT
```

```
     V   V   V   D   V   S   H   E   D   P   E   V   K   F   N   W   Y   V   D

GGC GTG GAG GTG CAT AAT GCC AAG ACC AAG CCT AGG GAG GAG CAG TAC CAG TCT ACC
 G   V   E   V   H   N   A   K   T   K   P   R   E   E   Q   Y   Q   S   T

TAT CGG GTG GTG TCC GTG CTG ACA GTG CTG CAT CAG GAC TGG CTG AAC GGC AAG GAG
 Y   R   V   V   S   V   L   T   V   L   H   Q   D   W   L   N   G   K   E

TAT AAG TGC AAG GTG TCT AAT AAG GCC CTG CCC GCC TCC ATC GAG AAG ACC ATC TCT
 Y   K   C   K   V   S   N   K   A   L   P   A   S   I   E   K   T   I   S

AAG GCC AAG GGC CAG CCA AGA GAG CCC CAG GTG TAC ACA CTG CCC CCT TCC CGC GAC
 K   A   K   G   Q   P   R   E   P   Q   V   Y   T   L   P   P   S   R   D

GAG CTG ACC AAG AAC CAG GTG AGC CTG ACA TGT CTG GTG AAG GGC TTC TAT CCC AGC
 E   L   T   K   N   Q   V   S   L   T   C   L   V   K   G   F   Y   P   S

GAC ATC GCT GTG GAG TGG GAG TCT AAT GGC CAG CCT GAG AAC AAT TAC AAG ACC ACA
 D   I   A   V   E   W   E   S   N   G   Q   P   E   N   N   Y   K   T   T

CCA CCC GTG CTG GAC TCC GAT GGC AGC TTC TTT CTG TAT TCT AAG CTG ACC GTG GAT
 P   P   V   L   D   S   D   G   S   F   F   L   Y   S   K   L   T   V   D

AAG TCC AGG TGG CAG CAG GGC AAC GTG TTT TCT TGC TCC GTG ATG CAC GAG GCC CTG
 K   S   R   W   Q   Q   G   N   V   F   S   C   S   V   M   H   E   A   L

CAC AAT CAT TAC ACA CAG AAG AGC CTG TCT CTG TCC CCA GGC AAG GCC GTG GGC CAG
 H   N   H   Y   T   Q   K   S   L   S   L   S   P   G   K   A   V   G   Q

GAC ACC CAG GAG GTG ATC GTG GTG CCC CAC TCC CTG CCC TTC AAG GTG GTG GTG ATC
 D   T   Q   E   V   I   V   V   P   H   S   L   P   F   K   V   V   V   I

TCC GCC ATC CTG GCC CTG GTG GTG CTG ACC ATC ATC TCC CTG ATC ATC CTG ATC ATG
 S   A   I   L   A   L   V   V   L   T   I   I   S   L   I   I   L   I   M

CTG TGG CAG AAG AAG CCC AGG TAA TGA
 L   W   Q   K   K   P   R   *   *
```

6.1.2 HC-scTv

```
ATG AAA TGG GTC ACC TTT ATC TCC CTG CTG TTC CTG TTC TCC TCC GCC TAC CAA CAA
 M   K   W   V   T   F   I   S   L   L   F   L   F   S   S   A   Y   Q   Q

AAA GAG GTC GAG CAG AAC AGC GGC CCT CTG TCT GTT CCT GAG GGC GCT ATC GCC TCT
 K   E   V   E   Q   N   S   G   P   L   S   V   P   E   G   A   I   A   S

CTG AAC TGC ACC TAC TCC GAC AGA GGC TCC CAG AGC TTC TTC TGG TAC AGA CAG TAC
 L   N   C   T   Y   S   D   R   G   S   Q   S   F   F   W   Y   R   Q   Y

TCC GGC AAG TCC CCT GAG CTG ATC ATG TCC ATC TAC CAA GAG GGC GAC AAA GAG GAC
 S   G   K   S   P   E   L   I   M   S   I   Y   Q   E   G   D   K   E   D

GGC CGG TTT ACC GCT CAG CTG AAC AAG GCC TCT CAG TAC GTG TCC CTG CTG ATC CGG
 G   R   F   T   A   Q   L   N   K   A   S   Q   Y   V   S   L   L   I   R

GAC TCC CAG CCT TCT GAT TCT GCC ACC TAC CTG TGT GCC GCC GTG ATC GAC AAT GAC
 D   S   Q   P   S   D   S   A   T   Y   L   C   A   A   V   I   D   N   D

CAA GGC GGC ATC CTG ACC TTC GGC ACC GGA ACC AGA CTG ACA ATC ATC CCC AAC ATC
```

```
     Q   G   G   I   L   T   F   G   T   G   T   R   L   T   I   I   P   N   I
CAG AAC GGA GGC GGC GGA TCT GGC GGC GGA GGA AGC GGA GGC GGA GGT TCT GGC GGT
 Q   N   G   G   G   G   S   G   G   G   G   S   G   G   G   G   S   G   G

GGT GGT TCT GGC GGA GGC GGA AGC AAA GCT GGT GTC ACC CAG ACA CCT AGA TAC CTG
 G   G   S   G   G   G   G   S   K   A   G   V   T   Q   T   P   R   Y   L

ATC AAG ACC AGA GGC CAG CAA GTG ACA CTG TCC TGC TCT CCC ATT CCT GGC CAC AGA
 I   K   T   R   G   Q   Q   V   T   L   S   C   S   P   I   P   G   H   R

GCC GTG TCC TGG TAT CAG CAG ACA CCA GGC CAG GGC CTG CAG TTT CTG TTC GAG TAT
 A   V   S   W   Y   Q   Q   T   P   G   Q   G   L   Q   F   L   F   E   Y

GTG CAC GGC GAG GAA CGG AAC AAG GGC AAC TTC CCC GGC AGA TTC TCC GGC AGA CAG
 V   H   G   E   E   R   N   K   G   N   F   P   G   R   F   S   G   R   Q

TTC TCC AAC TCC TCC AGC GAG ATG AAC ATC TCC AAC CTG GAA CTG GGC GAC AGC GCC
 F   S   N   S   S   S   E   M   N   I   S   N   L   E   L   G   D   S   A

CTG TAC CTG TGT GCT TCT TCT CCT TGG GAC TCC CCT AAC GTG CAG TAC TTC GGC CCT
 L   Y   L   C   A   S   S   P   W   D   S   P   N   V   Q   Y   F   G   P

GGC ACC AGA CTG ACC GTG ACC GAG GAT CTG AAG AAC GAA CCC AAG TCC TGC GAC AAG
 G   T   R   L   T   V   T   E   D   L   K   N   E   P   K   S   C   D   K

ACC CAC ACC TGT CCC CCT TGT CCT GTG CAG CTG CAG CAG TCT GGA CCC GAG CTC GTG
 T   H   T   C   P   P   C   P   V   Q   L   Q   Q   S   G   P   E   L   V

AAG CCT GGC GCC TCC GTG AAG ATG TCC TGC AAG GCC TCC GGC TAC AAG TTC ACC TCC
 K   P   G   A   S   V   K   M   S   C   K   A   S   G   Y   K   F   T   S

TAC GTG ATG CAT TGG GTC AAG CAG AAG CCC GGC CAG GGC CTG GAA TGG ATC GGC TAC
 Y   V   M   H   W   V   K   Q   K   P   G   Q   G   L   E   W   I   G   Y

ATC AAC CCC TAC AAC GAC GTG ACC AAG TAC AAC GAG AAG TTC AAG GGC AAG GCC ACC
 I   N   P   Y   N   D   V   T   K   Y   N   E   K   F   K   G   K   A   T

CTG ACC TCC GAC AAG TCC TCC TCC ACC GCC TAC ATG GAA CTG TCC TCC CTG ACC AGC
 L   T   S   D   K   S   S   S   T   A   Y   M   E   L   S   S   L   T   S

GAG GAC TCC GCC GTG CAC TAC TGT GCC AGA GGC TCC TAC TAC GAC TAC GAC GGC TTC
 E   D   S   A   V   H   Y   C   A   R   G   S   Y   Y   D   Y   D   G   F

GTG TAC TGG GGC CAG GGC ACC CTC GTG ACC GTG TCA TCT GCT TCC ACC AAG GGC CCA
 V   Y   W   G   Q   G   T   L   V   T   V   S   S   A   S   T   K   G   P

TCC GTG TTC CCT CTG GCC CCT TCC AGC AAG TCT ACC TCT GGC GGC ACA GCC GCT CTG
 S   V   F   P   L   A   P   S   S   K   S   T   S   G   G   T   A   A   L

GGC TGC CTC GTG AAG GAC TAC TTC CCC GAA CCG GTG ACC GTG TCT TGG AAC TCT GGC
 G   C   L   V   K   D   Y   F   P   E   P   V   T   V   S   W   N   S   G

GCC CTG ACA TCC GGC GTG CAC ACC TTT CCA GCT GTG CTG CAG TCC TCC GGC CTG TAC
 A   L   T   S   G   V   H   T   F   P   A   V   L   Q   S   S   G   L   Y

TCC CTG TCC TCC GTC GTG ACC GTG CCT TCC AGC TCT CTG GGC ACC CAG ACC TAC ATC
 S   L   S   S   V   V   T   V   P   S   S   S   L   G   T   Q   T   Y   I

TGC AAC GTG AAC CAC AAG CCC TCC AAC ACC AAG GTG GAC AAG AAG GTG GCC GTG GGC
 C   N   V   N   H   K   P   S   N   T   K   V   D   K   K   V   A   V   G
```

```
CAG GAC ACC CAG GAG GTG ATC GTG GTG CCC CAC TCC CTG CCC TTC AAG GTG GTG GTG
 Q   D   T   Q   E   V   I   V   V   P   H   S   L   P   F   K   V   V   V

ATC TCC GCC ATC CTG GCC CTG GTG GTG CTG ACC ATC ATC TCC CTG ATC ATC CTG ATC
 I   S   A   I   L   A   L   V   V   L   T   I   I   S   L   I   I   L   I

ATG CTG TGG CAG AAG AAG CCC AGG TAA TGA
 M   L   W   Q   K   K   P   R   *   *
```

6.1.3 LC-scTv

```
ATG AAG TGG GTC ACC TTT ATC GAG ACC CTG TTT CTG TTC TCA AGC GCC TAC TCT CAA
 M   K   W   V   T   F   I   E   T   L   F   L   F   S   S   A   Y   S   Q

AAA GAG GTC GAG CAG AAC AGC GGC CCT CTG TCT GTT CCT GAG GGC GCT ATC GCC TCT
 K   E   V   E   Q   N   S   G   P   L   S   V   P   E   G   A   I   A   S

CTG AAC TGC ACC TAC TCC GAC AGA GGC TCC CAG AGC TTC TTC TGG TAC AGA CAG TAC
 L   N   C   T   Y   S   D   R   G   S   Q   S   F   F   W   Y   R   Q   Y

TCC GGC AAG TCC CCT GAG CTG ATC ATG TCC ATC TAC CAA GAG GGC GAC AAA GAG GAC
 S   G   K   S   P   E   L   I   M   S   I   Y   Q   E   G   D   K   E   D

GGC CGG TTT ACC GCT CAG CTG AAC AAG GCC TCT CAG TAC GTG TCC CTG CTG ATC CGG
 G   R   F   T   A   Q   L   N   K   A   S   Q   Y   V   S   L   L   I   R

GAC TCC CAG CCT TCT GAT TCT GCC ACC TAC CTG TGT GCC GCC GTG ATC GAC AAT GAC
 D   S   Q   P   S   D   S   A   T   Y   L   C   A   A   V   I   D   N   D

CAA GGC GGC ATC CTG ACC TTC GGC ACC GGA ACC AGA CTG ACA ATC ATC CCC AAC ATC
 Q   G   G   I   L   T   F   G   T   G   T   R   L   T   I   I   P   N   I

CAG AAC GGA GGC GGC GGA TCT GGC GGC GGA GGA AGC GGA GGC GGA GGT TCT GGC GGT
 Q   N   G   G   G   G   S   G   G   G   G   S   G   G   G   G   S   G   G

GGT GGT TCT GGC GGA GGC GGA AGC AAA GCT GGT GTC ACC CAG ACA CCT AGA TAC CTG
 G   G   S   G   G   G   G   S   K   A   G   V   T   Q   T   P   R   Y   L

ATC AAG ACC AGA GGC CAG CAA GTG ACA CTG TCC TGC TCT CCC ATT CCT GGC CAC AGA
 I   K   T   R   G   Q   Q   V   T   L   S   C   S   P   I   P   G   H   R

GCC GTG TCC TGG TAT CAG CAG ACA CCA GGC CAG GGC CTG CAG TTT CTG TTC GAG TAT
 A   V   S   W   Y   Q   Q   T   P   G   Q   G   L   Q   F   L   F   E   Y

GTG CAC GGC GAG GAA CGG AAC AAG GGC AAC TTC CCC GGC AGA TTC TCC GGC AGA CAG
 V   H   G   E   E   R   N   K   G   N   F   P   G   R   F   S   G   R   Q

TTC TCC AAC TCC TCC AGC GAG ATG AAC ATC TCC AAC CTG GAA CTG GGC GAC AGC GCC
 F   S   N   S   S   S   E   M   N   I   S   N   L   E   L   G   D   S   A

CTG TAC CTG TGT GCT TCT TCT CCT TGG GAC TCC CCT AAC GTG CAG TAC TTC GGC CCT
 L   Y   L   C   A   S   S   P   W   D   S   P   N   V   Q   Y   F   G   P

GGC ACC AGA CTG ACC GTG ACC GAG GAT CTG AAG AAC GAA CCC AAG TCC TGC GAC AAG
 G   T   R   L   T   V   T   E   D   L   K   N   E   P   K   S   C   D   K

ACC CAC ACC TGT CCC CCT TGT CCT ATC GTG CTG ACC CAG TCC CCC GCC ATC ATG TCT
 T   H   T   C   P   P   C   P   I   V   L   T   Q   S   P   A   I   M   S
```

```
GCT TCT CCC GGC GAG AAA GTG ACC ATG ACC TGC TCC GCC ACC TCC TCC GTG TCC TAC
 A   S   P   G   E   K   V   T   M   T   C   S   A   T   S   S   V   S   Y

ATG CAC TGG TAT CAG CAG AAG TCC GGC ACC TCC CCC AAG CGG TGG ATC TAC GAC ACC
 M   H   W   Y   Q   Q   K   S   G   T   S   P   K   R   W   I   Y   D   T

TCC AAG CTG GCC TCT GGC GTG CCC GCT AGA TTC TCC GGC TCT GGC TCC GGC ACC TCC
 S   K   L   A   S   G   V   P   A   R   F   S   G   S   G   S   G   T   S

TAC TCC CTG ACC ATC TCC TCC ATG GAA GCC GAG GAT GCC GCC ACC TAC TAC TGC CAG
 Y   S   L   T   I   S   S   M   E   A   E   D   A   A   T   Y   Y   C   Q

CAG TGG TCC TCC AAC CCC CTG ACC TTT GGC GCT GGC ACC AAG CTG GAA CTG AAG CGG
 Q   W   S   S   N   P   L   T   F   G   A   G   T   K   L   E   L   K   R

ACC GTG GCC GCT CCC TCC GTG TTC ATC TTC CCA CCT TCC GAC GAG CAG CTG AAG TCC
 T   V   A   A   P   S   V   F   I   F   P   P   S   D   E   Q   L   K   S

GGC ACC GCT TCT GTC GTG TGC CTG CTG AAC AAC TTC TAC CCC CGC GAG GCC AAG GTG
 G   T   A   S   V   V   C   L   L   N   N   F   Y   P   R   E   A   K   V

CAG TGG AAG GTG GAC AAC GCC CTG CAG TCC GGC AAC TCC CAG GAA TCC GTG ACC GAG
 Q   W   K   V   D   N   A   L   Q   S   G   N   S   Q   E   S   V   T   E

CAG GAC TCC AAG GAC AGC ACC TAC TCC CTG TCT AAC ACC CTG ACA CTG TCC AAG GCC
 Q   D   S   K   D   S   T   Y   S   L   S   N   T   L   T   L   S   K   A

GAC TAC GAG AAG CAC AAG GTG TAC GCC TGC GAA GTG ACC CAC CAG GGC CTG TCT AGC
 D   Y   E   K   H   K   V   Y   A   C   E   V   T   H   Q   G   L   S   S

CCC GTG ACC AAG TCT TTC AAC CGG GGC GAG TGC TAA TGA
 P   V   T   K   S   F   N   R   G   E   C   *   *
```

6.1.4 ScFc-scTv

```
ATG AAG TGG GTC ACC TTT ATC AGT CTG CTG TTT CTG TTC TCT AGT GCC TAT TCT CAA
 M   K   W   V   T   F   I   S   L   L   F   L   F   S   S   A   Y   S   Q

AAA GAG GTC GAG CAG AAC AGC GGC CCT CTG TCT GTT CCT GAG GGC GCT ATC GCC TCT
 K   E   V   E   Q   N   S   G   P   L   S   V   P   E   G   A   I   A   S

CTG AAC TGC ACC TAC TCC GAC AGA GGC TCC CAG AGC TTC TTC TGG TAC AGA CAG TAC
 L   N   C   T   Y   S   D   R   G   S   Q   S   F   F   W   Y   R   Q   Y

TCC GGC AAG TCC CCT GAG CTG ATC ATG TCC ATC TAC CAA GAG GGC GAC AAA GAG GAC
 S   G   K   S   P   E   L   I   M   S   I   Y   Q   E   G   D   K   E   D

GGC CGG TTT ACC GCT CAG CTG AAC AAG GCC TCT CAG TAC GTG TCC CTG CTG ATC CGG
 G   R   F   T   A   Q   L   N   K   A   S   Q   Y   V   S   L   L   I   R

GAC TCC CAG CCT TCT GAT TCT GCC ACC TAC CTG TGT GCC GCC GTG ATC GAC AAT GAC
 D   S   Q   P   S   D   S   A   T   Y   L   C   A   A   V   I   D   N   D

CAA GGC GGC ATC CTG ACC TTC GGC ACC GGA ACC AGA CTG ACA ATC ATC CCC AAC ATC
 Q   G   G   I   L   T   F   G   T   G   T   R   L   T   I   I   P   N   I

CAG AAC GGC GGT GGT GGT TCT GGC GGC GGA GGA AGC GGA GGC GGA GGT TCT GGC GGT
 Q   N   G   G   G   G   S   G   G   G   G   S   G   G   G   G   S   G   G
```

117

```
GGT GGT TCT GGC GGC GGA GGA AGC AAA GCT GGT GTC ACC CAG ACA CCT AGA TAC CTG
 G   G   S   G   G   G   G   S   K   A   G   V   T   Q   T   P   R   Y   L

ATC AAG ACC AGA GGC CAG CAA GTG ACA CTG TCC TGC TCT CCC ATT CCT GGC CAC AGA
 I   K   T   R   G   Q   Q   V   T   L   S   C   S   P   I   P   G   H   R

GCC GTG TCC TGG TAT CAG CAG ACA CCA GGC CAG GGC CTG CAG TTT CTG TTC GAG TAT
 A   V   S   W   Y   Q   Q   T   P   G   Q   G   L   Q   F   L   F   E   Y

GTG CAC GGC GAG GAA CGG AAC AAG GGC AAC TTC CCC GGC AGA TTC TCC GGC AGA CAG
 V   H   G   E   E   R   N   K   G   N   F   P   G   R   F   S   G   R   Q

TTC TCC AAC TCC TCC AGC GAG ATG AAC ATC TCC AAC CTG GAA CTG GGC GAC AGC GCC
 F   S   N   S   S   S   E   M   N   I   S   N   L   E   L   G   D   S   A

CTG TAC CTG TGT GCT TCT TCT CCT TGG GAC TCC CCT AAC GTG CAG TAC TTC GGC CCT
 L   Y   L   C   A   S   S   P   W   D   S   P   N   V   Q   Y   F   G   P

GGC ACC AGA CTG ACC GTG ACC GAG GAT CTG AAG AAC GAG CCC AAG TCC TGT GAT AAG
 G   T   R   L   T   V   T   E   D   L   K   N   E   P   K   S   C   D   K

ACC CAT ACA TGC CCA CCT TGT CCA GCT CCA CCT GTT GCT GGC CCT TCC GTG TTC CTG
 T   H   T   C   P   P   C   P   A   P   P   V   A   G   P   S   V   F   L

TTC CCC CCC AAG CCC AAG GAC ACC CTG ATG ATC TCC AGG ACC CCC GAG GTG ACC TGC
 F   P   P   K   P   K   D   T   L   M   I   S   R   T   P   E   V   T   C

GTG TGG GAT GTG TCT CAC GAG GAC CCT GAA GTG AAG TTC AAT TGG TAC GTG GAC GGC
 V   W   D   V   S   H   E   D   P   E   V   K   F   N   W   Y   V   D   G

GTG GAA GTG CAC AAC GCC AAG ACA AAG CCC TGC GAG GAA CAG TAC GGC TCC ACC TAC
 V   E   V   H   N   A   K   T   K   P   C   E   E   Q   Y   G   S   T   Y

AGA TGC GTG TCC GTG CTG ACA GTG CTG CAC CAG GAT TGG CTG AAC GGC AAA GAG TAC
 R   C   V   S   V   L   T   V   L   H   Q   D   W   L   N   G   K   E   Y

AAG TGC AAG GTG TCC AAC AAG GCC CTG CCT GCT CCT ATC GAA AAG ACC ATC TCC AAG
 K   C   K   V   S   N   K   A   L   P   A   P   I   E   K   T   I   S   K

GCC AAG GGA CAG CCC AGG GAA CCC CAG GTT TAC ACC TTG CCT CCA TCT CGG GAC GAG
 A   K   G   Q   P   R   E   P   Q   V   Y   T   L   P   P   S   R   D   E

CTG ACC AAG AAC CAG GTG TCC CTG ACC TGT CTC GTG AAG GGC TTC TAC CCC TCC GAT
 L   T   K   N   Q   V   S   L   T   C   L   V   K   G   F   Y   P   S   D

ATC GCC GTC GAG TGG GAG TCT AAT GGC CAG CCA GAG AAC AAC TAC AAG ACA ACC CCT
 I   A   V   E   W   E   S   N   G   Q   P   E   N   N   Y   K   T   T   P

CCT GTG CTG GAC TCC GAC GGC TCA TTC TTC CTG TAC TCC AAG CTG ACT GTG GAT AAG
 P   V   L   D   S   D   G   S   F   F   L   Y   S   K   L   T   V   D   K

TCC CGG TGG CAG CAG GGC AAC GTG TTC TCC TGT TCT GTG ATG CAC GAG GCC CTG CAC
 S   R   W   Q   Q   G   N   V   F   S   C   S   V   M   H   E   A   L   H

AAC CAC TAC ACC CAG AAG TCT CTG TCC CTG TCT CCT GGC AAA GGC GGC GGT GGA TCT
 N   H   Y   T   Q   K   S   L   S   L   S   P   G   K   G   G   G   G   S

GGT GGT GGT GGC TCT GGC GGC GGA GGT TCA GGT GGC GGA GGA TCA GGC GGT GGC GGT
 G   G   G   G   S   G   G   G   G   S   G   G   G   G   S   G   G   G   G
```

```
TCC GGC GGT GGT GGA AGT GAT AAG ACA CAC ACA TGC CCA CCT TGT CCT GCA CCT CCA
 S   G   G   G   G   S   D   K   T   H   T   C   P   P   C   P   A   P   P

GTG GCT GGC CCA TCT GTC TTT CTG TTT CCA CCT AAG CCT AAG GAT ACA CTC ATG ATC
 V   A   G   P   S   V   F   L   F   P   P   K   P   K   D   T   L   M   I

AGC CGC ACA CCT GAA GTC ACT TGT GTC TGG GAC GTG TCC CAT GAA GAT CCC GAA GTC
 S   R   T   P   E   V   T   C   V   W   D   V   S   H   E   D   P   E   V

AAG TTT AAT TGG TAT GTC GAT GGC GTC GAG GTC CAC AAT GCT AAG ACC AAG CCT TGT
 K   F   N   W   Y   V   D   G   V   E   V   H   N   A   K   T   K   P   C

GAA GAA CAA TAT GGC AGC ACC TAT CGC TGT GTG TCT GTG CTC ACC GTC CTG CAT CAA
 E   E   Q   Y   G   S   T   Y   R   C   V   S   V   L   T   V   L   H   Q

GAC TGG CTG AAT GGG AAA GAA TAC AAA TGT AAA GTC TCT AAC AAG GCT CTC CCC GCA
 D   W   L   N   G   K   E   Y   K   C   K   V   S   N   K   A   L   P   A

CCA ATC GAG AAA ACC ATC AGC AAG GCT AAA GGC CAG CCT CGC GAG CCT CAG GTG TAC
 P   I   E   K   T   I   S   K   A   K   G   Q   P   R   E   P   Q   V   Y

ACA TTG CCA CCT TCC AGA GAT GAA CTC ACA AAA AAT CAA GTC TCC CTG ACA TGC CTG
 T   L   P   P   S   R   D   E   L   T   K   N   Q   V   S   L   T   C   L

GTT AAG GGG TTT TAC CCT AGC GAC ATT GCC GTG GAA TGG GAA TCC AAC GGC CAA CCT
 V   K   G   F   Y   P   S   D   I   A   V   E   W   E   S   N   G   Q   P

GAG AAC AAT TAT AAG ACC ACA CCA CCA GTG CTG GAT AGC GAC GGC TCA TTT TTT CTC
 E   N   N   Y   K   T   T   P   P   V   L   D   S   D   G   S   F   F   L

TAC TCT AAA CTC ACA GTG GAC AAG AGC AGA TGG CAG CAA GGG AAT GTG TTT AGC TGC
 Y   S   K   L   T   V   D   K   S   R   W   Q   Q   G   N   V   F   S   C

TCC GTG ATG CAT GAA GCT CTC CAC AAT CAT TAT ACC CAG AAA AGC CTG TCT CTG AGC
 S   V   M   H   E   A   L   H   N   H   Y   T   Q   K   S   L   S   L   S

CCC GGC AAA GCC GTG GGC CAG GAC ACC CAG GAG GTG ATC GTG GTG CCC CAC TCC CTG
 P   G   K   A   V   G   Q   D   T   Q   E   V   I   V   V   P   H   S   L

CCC TTC AAG GTG GTG GTG ATC TCC GCC ATC CTG GCC CTG GTG GTG CTG ACC ATC ATC
 P   F   K   V   V   V   I   S   A   I   L   A   L   V   V   L   T   I   I

TCC CTG ATC ATC CTG ATC ATG CTG TGG CAG AAG AAG CCC AGG TAA TGA
 S   L   I   I   L   I   M   L   W   Q   K   K   P   R   *   *
```

6.1.5 scTv

```
ATG AAA TGG GTC ACC TTT ATC TCC CTG CTG TTC CTG TTC TCC TCC GCC TAC TCT CAA
 M   K   W   V   T   F   I   S   L   L   F   L   F   S   S   A   Y   S   Q

AAA GAG GTC GAG CAG AAC AGC GGC CCT CTG TCT GTT CCT GAG GGC GCT ATC GCC TCT
 K   E   V   E   Q   N   S   G   P   L   S   V   P   E   G   A   I   A   S

CTG AAC TGC ACC TAC TCC GAC AGA GGC TCC CAG AGC TTC TTC TGG TAC AGA CAG TAC
 L   N   C   T   Y   S   D   R   G   S   Q   S   F   F   W   Y   R   Q   Y

TCC GGC AAG TCC CCT GAG CTG ATC ATG TCC ATC TAC CAA GAG GGC GAC AAA GAG GAC
 S   G   K   S   P   E   L   I   M   S   I   Y   Q   E   G   D   K   E   D
```

```
GGC CGG TTT ACC GCT CAG CTG AAC AAG GCC TCT CAG TAC GTG TCC CTG CTG ATC CGG
 G   R   F   T   A   Q   L   N   K   A   S   Q   Y   V   S   L   L   I   R

GAC TCC CAG CCT TCT GAT TCT GCC ACC TAC CTG TGT GCC GCC GTG ATC GAC AAT GAC
 D   S   Q   P   S   D   S   A   T   Y   L   C   A   A   V   I   D   N   D

CAA GGC GGC ATC CTG ACC TTC GGC ACC GGA ACC AGA CTG ACA ATC ATC CCC AAC ATC
 Q   G   G   I   L   T   F   G   T   G   T   R   L   T   I   I   P   N   I

CAG AAC GGT GGA GGT GGA TCA GGT GGA GGA GGT TCC GGT GGA GGA GGT TCA GGA GGT
 Q   N   G   G   G   G   S   G   G   G   G   S   G   G   G   G   S   G   G

GGT GGA TCT AAA GCT GGT GTC ACC CAG ACA CCT AGA TAC CTG ATC AAG ACC AGA GGC
 G   G   S   K   A   G   V   T   Q   T   P   R   Y   L   I   K   T   R   G

CAG CAA GTG ACA CTG TCC TGC TCT CCC ATT CCT GGC CAC AGA GCC GTG TCC TGG TAT
 Q   Q   V   T   L   S   C   S   P   I   P   G   H   R   A   V   S   W   Y

CAG CAG ACA CCA GGC CAG GGC CTG CAG TTT CTG TTC GAG TAT GTG CAC GGC GAG GAA
 Q   Q   T   P   G   Q   G   L   Q   F   L   F   E   Y   V   H   G   E   E

CGG AAC AAG GGC AAC TTC CCC GGC AGA TTC TCC GGC AGA CAG TTC TCC AAC TCC TCC
 R   N   K   G   N   F   P   G   R   F   S   G   R   Q   F   S   N   S   S

AGC GAG ATG AAC ATC TCC AAC CTG GAA CTG GGC GAC AGC GCC CTG TAC CTG TGT GCT
 S   E   M   N   I   S   N   L   E   L   G   D   S   A   L   Y   L   C   A

TCT TCT CCT TGG GAC TCC CCT AAC GTG CAG TAC TTC GGC CCT GGC ACC AGA CTG ACC
 S   S   P   W   D   S   P   N   V   Q   Y   F   G   P   G   T   R   L   T

GTG ACC GAG GAT CTG AAG AAC GCC GTG GGC CAG GAC ACC CAG GAG GTG ATC GTG GTG
 V   T   E   D   L   K   N   A   V   G   Q   D   T   Q   E   V   I   V   V

CCC CAC TCC CTG CCC TTC AAG GTG GTG GTG ATC TCC GCC ATC CTG GCC CTG GTG GTG
 P   H   S   L   P   F   K   V   V   V   I   S   A   I   L   A   L   V   V

CTG ACC ATC ATC TCC CTG ATC ATC CTG ATC ATG CTG TGG CAG AAG AAG CCC AGG TAA
 L   T   I   I   S   L   I   I   L   I   M   L   W   Q   K   K   P   R   *

TGA
 *
```

6.1.6 TCER®

6.1.6.1 Chain 1

```
ATG AAA TGG GTC ACC TTT ATC TCC CTG CTG TTC CTG TTC TCC TCC GCC TAC TCT CAA
 M   K   W   V   T   F   I   S   L   L   F   L   F   S   S   A   Y   S   Q

AAA GAG GTC GAG CAG AAC AGC GGC CCT CTG TCT GTT CCT GAG GGC GCT ATC GCC TCT
 K   E   V   E   Q   N   S   G   P   L   S   V   P   E   G   A   I   A   S

CTG AAC TGC ACC TAC TCC GAC AGA GGC TCC CAG AGC TTC TTC TGG TAC AGA CAG TAC
 L   N   C   T   Y   S   D   R   G   S   Q   S   F   F   W   Y   R   Q   Y

TCC GGC AAG TCC CCT GAG CTG ATC ATG TCC ATC TAC CAA GAG GGC GAC AAA GAG GAC
 S   G   K   S   P   E   L   I   M   S   I   Y   Q   E   G   D   K   E   D
```

```
GGC CGG TTT ACC GCT CAG CTG AAC AAG GCC TCT CAG TAC GTG TCC CTG CTG ATC CGG
 G   R   F   T   A   Q   L   N   K   A   S   Q   Y   V   S   L   L   I   R

GAC TCC CAG CCT TCT GAT TCT GCC ACC TAC CTG TGT GCC GCC GTG ATC GAC AAT GAC
 D   S   Q   P   S   D   S   A   T   Y   L   C   A   A   V   I   D   N   D

CAA GGC GGC ATC CTG ACC TTC GGC ACC GGA ACC AGA CTG ACA ATC ATC CCC AAC ATC
 Q   G   G   I   L   T   F   G   T   G   T   R   L   T   I   I   P   N   I

CAG AAC GGC GGA GGA TCT GGC GGA GGC GGA GAT ATC CAG ATG ACC CAG TCT CCT TCC
 Q   N   G   G   G   S   G   G   G   G   D   I   Q   M   T   Q   S   P   S

AGC CTG TCC GCT TCT GTG GGC GAC AGA GTG ACC ATC ACC TGT AGA GCC TCT CAG GAC
 S   L   S   A   S   V   G   D   R   V   T   I   T   C   R   A   S   Q   D

ATC CGG AAC TAC CTG AAC TGG TAT CAG CAG AAG CCT GGC AAG GCC CCA AAG CTG CTG
 I   R   N   Y   L   N   W   Y   Q   Q   K   P   G   K   A   P   K   L   L

ATC TAC TAC ACC TCT CGG CTG CAC TCT GGC GTG CCC TCT AGA TTT TCT GGC TCC GGC
 I   Y   Y   T   S   R   L   H   S   G   V   P   S   R   F   S   G   S   G

TCT GGC ACC GAC TAT ACC CTG ACT ATC TCC AGC CTG CAG CCT GAG GAT ATC GCT ACC
 S   G   T   D   Y   T   L   T   I   S   S   L   Q   P   E   D   I   A   T

TAC TTC TGC CAG CAA GGC CAG ACA CTG CCC TGG ACA TTT GGC CAG GGC ACC AAG GTG
 Y   F   C   Q   Q   G   Q   T   L   P   W   T   F   G   Q   G   T   K   V

GAA ATC AAA GAG CCC AAG TCC TCC GAC AAG ACC CAC ACC TGT CCT CCA TGT CCT GCT
 E   I   K   E   P   K   S   S   D   K   T   H   T   C   P   P   C   P   A

CCT CCA GTG GCT GGC CCT TCC GTG TTT CTG TTC CCT CCA AAG CCT AAG GAC ACC CTG
 P   P   V   A   G   P   S   V   F   L   F   P   P   K   P   K   D   T   L

ATG ATC TCT CGG ACC CCT GAA GTG ACC TGC GTG GTG GTG GAT GTG TCT CAC GAG GAT
 M   I   S   R   T   P   E   V   T   C   V   V   V   D   V   S   H   E   D

CCC GAA GTG AAG TTC AAT TGG TAC GTG GAC GGC GTG GAA GTG CAC AAC GCC AAG ACC
 P   E   V   K   F   N   W   Y   V   D   G   V   E   V   H   N   A   K   T

AAG CCT AGA GAG GAA CAG TAC CAG TCC ACC TAC AGA GTG GTG TCC GTG CTG ACC GTG
 K   P   R   E   E   Q   Y   Q   S   T   Y   R   V   V   S   V   L   T   V

CTG CAC CAG GAT TGG CTG AAC GGC AAA GAG TAC AAG TGC AAG GTG TCC AAC AAG GCC
 L   H   Q   D   W   L   N   G   K   E   Y   K   C   K   V   S   N   K   A

CTG CCT GCC TCC ATC GAA AAG ACC ATC TCC AAG GCC AAG GGA CAG CCC AGA GAA CCC
 L   P   A   S   I   E   K   T   I   S   K   A   K   G   Q   P   R   E   P

CAG GTG TAC ACA CTG CCA CCT TGC AGA GAT GAG CTG ACC AAG AAC CAG GTG TCC CTG
 Q   V   Y   T   L   P   P   C   R   D   E   L   T   K   N   Q   V   S   L

TGG TGT CTG GTC AAG GGC TTC TAC CCC TCC GAT ATC GCC GTG GAA TGG GAG TCT AAT
 W   C   L   V   K   G   F   Y   P   S   D   I   A   V   E   W   E   S   N

GGC CAG CCT GAG AAC AAC TAC AAG ACA ACC CCT CCT GTG CTG GAC TCC GAC GGC TCA
 G   Q   P   E   N   N   Y   K   T   T   P   P   V   L   D   S   D   G   S

TTC TTC CTG TAC TCC AAG CTG ACA GTG GAC AAG TCC AGA TGG CAG CAG GGC AAC GTG
 F   F   L   Y   S   K   L   T   V   D   K   S   R   W   Q   Q   G   N   V

TTC TCC TGC TCC GTG ATG CAC GAG GCC CTG CAC AAT CAC TAC ACC CAG AAG TCC CTG
```

```
     F    S    C    S    V    M    H    E    A    L    H    N    H    Y    T    Q    K    S    L
TCT CTG TCC CCT GCC GTG GGC CAG GAC ACC CAG GAG GTG ATC GTG GTG CCC CAC TCC
 S   L   S   P   A   V   G   Q   D   T   Q   E   V   I   V   V   P   H   S

CTG CCC TTC AAG GTG GTG GTG ATC TCC GCC ATC CTG GCC CTG GTG GTG CTG ACC ATC
 L   P   F   K   V   V   V   I   S   A   I   L   A   L   V   V   L   T   I

ATC TCC CTG ATC ATC CTG ATC ATG CTG TGG CAG AAG AAG CCC AGG TAA TGA
 I   S   L   I   I   L   I   M   L   W   Q   K   K   P   R   *   *
```

6.1.6.2   Chain 2

```
ATG AAA TGG GTC ACC TTT ATC TCC CTG CTG TTC CTG TTC TCC AGC GCC TAC TCT GAG
 M   K   W   V   T   F   I   S   L   L   F   L   F   S   S   A   Y   S   E

GTG CAG CTG GTT CAG TCT GGC GCC GAA GTG AAG AAA CCT GGC GCC TCT GTG AAG GTG
 V   Q   L   V   Q   S   G   A   E   V   K   K   P   G   A   S   V   K   V

TCC TGC AAG GCT TCC GGC TAC TCC TTC ACC GGC TAC ACA ATG AAC TGG GTC CGA CAG
 S   C   K   A   S   G   Y   S   F   T   G   Y   T   M   N   W   V   R   Q

GCT CCT GGA CAG GGA CTT GAA TGG ATG GGC CTG ATC AAC CCC TAC AAG GGC GTG TCC
 A   P   G   Q   G   L   E   W   M   G   L   I   N   P   Y   K   G   V   S

ACC TAC GCT CAG AAA TTC CAG GAC AGA GTG ACC CTG ACC GTG GAC AAG TCT ACC TCC
 T   Y   A   Q   K   F   Q   D   R   V   T   L   T   V   D   K   S   T   S

ACC GCC TAC ATG GAA CTG TCC AGC CTG AGA TCT GAG GAC ACC GCC GTG TAC TAC TGT
 T   A   Y   M   E   L   S   S   L   R   S   E   D   T   A   V   Y   Y   C

GCC AGA TCC GGC TAT TAC GGC GAC TCC GAC TGG TAC TTC GAT GTG TGG GGA CAG GGC
 A   R   S   G   Y   Y   G   D   S   D   W   Y   F   D   V   W   G   Q   G

ACC CTG GTC ACA GTT AGT TCT GGC GGA GGA AGT GGC GGA GGC GGA AAA GCT GGT GTC
 T   L   V   T   V   S   S   G   G   G   S   G   G   G   G   K   A   G   V

ACC CAG ACA CCT AGA TAC CTG ATC AAG ACC AGA GGC CAG CAA GTG ACA CTG TCC TGC
 T   Q   T   P   R   Y   L   I   K   T   R   G   Q   Q   V   T   L   S   C

TCT CCC ATT CCT GGC CAC AGA GCC GTG TCC TGG TAT CAG CAG ACA CCA GGC CAG GGC
 S   P   I   P   G   H   R   A   V   S   W   Y   Q   Q   T   P   G   Q   G

CTG CAG TTT CTG TTC GAG TAT GTG CAC GGC GAG GAA CGG AAC AAG GGC AAC TTC CCC
 L   Q   F   L   F   E   Y   V   H   G   E   E   R   N   K   G   N   F   P

GGC AGA TTC TCC GGC AGA CAG TTC TCC AAC TCC TCC AGC GAG ATG AAC ATC TCC AAC
 G   R   F   S   G   R   Q   F   S   N   S   S   S   E   M   N   I   S   N

CTG GAA CTG GGC GAC AGC GCC CTG TAC CTG TGT GCT TCT TCT CCT TGG GAC TCC CCT
 L   E   L   G   D   S   A   L   Y   L   C   A   S   S   P   W   D   S   P

AAC GTG CAG TAC TTC GGC CCT GGC ACC AGA CTG ACC GTG ACC GAG GAT CTG AAG AAC
 N   V   Q   Y   F   G   P   G   T   R   L   T   V   T   E   D   L   K   N

GAG CCC AAG TCC TCC GAC AAG ACC CAC ACC TGT CCT CCA TGT CCA GCT CCA CCT GTT
 E   P   K   S   S   D   K   T   H   T   C   P   P   C   P   A   P   P   V

GCT GGC CCT TCC GTG TTT CTG TTT CCT CCA AAG CCT AAG GAC ACC CTG ATG ATC TCT
```

```
     A    G    P    S    V    F    L    F    P    P    K    P    K    D    T    L    M    I    S

CGG  ACC  CCT  GAA  GTG  ACC  TGC  GTG  GTG  GTG  GAT  GTG  TCT  CAC  GAG  GAC  CCA  GAA  GTG
 R    T    P    E    V    T    C    V    V    V    D    V    S    H    E    D    P    E    V

AAG  TTC  AAT  TGG  TAC  GTG  GAC  GGC  GTG  GAA  GTG  CAC  AAC  GCC  AAG  ACC  AAG  CCT  AGA
 K    F    N    W    Y    V    D    G    V    E    V    H    N    A    K    T    K    P    R

GAG  GAA  CAG  TAC  CAG  AGC  ACC  TAC  AGA  GTG  GTG  TCC  GTG  CTG  ACC  GTG  CTG  CAC  CAG
 E    E    Q    Y    Q    S    T    Y    R    V    V    S    V    L    T    V    L    H    Q

GAT  TGG  CTG  AAC  GGC  AAA  GAG  TAC  AAG  TGC  AAG  GTG  TCC  AAC  AAG  GCC  CTG  CCT  GCC
 D    W    L    N    G    K    E    Y    K    C    K    V    S    N    K    A    L    P    A

TCC  ATC  GAA  AAG  ACC  ATC  TCC  AAG  GCC  AAG  GGA  CAG  CCC  CGG  GAA  CCT  CAA  GTC  TGT
 S    I    E    K    T    I    S    K    A    K    G    Q    P    R    E    P    Q    V    C

ACC  TTG  CCT  CCT  AGC  CGG  GAC  GAG  CTG  ACC  AAG  AAT  CAG  GTG  TCC  CTG  AGC  TGT  GCC
 T    L    P    P    S    R    D    E    L    T    K    N    Q    V    S    L    S    C    A

GTG  AAG  GGC  TTC  TAC  CCT  TCC  GAT  ATC  GCC  GTC  GAG  TGG  GAG  TCT  AAT  GGC  CAG  CCA
 V    K    G    F    Y    P    S    D    I    A    V    E    W    E    S    N    G    Q    P

GAG  AAC  AAC  TAC  AAG  ACA  ACC  CCT  CCT  GTG  CTG  GAC  TCC  GAC  GGC  TCA  TTC  TTC  CTG
 E    N    N    Y    K    T    T    P    P    V    L    D    S    D    G    S    F    F    L

GTG  TCC  AAG  CTG  ACA  GTG  GAT  AAG  TCC  AGA  TGG  CAG  CAG  GGC  AAC  GTG  TTC  TCC  TGC
 V    S    K    L    T    V    D    K    S    R    W    Q    Q    G    N    V    F    S    C

TCC  GTG  ATG  CAC  GAG  GCC  CTG  CAC  AAT  CAC  TAC  ACA  CAG  AAG  TCT  CTG  TCC  CTG  TCT
 S    V    M    H    E    A    L    H    N    H    Y    T    Q    K    S    L    S    L    S

CCT  GGC  AAG  TGA  TAA
 P    G    K    *    *
```

7 References

1. Dhimolea, E. & Reichert, J. M. World Bispecific Antibody Summit, September 27–28, 2011, Boston, MA. *Mabs* **4**, 4–13 (2012).

2. Ellerman, D. Bispecific T-cell engagers: Towards understanding variables influencing the in vitro potency and tumor selectivity and their modulation to enhance their efficacy and safety. *Methods* **154**, 102–117 (2019).

3. Symmetry breaking: bispecific antibodies, the beginnings, and 50 years on.

4. Grand View Research. *Cancer Immunotherapy Market Growth & Trends* https://www.grandviewresearch.com/press-release/global-cancer-immunotherapy-market (2021).

5. Reichert, J. M., Rosensweig, C. J., Faden, L. B. & Dewitz, M. C. Monoclonal antibody successes in the clinic. *Nat Biotechnol* **23**, 1073–1078 (2005).

6. Wu, Z. & Cheung, N. V. T cell engaging bispecific antibody (T-BsAb): From technology to therapeutics. *Pharmacol Therapeut* **182**, 161–175 (2018).

7. Chandran, S. S. & Klebanoff, C. A. T cell receptor-based cancer immunotherapy: Emerging efficacy and pathways of resistance. *Immunol Rev* **290**, 127–147 (2019).

8. Boldt & Claytoon. Why doesn't immunotherapy work for everyone? https://www.mdanderson.org/cancerwise/why-doesnt-immunotherapy-work-for-everyone.h00-159385101.html (2020).

9. Lowe, K. L. *et al.* Novel TCR-based biologics: mobilising T cells to warm 'cold' tumours. *Cancer Treat Rev* **77**, 35–43 (2019).

10. Tsimberidou, A.-M. *et al.* T-cell receptor-based therapy: an innovative therapeutic approach for solid tumors. *J Hematol Oncol* **14**, 102 (2021).

11. Nimmerjahn, F. & Ravetch, J. V. Translating basic mechanisms of IgG effector activity into next generation cancer therapies. *Cancer Immun* **12**, 13 (2012).

12. Scott, A. M., Wolchok, J. D. & Old, L. J. Antibody therapy of cancer. *Nat Rev Cancer* **12**, 278–287 (2012).

13. Redman, J. M., Hill, E. M., AlDeghaither, D. & Weiner, L. M. Mechanisms of action of therapeutic antibodies for cancer. *Mol Immunol* **67**, 28–45 (2015).

14. Natsume, A., Niwa, R. & Satoh, M. Improving effector functions of antibodies for cancer treatment: Enhancing ADCC and CDC. *Drug Des Dev Ther* **Volume 3**, 7–16 (2008).

15. Brinkmann, U. & Kontermann, R. E. The making of bispecific antibodies. *Mabs* **9**, 182–212 (2017).

16. Lopez-Albaitero, A. *et al.* Overcoming resistance to HER2-targeted therapy with a novel HER2/CD3 bispecific antibody. *Oncoimmunology* **6**, 00–00 (2017).

17. Wang, L., Hoseini, S. S., Xu, H., Ponomarev, V. & Cheung, N.-K. Silencing Fc Domains in T cell–Engaging Bispecific Antibodies Improves T-cell Trafficking and Antitumor Potency. *Cancer Immunol Res* **7**, 2013–2024 (2019).

18. Liu, L. *et al.* MGD011, A CD19 x CD3 Dual-Affinity Retargeting Bi-specific Molecule Incorporating Extended Circulating Half-life for the Treatment of B-Cell Malignancies. *Clin Cancer Res* **23**, 1506–1518 (2017).

19. Segal, D. M., Weiner, G. J. & Weiner, L. M. Bispecific antibodies in cancer therapy. *Curr Opin Immunol* **11**, 558–562 (1999).

20. Dall'Acqua, W., Simon, A. L., Mulkerrin, M. G. & Carter, P. Contribution of Domain Interface Residues to the Stability of Antibody C H 3 Domain Homodimers. *Biochemistry-us* **37**, 9266–9273 (1998).

21. Crick, F. H. C. The packing of -helices: simple coiled-coils. *Acta Crystallogr* **6**, 689–697 (1953).

22. Ridgway, J. B. B., Presta, L. G. & Carter, P. 'Knobs-into-holes' engineering of antibody CH3 domains for heavy chain heterodimerization. *Protein Eng Des Sel* **9**, 617–621 (1996).

23. Merchant, A. M. *et al.* An efficient route to human bispecific IgG. *Nature Biotechnology* 677–681 (1998).

24. Husain, B. & Ellerman, D. Expanding the Boundaries of Biotherapeutics with Bispecific Antibodies. *Biodrugs* **32**, 441–464 (2018).

25. Frankel, S. R. & Baeuerle, P. A. Targeting T cells to tumor cells using bispecific antibodies. *Curr Opin Chem Biol* **17**, 385–392 (2013).

26. Bargou, R. *et al.* Tumor Regression in Cancer Patients by Very Low Doses of a T Cell–Engaging Antibody. *Science* **321**, 974–977 (2008).

27. Velasquez, M. P., Bonifant, C. L. & Gottschalk, S. Redirecting T cells to hematological malignancies with bispecific antibodies. *Blood* **131**, 30–38 (2018).

28. Vafa, O. & Trinklein, N. D. Perspective: Designing T-Cell Engagers With Better Therapeutic Windows. *Frontiers Oncol* **10**, 446 (2020).

29. Matsui, K. *et al.* Low affinity interaction of peptide-MHC complexes with T cell receptors. *Science* **254**, 1788–1791 (1991).

30. Mullard, A. FDA approval of Immunocore's first-in-class TCR therapeutic broadens depth of the T cell engager platform. *Nat Rev Drug Discov* (2022) doi:10.1038/d41573-022-00031-3.

31. AbbVie Oncology Pipeline. https://www.abbviescience.com/oncology/pipeline.

32. Murphy, K. *Janeway's Immunobiology (8th ed, 2012).pdf*. vol. 8th (Garland Science, 2012).

33. Shahinian, A. *et al.* Differential T cell costimulatory requirements in CD28-deficient mice. *Science* **261**, 609–612 (1993).

34. Birnbaum, M. E. *et al.* Molecular architecture of the αβ T cell receptor–CD3 complex. *Proc National Acad Sci* **111**, 17576–17581 (2014).

35. Liddy, N. Molecular engineering of high affinity T-cell receptors for bispecific therapeutics. (2013).

36. Cole, D. K. *et al.* Human TCR-Binding Affinity is Governed by MHC Class Restriction. *J Immunol* **178**, 5727–5734 (2007).

37. Aleksic, M. *et al.* Different affinity windows for virus and cancer-specific T-cell receptors: implications for therapeutic strategies. *Eur J Immunol* **42**, 3174–9 (2012).

38. Holland, C. J. *et al.* Specificity of bispecific T cell receptors and antibodies targeting peptide-HLA. *J Clin Invest* **130**, 2673–2688 (2020).

39. Wooldridge, L. *et al.* A single autoimmune T cell receptor recognizes more than a million different peptides. *J Biological Chem* **287**, 1168–77 (2012).

40. Birnbaum, M. E. *et al.* Deconstructing the peptide-MHC specificity of T cell recognition. *Cell* **157**, 1073–87 (2014).

41. Cole, D. K. *et al.* Structural Mechanism Underpinning Cross-reactivity of a CD8+ T-cell Clone That Recognizes a Peptide Derived from Human Telomerase Reverse Transcriptase*. *J Biol Chem* **292**, 802–813 (2017).

42. Garrido, F., Cabrera, T. & Aptsiauri, N. "Hard" and "soft" lesions underlying the HLA class I alterations in cancer cells: Implications for immunotherapy. *Int J Cancer* **127**, 249–256 (2010).

43. Purbhoo, M. A. *et al.* Quantifying and Imaging NY-ESO-1/LAGE-1-Derived Epitopes on Tumor Cells Using High Affinity T Cell Receptors. *J Immunol* **176**, 7308–7316 (2006).

44. Li, Y. *et al.* Directed evolution of human T-cell receptors with picomolar affinities by phage display. *Nat Biotechnol* **23**, 349–54 (2005).

45. Health, N. C. I. at the N. I. of. National Cancer Institue - Tumor-specific antigen. https://www.cancer.gov/publications/dictionaries/cancer-terms/def/tumor-specific-antigen.

46. Wagner, S., Mullins, C. S. & Linnebacher, M. Colorectal cancer vaccines: Tumor-associated antigens vs neoantigens. *World J Gastroentero* **24**, 5418–5432 (2018).

47. Smith, C. C. *et al.* Alternative tumour-specific antigens. *Nat Rev Cancer* **19**, 465–478 (2019).

48. Xu, Y., Zou, R., Wang, J., Wang, Z. W. & Zhu, X. The role of the cancer testis antigen PRAME in tumorigenesis and immunotherapy in human cancer. *Cell Proliferat* **53**, e12770 (2020).

49. Stone, J. D., Chervin, A. S., Aggen, D. H. & Kranz, D. M. Chapter eight T Cell Receptor Engineering. *Methods Enzymol* **503**, 189–222 (2012).

50. Ikeda, H. *et al.* Characterization of an Antigen That Is Recognized on a Melanoma Showing Partial HLA Loss by CTL Expressing an NK Inhibitory Receptor. *Immunity* **6**, 199–208 (1997).

51. Tessari, A. *et al.* Expression of NY-ESO-1, MAGE-A3, PRAME and WT1 in different subgroups of breast cancer: An indication to immunotherapy? *Breast* **42**, 68–73 (2018).

52. Neumann, E. *et al.* Heterogeneous expression of the tumor-associated antigens RAGE-1, PRAME, and glycoprotein 75 in human renal cell carcinoma: candidates for T-cell-based immunotherapies? *Cancer Res* **58**, 4090–5 (1998).

53. Zhang, W. *et al.* PRAME expression and promoter hypomethylation in epithelial ovarian cancer. *Oncotarget* **7**, 45352–45369 (2016).

54. Bankovic, J. *et al.* Identification of genes associated with non-small-cell lung cancer promotion and progression. *Lung Cancer* **67**, 151–9 (2010).

55. Van, B. N. *et al.* PRAME, a gene encoding an antigen recognized on a human melanoma by cytolytic T cells, is expressed in acute leukaemia cells. *Br. J Haematol* **102**, 1376–1379 (1998).

56. Iura, K. *et al.* Cancer-testis antigen expression in synovial sarcoma: NY-ESO-1, PRAME, MAGEA4, and MAGEA1. *Hum Pathol* **61**, 130–139 (2017).

57. Iura, K. *et al.* Cancer-testis antigens PRAME and NY-ESO-1 correlate with tumour grade and poor prognosis in myxoid liposarcoma. *J Pathology Clin Res* **1**, 144–59 (2015).

58. Hemminger, J. A. *et al.* Expression of cancer-testis antigens MAGEA1, MAGEA3, ACRBP, PRAME, SSX2, and CTAG2 in myxoid and round cell liposarcoma. *Modern Pathol* **27**, 1238–45 (2014).

59. Oberthuer, A., Hero, B., Spitz, R., Berthold, F. & Fischer, M. The tumor-associated antigen PRAME is universally expressed in high-stage neuroblastoma and associated with poor outcome. *Clin Cancer Res* **10**, 4307–13 (2004).

60. immatics Technology Overview. https://immatics.com/technologies/#1587996332625-7a8caf01-0299.

61. Robbins, P. F. *et al.* Mining exomic sequencing data to identify mutated antigens recognized by adoptively transferred tumor-reactive T cells. *Nat Med* **19**, 747–52 (2013).

62. Castle, J. C. *et al.* Exploiting the mutanome for tumor vaccination. *Cancer Res* **72**, 1081–91 (2012).

63. Matsushita, H. *et al.* Cancer exome analysis reveals a T-cell-dependent mechanism of cancer immunoediting. *Nature* **482**, 400–4 (2012).

64. Rooij, N. van *et al.* Tumor exome analysis reveals neoantigen-specific T-cell reactivity in an ipilimumab-responsive melanoma. *J Clin Oncol* **31**, e439-42 (2013).

65. Boon, T., Coulie, P. G., Eynde, B. J. V. den & Bruggen, P. van der. Human T cell responses against melanoma. *Immunology* **24**, 175–208 (2006).

66. Mellman, I., Coukos, G. & Dranoff, G. Cancer immunotherapy comes of age. *Nature* **480**, 480–9 (2011).

67. Chen, D. S. & Mellman, I. Oncology meets immunology: the cancer-immunity cycle. *Immunity* **39**, 1–10 (2013).

68. Staerz, U. D., Kanagawa, O. & Bevan, M. J. Hybrid antibodies can target sites for attack by T cells. *Nature* **314**, 628–631 (1985).

69. Mau-Sørensen, M. *et al.* A phase I trial of intravenous catumaxomab: a bispecific monoclonal antibody targeting EpCAM and the T cell coreceptor CD3. *Cancer Chemoth Pharm* **75**, 1065–1073 (2015).

70. Teachey, D. T. *et al.* Cytokine release syndrome after blinatumomab treatment related to abnormal macrophage activation and ameliorated with cytokine-directed therapy. *Blood* **121**, 5154–7 (2013).

71. Yiu, H. H., Graham, A. L. & Stengel, R. F. Dynamics of a Cytokine Storm. *Plos One* **7**, e45027 (2012).

72. Saber, H., Valle, P. D., Ricks, T. K. & Leighton, J. K. An FDA oncology analysis of CD3 bispecific constructs and first-in-human dose selection. *Regul Toxicol Pharm* **90**, 144–152 (2017).

73. Caspi, R. R. Immunotherapy of autoimmunity and cancer: the penalty for success. *Nat Rev Immunol* **8**, 970–6 (2008).

74. Liddy, N. *et al.* Monoclonal TCR-redirected tumor cell killing. *Nat Med* **18**, 980–987 (2012).

75. Leong, S. R. *et al.* An anti-CD3/anti–CLL-1 bispecific antibody for the treatment of acute myeloid leukemia. *Blood* **129**, 609–618 (2017).

76. Valldorf, B. *et al.* Antibody display technologies: selecting the cream of the crop. *Biol Chem* **0**, 000010151520200377 (2021).

77. Boulter, J. M. *et al.* Stable, soluble T-cell receptor molecules for crystallization and therapeutics. *Protein Eng Des Sel* **16**, 707–711 (2003).

78. Wagner, E. K. *et al.* Human cytomegalovirus-specific T-cell receptor engineered for high affinity and soluble expression using mammalian cell display. *J Biol Chem* **294**, 5790–5804 (2019).

79. Holler, P. D. *et al.* In vitro evolution of a T cell receptor with high affinity for peptide/MHC. *Proc National Acad Sci* **97**, 5387–5392 (2000).

80. Lu, R.-M. *et al.* Development of therapeutic antibodies for the treatment of diseases. *J Biomed Sci* **27**, 1 (2020).

81. Bradbury, A. R. M., Sidhu, S., Dübel, S. & McCafferty, J. Beyond natural antibodies: the power of in vitro display technologies. *Nat Biotechnol* **29**, 245–254 (2011).

82. Frenzel, A. *et al.* Designing Human Antibodies by Phage Display. *Transfus Med Hemoth* **44**, 312–318 (2017).

83. Smith, G. Filamentous fusion phage: novel expression vectors that display cloned antigens on the virion surface. *Science* **228**, 1315–1317 (1985).

84. Parmley, S. F. & Smith, G. P. Antibody-selectable filamentous fd phage vectors: affinity purification of target genes. *Gene* **73**, 305–318 (1988).

85. McCafferty, J., Griffiths, A. D., Winter, G. & Chiswell, D. J. Phage antibodies: filamentous phage displaying antibody variable domains. *Nature* **348**, 552–554 (1990).

86. Mazor, Y., Blarcom, T. V., Carroll, S. & Georgiou, G. Selection of full-length IgGs by tandem display on filamentous phage particles and Escherichia   coli fluorescence-activated cell sorting screening. *Febs J* **277**, 2291–2303 (2010).

87. Vaughan, T. J. *et al.* Human Antibodies with Sub-nanomolar Affinities Isolated from a Large Non-immunized Phage Display Library. *Nat Biotechnol* **14**, 309–314 (1996).

88. Hoet, R. M. *et al.* Generation of high-affinity human antibodies by combining donor-derived and synthetic complementarity-determining-region diversity. *Nat Biotechnol* **23**, 344–348 (2005).

89. Sellmann, C. *et al.* A One-Step Process for the Construction of Phage Display scFv and VHH Libraries. *Mol Biotechnol* **62**, 228–239 (2020).

90. Schwimmer, L. J. *et al.* Discovery of diverse and functional antibodies from large human repertoire antibody libraries. *J Immunol Methods* **391**, 60–71 (2013).

91. Tiller, T. *et al.* A fully synthetic human Fab antibody library based on fixed VH/VL framework pairings with favorable biophysical properties. *Mabs* **5**, 445–470 (2013).

92. Onda, T. *et al.* A phage display system for detection of T cell receptor-antigen interactions. *Mol Immunol* **32**, 1387–1397 (1995).

93. Boder, E. T. & Wittrup, K. D. Yeast surface display for screening combinatorial polypeptide libraries. *Nat Biotechnol* **15**, 553–557 (1997).

94. Wang, Z., Mathias, A., Stavrou, S. & Neville, D. M. A new yeast display vector permitting free scFv amino termini can augment ligand binding affinities. *Protein Eng Des Sel* **18**, 337–343 (2005).

95. Rakestraw, J. A., Aird, D., Aha, P. M., Baynes, B. M. & Lipovšek, D. Secretion-and-capture cell-surface display for selection of target-binding proteins. *Protein Eng Des Sel* **24**, 525–530 (2011).

96. Rhiel, L. *et al.* REAL-Select: Full-Length Antibody Display and Library Screening by Surface Capture on Yeast Cells. *Plos One* **9**, e114887 (2014).

97. Chao, G. *et al.* Isolating and engineering human antibodies using yeast surface display. *Nat Protoc* **1**, 755–768 (2006).

98. Sivelle, C. *et al.* Fab is the most efficient format to express functional antibodies by yeast surface display. *Mabs* **10**, 01–34 (2018).

99. Beucken, T. van den *et al.* Affinity maturation of Fab antibody fragments by fluorescent-activated cell sorting of yeast-displayed libraries. *Febs Lett* **546**, 288–294 (2003).

100. Weaver-Feldhaus, J. M. *et al.* Yeast mating for combinatorial Fab library generation and surface display. *Febs Lett* **564**, 24–34 (2004).

101. Smith, S. N., Harris, D. T. & Kranz, D. M. T Cell Receptor Engineering and Analysis Using the Yeast Display Platform. *Methods Mol Biology* **1319**, 95–141 (2015).

102. Benatuil, L., Perez, J. M., Belk, J. & Hsieh, C.-M. An improved yeast transformation method for the generation of very large human antibody libraries. *Protein Eng Des Sel* **23**, 155–159 (2010).

103. Blaise, L. *et al.* Construction and diversification of yeast cell surface displayed libraries by yeast mating: application to the affinity maturation of Fab antibody fragments. *Gene* **342**, 211–218 (2004).

104. Rosowski, S. *et al.* A novel one-step approach for the construction of yeast surface display Fab antibody libraries. *Microb Cell Fact* **17**, 3 (2018).

105. Boder, E. T., Raeeszadeh-Sarmazdeh, M. & Price, J. V. Engineering antibodies by yeast display. *Arch Biochem Biophys* **526**, 99–106 (2012).

106. Bowley, D. R., Labrijn, A. F., Zwick, M. B. & Burton, D. R. Antigen selection from an HIV-1 immune antibody library displayed on yeast yields many novel antibodies compared to selection from the same library displayed on phage. *Protein Eng Des Sel* **20**, 81–90 (2007).

107. Doerner, A., Rhiel, L., Zielonka, S. & Kolmar, H. Therapeutic antibody engineering by high efficiency cell screening. *Febs Lett* **588**, 278–287 (2014).

108. Schröter, C. *et al.* Selection of Antibodies with Tailored Properties by Application of High-Throughput Multiparameter Fluorescence-Activated Cell Sorting of Yeast-Displayed Immune Libraries. *Mol Biotechnol* **60**, 727–735 (2018).

109. Rappazzo, C. G. *et al.* Broad and potent activity against SARS-like viruses by an engineered human monoclonal antibody. *Science* **371**, 823–829 (2021).

110. Simons, J. F. *et al.* Affinity maturation of antibodies by combinatorial codon mutagenesis versus error-prone PCR. *Mabs* **12**, 1803646 (2020).

111. Bunk, S. *et al.* Abstract 2789: Development of highly potent T-cell receptor bispecifics with picomolar activity against tumor-specific HLA ligands. *Immunology* 2789–2789 (2018) doi:10.1158/1538-7445.am2018-2789.

112. Bunk, S. *et al.* Effective Targeting of PRAME-Positive Tumors with Bispecific T Cell-Engaging Receptor (TCER®) Molecules. *Blood* **134**, 3368–3368 (2019).

113. Parthiban, K. *et al.* A comprehensive search of functional sequence space using large mammalian display libraries created by gene editing. *Mabs* **11**, 884–898 (2019).

114. Waldmeier, L. *et al.* Transpo-mAb display: Transposition-mediated B cell display and functional screening of full-length IgG antibody libraries. *Mabs* **8**, 726–740 (2016).

115. Zhou, C., Jacobsen, F. W., Cai, L., Chen, Q. & Shen, D. Development of a novel mammalian cell surface antibody display platform. *Mabs* **2**, 508–518 (2010).

116. Gaidukov, L. *et al.* A multi-landing pad DNA integration platform for mammalian cell engineering. *Nucleic Acids Res* **46**, gky216- (2018).

117. Chen, C., Li, N., Zhao, Y. & Hang, H. Coupling recombinase-mediated cassette exchange with somatic hypermutation for antibody affinity maturation in CHO cells. *Biotechnol Bioeng* **113**, 39–51 (2016).

118. Olorunniji, F. J., Rosser, S. J. & Stark, W. M. Site-specific recombinases: molecular machines for the Genetic Revolution. *Biochem J* **473**, 673–684 (2016).

119. Chi, X., Zheng, Q., Jiang, R., Chen-Tsai, R. Y. & Kong, L.-J. A system for site-specific integration of transgenes in mammalian cells. *Plos One* **14**, e0219842 (2019).

120. Phan, Q. V., Contzen, J., Seemann, P. & Gossen, M. Site-specific chromosomal gene insertion: Flp recombinase versus Cas9 nuclease. *Sci Rep-uk* **7**, 17771 (2017).

121. Bowers, P. M. *et al.* Mammalian cell display for the discovery and optimization of antibody therapeutics. *Methods* **65**, 44–56 (2014).

122. Beerli, R. R. *et al.* Isolation of human monoclonal antibodies by mammalian cell display. *Proc National Acad Sci* **105**, 14336–14341 (2008).

123. Breous-Nystrom, E. *et al.* Retrocyte Display® technology: Generation and screening of a high diversity cellular antibody library. *Methods* **65**, 57–67 (2014).

124. Ho, M. & Pastan, I. Therapeutic Antibodies, Methods and Protocols. *Methods Mol Biology* **525**, 337–352 (2008).

125. Birch, J. R. & Racher, A. J. Antibody production. *Adv Drug Deliver Rev* **58**, 671–685 (2006).

126. Wurm, F. M. Production of recombinant protein therapeutics in cultivated mammalian cells. *Nat Biotechnol* **22**, 1393–1398 (2004).

127. Dyson, M. R. *et al.* Beyond affinity: selection of antibody variants with optimal biophysical properties and reduced immunogenicity from mammalian display libraries. *Mabs* **12**, 1829335 (2020).

128. Nguyen, A. W., Le, K. C. & Maynard, J. A. Identification of high affinity HER2 binding antibodies using CHO Fab surface display. *Protein Eng Des Sel* **31**, 91–101 (2018).

129. King, D., Bowers, P., Kehry, M. & Horlick, R. Mammalian Cell Display and Somatic Hypermutation In Vitro for Human Antibody Discovery. *Curr Drug Discov Technologies* **11**, 56–64 (2014).

130. Zhou, C., Jacobsen, F. W., Cai, L., Chen, Q. & Shen, D. Development of a novel mammalian cell surface antibody display platform. *Mabs* **2**, 508–518 (2010).

131. Ho, S. C. L. *et al.* IRES-mediated Tricistronic vectors for enhancing generation of high monoclonal antibody expressing CHO cell lines. *J Biotechnol* **157**, 130–139 (2012).

132. McConnell, A. D. *et al.* High Affinity Humanized Antibodies without Making Hybridomas; Immunization Paired with Mammalian Cell Display and In Vitro Somatic Hypermutation. *Plos One* **7**, e49458 (2012).

133. Plewa, C. A. *et al.* AgenTus Therapeutics to Present on the Anti-tumor Activities of Two Proprietary T Cell Receptors (TCRs) at CAR-TCR Summit in Boston, MA. *A mammalian display-based platform for T Cell Receptor (TCR) discovery and identification of novel TCRs*

targeting NY-ESO-1 https://investor.agenusbio.com/news-releases/news-release-details/agentus-therapeutics-present-anti-tumor-activities-two/ (2018).

134. Martin, A. & Scharff, M. D. Somatic hypermutation of the AID transgene in B and non-B cells. *Proc National Acad Sci* **99**, 12304–12308 (2002).

135. Maul, R. W. & Gearhart, P. J. Chapter six AID and Somatic Hypermutation. *Adv Immunol* **105**, 159–191 (2010).

136. Shivarov, V., Shinkura, R. & Honjo, T. Dissociation of in vitro DNA deamination activity and physiological functions of AID mutants. *Proc National Acad Sci* **105**, 15866–15871 (2008).

137. Bowers, P. M. *et al.* Coupling mammalian cell surface display with somatic hypermutation for the discovery and maturation of human antibodies. *Proc National Acad Sci* **108**, 20455–20460 (2011).

138. Chen, S. *et al.* Affinity maturation of anti-TNF-alpha scFv with somatic hypermutation in non-B cells. *Protein Cell* **3**, 460–469 (2012).

139. Yoshikawa, K. *et al.* AID Enzyme-Induced Hypermutation in an Actively Transcribed Gene in Fibroblasts. *Science* **296**, 2033–2036 (2002).

140. Zheng, N.-Y., Wilson, K., Jared, M. & Wilson, P. C. Intricate targeting of immunoglobulin somatic hypermutation maximizes the efficiency of affinity maturation. *J Exp Medicine* **201**, 1467–1478 (2005).

141. Wirth, D. *et al.* Road to precision: recombinase-based targeting technologies for genome engineering. *Curr Opin Biotech* **18**, 411–419 (2007).

142. Branda, C. S. & Dymecki, S. M. Talking about a Revolution The Impact of Site-Specific Recombinases on Genetic Analyses in Mice. *Dev Cell* **6**, 7–28 (2004).

143. Baer, A. & Bode, J. Coping with kinetic and thermodynamic barriers: RMCE, an efficient strategy for the targeted integration of transgenes. *Curr Opin Biotech* **12**, 473–480 (2001).

144. Schlake, T. & Bode, J. Use of Mutated FLP Recognition Target (FRT) Sites for the Exchange of Expression Cassettes at Defined Chromosomal Loci. *Biochemistry-us* **33**, 12746–12751 (1994).

145. Lee, G. & Saito, I. Role of nucleotide sequences of loxP spacer region in Cre-mediated recombination. *Gene* **216**, 55–65 (1998).

146. Lauth, M., Spreafico, F., Dethleffsen, K. & Meyer, M. Stable and efficient cassette exchange under non-selectable conditions by combined use of two site-specific recombinases. *Nucleic Acids Res* **30**, e115–e115 (2002).

147. Buchholz, F., Angrand, P.-O. & Stewart, A. F. Improved properties of FLP recombinase evolved by cycling mutagenesis. *Nat Biotechnol* **16**, 657–662 (1998).

148. Thyagarajan, B., Olivares, E. C., Hollis, R. P., Ginsburg, D. S. & Calos, M. P. Site-Specific Genomic Integration in Mammalian Cells Mediated by Phage ΦC31 Integrase. *Mol Cell Biol* **21**, 3926–3934 (2001).

149. Giard, D. J. *et al.* In Vitro Cultivation of Human Tumors: Establishment of Cell Lines Derived From a Series of Solid Tumors2. *Jnci J National Cancer Inst* **51**, 1417–1423 (1973).

150. Puck, T. T., Cieciura, S. J. & Robinson, A. GENETICS OF SOMATIC MAMMALIAN CELLS. *J Exp Medicine* **108**, 945–956 (1958).

151. Creasey, A. A. *et al.* Biological properties of human melanoma cells in culture. *Vitro* **15**, 342–350 (1979).

152. Uozumi, K. *et al.* Establishment and characterization of a new human megakaryoblastic cell line (SET-2) that spontaneously matures to megakaryocytes and produces platelet-like particles. *Leukemia* **14**, 142–152 (2000).

153. Stein, G. H. T98G: An anchorage-independent human tumor cell line that exhibits stationary phase G1 arrest in vitro. *J Cell Physiol* **99**, 43–54 (1979).

154. Stinson, S. F. *et al.* Morphological and immunocytochemical characteristics of human tumor cell lines for use in a disease-oriented anticancer drug screen. *Anticancer Research* 1035–1054 (1992).

155. Vree, P. J. P. de *et al.* Targeted sequencing by proximity ligation for comprehensive variant detection and local haplotyping. *Nat Biotechnol* **32**, 1019–1025 (2014).

156. Garboczi, D. N., Hung, D. T. & Wiley, D. C. HLA-A2-peptide complexes: refolding and crystallization of molecules expressed in Escherichia coli and complexed with single antigenic peptides. *Proc National Acad Sci* **89**, 3429–3433 (1992).

157. Rodenko, B. *et al.* Generation of peptide–MHC class I complexes through UV-mediated ligand exchange. *Nat Protoc* **1**, 1120–1132 (2006).

158. Atwell, S., Ridgway, J. B., Wells, J. A. & Carter, P. Stable heterodimers from remodeling the domain interface of a homodimer using a phage display library. *J Mol Biol* **270**, 26–35 (1997).

159. Armour, K. L., Clark, M. R., Hadley, A. G. & Williamson, L. M. Recombinant human IgG molecules lacking Fcγ receptor I binding and monocyte triggering activities. *Eur J Immunol* **29**, 2613–2624 (1999).

160. Morgan, A. *et al.* The N-terminal end of the CH2 domain of chimeric human IgG1 anti-HLA-DR is necessary for C1q, FcγRI and FcγRIII binding. *Immunology* 319–324 (1995) doi:10.1084/jem.173.4.1025.

161. Tao, M. H. & Morrison, S. L. Studies of aglycosylated chimeric mouse-human IgG. Role of carbohydrate in the structure and effector functions mediated by the human IgG constant region. *J Immunol* **143**, 2595–601. (1989).

162. Mason, D. M. *et al.* High-throughput antibody engineering in mammalian cells by CRISPR/Cas9-mediated homology-directed mutagenesis. *Biorxiv* 285015 (2018) doi:10.1101/285015.

163. Baughn, L. B. *et al.* Recombinase-Mediated Cassette Exchange as a Novel Method To Study Somatic Hypermutation in Ramos Cells. *Mbio* **2**, e00186-11 (2011).

164. Bassan, D., Gozlan, Y. M., Sharbi-Yunger, A., Tzehoval, E. & Eisenbach, L. Optimizing T-cell receptor avidity with somatic hypermutation. *Int J Cancer* **145**, 2816–2826 (2019).

165. Parola, C. *et al.* Antibody discovery and engineering by enhanced CRISPR-Cas9 integration of variable gene cassette libraries in mammalian cells. *Mabs* **11**, 1367–1380 (2019).

166. Raymond, C. S. & Soriano, P. High-Efficiency FLP and ΦC31 Site-Specific Recombination in Mammalian Cells. *Plos One* **2**, e162 (2007).

167. Nakano, M. *et al.* Efficient gene activation in cultured mammalian cells mediated by FLP recombinase-expressing recombinant adenovirus. *Nucleic Acids Res* **29**, e40–e40 (2001).

168. Chalberg, T. W. *et al.* Integration Specificity of Phage φC31 Integrase in the Human Genome. *J Mol Biol* **357**, 28–48 (2006).

169. Thyagarajan, B., Guimarães, M. J., Groth, A. C. & Calos, M. P. Mammalian genomes contain active recombinase recognition sites. *Gene* **244**, 47–54 (2000).

170. Loonstra, A. *et al.* Growth inhibition and DNA damage induced by Cre recombinase in mammalian cells. *Proc National Acad Sci* **98**, 9209–9214 (2001).

171. Schmidt, E. E., Taylor, D. S., Prigge, J. R., Barnett, S. & Capecchi, M. R. Illegitimate Cre-dependent chromosome rearrangements in transgenic mouse spermatids. *Proc National Acad Sci* **97**, 13702–13707 (2000).

172. Baser, B., Spehr, J., Büssow, K. & Heuvel, J. van den. A method for specifically targeting two independent genomic integration sites for co-expression of genes in CHO cells. *Methods* **95**, 3–12 (2016).

173. Callesen, M. M. *et al.* Recombinase-Mediated Cassette Exchange (RMCE)-in Reporter Cell Lines as an Alternative to the Flp-in System. *Plos One* **11**, e0161471 (2016).

174. Erlendsson, S. & Teilum, K. Binding Revisited—Avidity in Cellular Function and Signaling. *Frontiers Mol Biosci* **7**, 615565 (2021).

175. Hoffmann, T., Krackhardt, A. M. & Antes, I. Quantitative Analysis of the Association Angle between T-cell Receptor Valpha/Vbeta Domains Reveals Important Features for Epitope Recognition. *Plos Comput Biol* **11**, e1004244 (2015).

176. Gezgin, G. *et al.* PRAME as a Potential Target for Immunotherapy in Metastatic Uveal Melanoma. *Jama Ophthalmol* **135**, 541–549 (2017).

177. Roszik, J. *et al.* Overexpressed PRAME is a potential immunotherapy target in sarcoma subtypes. *Clin Sarcoma Res* **7**, 11 (2017).

178. Wang, W.-L. *et al.* RNA expression profiling reveals PRAME, a potential immunotherapy target, is frequently expressed in solitary fibrous tumors. *Modern Pathol* **34**, 951–960 (2021).

179. Solopova, O. N. *et al.* Monoclonal Antibodies to PRAME Protein Slow the Development of PRAME-Expressing Tumor. *Dokl Biochem Biophys* **498**, 199–202 (2021).

180. Chang, A. Y. *et al.* A therapeutic T cell receptor mimic antibody targets tumor-associated PRAME peptide/HLA-I antigens. *J Clin Invest* **127**, 2705–2718 (2017).

181. Al-Khadairi, G. & Decock, J. Cancer Testis Antigens and Immunotherapy: Where Do We Stand in the Targeting of PRAME? *Cancers* **11**, 984 (2019).

182. Rajpal, A. *et al.* A general method for greatly improving the affinity of antibodies by using combinatorial libraries. *PNAS* (2014).

183. Wucherpfennig, K. W. The First Structures of T Cell Receptors Bound to Peptide–MHC. *J Immunol* **185**, 6391–6393 (2010).

184. Boulter, J. M. & Jakobsen, B. K. Stable, soluble, high-affinity, engineered T cell receptors: novel antibody-like proteins for specific targeting of peptide antigens. *Clin Exp Immunol* **142**, 454–60 (2005).

185. Thomas, S. *et al.* Human T cells expressing affinity-matured TCR display accelerated responses but fail to recognize low density of MHC-peptide antigen. *Blood* **118**, 319–329 (2011).

186. Harper, J. *et al.* An approved in vitro approach to preclinical safety and efficacy evaluation of engineered T cell receptor anti-CD3 bispecific (ImmTAC) molecules. *Plos One* **13**, e0205491 (2018).

187. Topp, M. S. *et al.* Safety and activity of blinatumomab for adult patients with relapsed or refractory B-precursor acute lymphoblastic leukaemia: a multicentre, single-arm, phase 2 study. *Lancet Oncol* **16**, 57–66 (2015).

188. Neelapu, S. S. *et al.* Chimeric antigen receptor T-cell therapy - assessment and management of toxicities. *Nat Rev Clin Oncol* **15**, 47–62 (2018).

189. Cameron, B. J. *et al.* Identification of a Titin-derived HLA-A1-presented peptide as a cross-reactive target for engineered MAGE A3-directed T cells. *Sci Transl Med* **5**, 197ra103 (2013).

190. Linette, G. P. *et al.* Cardiovascular toxicity and titin cross-reactivity of affinity-enhanced T cells in myeloma and melanoma. *Blood* **122**, 863–71 (2013).

191. Ziegler, S. F., Ramsdell, F. & Alderson, M. R. The activation antigen CD69. *Stem Cells* **12**, 456–465 (1994).

192. Mita, Y. *et al.* Crucial role of CD69 in anti-tumor immunity through regulating the exhaustion of tumor-infiltrating T cells. *Int Immunol* **30**, 559–567 (2018).

193. Yokoyama, W. M. *Specific and Non-specific Natural Killer Cell Responses to Viral Infection. In: Gupta, S., Paul, W.E., Steinman, R. (eds) Mechanisms of Lymphocyte Activation and Immune Regulation X.* (2005). doi:10.1007/0-387-24180-9_8.

194. Bowers, P. M., Boyle, W. J. & Damoiseaux, R. The Use of Somatic Hypermutation for the Affinity Maturation of Therapeutic Antibodies. *Methods Mol Biology* **1827**, 479–489 (2018).

195. Bassan, D. *et al.* Avidity optimization of a MAGE-A1-specific TCR with somatic hypermutation. *Eur J Immunol* **51**, 1505–1518 (2021).

196. Cowell, L. G., Kim, H.-J., Humaljoki, T., Berek, C. & Kepler, T. B. Enhanced Evolvability in Immunoglobulin V Genes Under Somatic Hypermutation. *J Mol Evol* **49**, 23–26 (1999).

197. Horlick, R. A. *et al.* Simultaneous Surface Display and Secretion of Proteins from Mammalian Cells Facilitate Efficient in Vitro Selection and Maturation of Antibodies. *J Biol Chem* **288**, 19861–19869 (2013).

8 Acknowledgement

First of all, I want to thank my both supervisors Prof. Dr. Roland Kontermann und Dr. Sebastian Bunk for giving me the opportunity to conduct my doctoral thesis as a joint project of the University Stuttgart and the Immatics Biotechnolgies GmbH. I want to thank both of you for your great supervision and support during this time. I also want to thank Prof. Dr. Matthias Peipp for being my second supervisor.

Special thanks go to all my colleagues at Immatics for helping me out at various occasions and for listening to my problems even if you didn't exactly know what I was talking about.

I would also like to thank my Homies Mina, Jules, Miri, Benso, Nienke, and Malte for starting this journey with me and for their constant support over more than ten years. You all made my studies more fun, and I am very thankful to have you in my life.

Furthermore, I would like to thank my family for their continuous support.
Thanks to my brothers-in-law, Frederic and Raphael, for distracting me with Bike & Burgers. And thanks to Mark, for always cheering things up with a funny teacher story. But especially I want to express my gratitude to my sister, Katharina, and my wife, Catherine, for always listening to me when things weren't going so well. Thank you all very much, you made these times easier and always managed to get me motivated again. And finally, thanks to my little daughter for keeping me up at night and for making reading paper even harder when being bone tired, but more importantly for all the cute moments in-between.

9 Declaration

I hereby declare that this work has been prepared exclusively by me without any illegitimate help.

All sources used have been quoted adequately.

Janine Dilchert

January 27th, 2023

10   Curriculum vitae

Name: Janine Dilchert

Professional carrier and education

Since 10|2022   **Trainee Medical** at AbbVie Deutschland GmbH & Co. KG

01|2019 – 09|2022   **PhD Student** at Immatics Biotechnologies GmbH in cooperation with the Institute for Cell Biology and Immunology, University of Stuttgart

07|2017 – 12|2018   **Research Associate** at Immatics Biotechnologies GmbH

04|2015 – 07|2017   **M.Sc. Medical Life Sciences**, Christian-Albrechts-University Kiel
Master's thesis: Analysis of Effector Machanisms Mediated by Engineered CD7-Antibodies, Prof. Dr. Matthias Peipp
(final grade 1.6)

10|2014 – 03|2015   **Master program Biology**, Christian-Albrechts-University Kiel

10|2011 – 09|2014   **B.Sc. Biology**, Christian-Albrechts-University Kiel
Bachelor's thesis: Der Einfluss von TGFβ auf TRAIL-vermittelte Signaltransduktionswege, PD Dr. Anna Trauzold
(final grade 1.8)

06|2010   **Abitur**, Gymnasium Wanne, Herne (final grade 1.3)